On Quantum Magnetism

in Cuprate Superconductors

C. N. A. van Duin
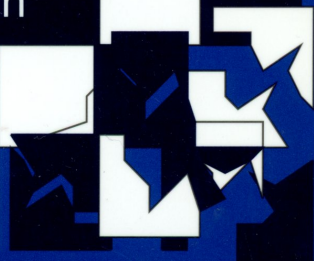
On Quantum Magnetism
in Cuprate Superconductors

On Quantum Magnetism
in Cuprate Superconductors

PROEFSCHRIFT

Ter verkrijging van
de graad van Doctor aan de Universiteit Leiden,
op gezag van de Rector Magnificus Dr. W.A. Wagenaar,
hoogleraar in de faculteit der Sociale Wetenschappen,
volgens het besluit van het College voor Promoties
te verdedigen op woensdag 26 mei 1999
te klokke 14.15 uur.

door

Cornelis Nicolaas Adrianus van Duin

geboren te Nijmegen
in 1970

Promotiecommissie:

Promotor: Prof. dr. ir. W. van Saarloos
Co-promotor: Dr. J. Zaanen
Referent: Prof. dr. ir. A. Pruisken (UvA)
Overige leden: Prof. dr. P. van Baal
Prof. dr. C. W. J. Beenakker
Dr. H. B. Brom
Prof. dr. L. J. de Jongh
Prof. dr. J. M. J. van Leeuwen
Dr. Th. M. Nieuwenhuizen (UvA)

Contents

1 Introduction

1.1 Cuprate superconductors

The cuprates came into the focus of attention after the discovery in 1986 of superconductivity in these materials by Müller and Bednorz [1] . Compared to conventional superconductors, such as mercury and tin, the cuprates exhibit a vanishing electrical resistance up to relatively high temperatures (30 K - 125 K). The obvious practical applications of a material which superconducts at reasonable temperatures triggered a great amount of research on the cuprates in the following years. The theories which had been successful in describing conventional superconductivity proved inadequate for the new materials. Indeed, conventional and cuprate superconductors have very different properties. The cuprates are doped Mott-insulators, while conventional superconductors are usually high electron density metals. The cuprates have a quasi two-dimensional structure, while conventional superconductors are isotropic. Because of the lower dimensionality and the smaller density of charge-carriers, fluctuations play a much more important role in the cuprates than in conventional superconductors. Also, the cuprates have a tendency towards antiferromagnetic order. This last point is somewhat unexpected, since superconductivity is related to attractive interactions between electrons, while antiferromagnetism arises as a result of repulsive interactions. Superconductivity and antiferromagnetism were therefore expected to be mutually exclusive phenomena. [1]

Thirteen years after their discovery, there is still no satisfactory theory describing the physics of the cuprate superconductors. It has in the mean time become clear that quantum mechanics and many-body effects play an important role in their physics.

The cuprates are a family of ceramic materials. Their common feature is the CuO_2 planes, shown in fig. 1-2. These planes are stacked in a lasagna-like structure. In the region between the planes sit rare-earth, oxygen and for some cuprates copper atoms. A cartoon of the crystallographic structure of La_2CuO_4 is drawn in figure 1-1. The layers are evenly spaced for this system. In other cuprate materials, such as $Y\ Ba_2Cu_3O_7$, there is an alternating structure of closely spaced and more widely spaced layers. The coupling between the layers, both magnetic and electric, is small with respect to the interactions in the layers. Many of the models used to describe the physics of the cuprates therefore rely on a two-dimensional description , where only the planes are taken into account. This is also the case for most of the work presented in this thesis. The coupling between the planes and the interaction with the degrees of freedom in the interstitial regions is invoked in cases where it is important. In chapter 4, a bilayer spin-model is discussed, which was originally

---

[1] Predating the discovery of superconductivity in the cuprates, a combination of antiferromagnetism and superconductivity had already been found in heavy fermion superconductors.

Cu O$_2$-plane

Interstitial
rare-earth and
oxygen atoms
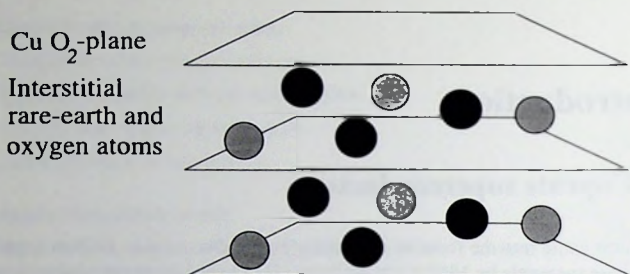
Figure 1-1. A sketch of the structure of La$_{2-x}$Sr$_x$CuO$_4$. No attempt at accuracy is made regarding the positions of the interstitial atoms.

proposed to describe some aspects of the spin-sector of Y Ba$_2$Cu$_3$O$_7$ [2]. This model takes into account the spin-spin coupling between the closely spaced CuO$_2$-layers.

The CuO$_2$ planes have a square-lattice structure, where the Cu-atoms form the sites of the lattice (fig. 1-2). Band-structure calculations show that the states close to the Fermi surface are related to the CuO$_2$-planes, supporting a quasi two-dimensional description. The undoped (no strontium) system has a half-filled Cu-band. This can be visualized in real space as there being one electron on every Cu-site in the plane. Since the band is found to be partially filled (in the band-structure approximation), there is no gap at the Fermi-surface and one would expect the system to be a conductor. However, correlation effects destroy the conductivity. The repulsive Coulomb-interaction between electrons causes a charge gap to open at the Fermi surface. This type of interactions-induced insulator is called a Mott insulator. The occurrence of this state at half-filling demonstrates the importance of many-body correlations in these materials.

Conductivity arises when electrons are removed from (or added to) the CuO$_2$-layers. In La$_2$CuO$_4$, this is done by replacing a percentage of the La^{2+}-atoms in the interstitial region with Sr^{3+}. In YBa$_2$Cu$_3$O$_7$, the oxygen-concentration outside the planes is varied. In both cases, the chemical structure is changed in the interstitial region, not in the planes, and the main effect on the in-plane physics is the introduction of holes.

In fig. 1-3, a generic phase-diagram is shown for the cuprate materials as a function of the hole-doping x and temperature T. At zero doping, the system is an antiferromagnetic insulator. Hole doping leads to a rapid depression of the Néel temperature. After the antiferromagnetism has disappeared, there is a region with spin-glass like behavior at low temperatures (the spin-dynamics slows down dramatically below a certain temperature, but there is no long-range magnetic order). This region is characterized by a gap, commonly called spin-gap or pseudo-gap, which disappears at a high, doping-dependent temperature $T^*(x)$. Photo-emission experiments suggest that this gap and the one in the superconducting phase have the same origin, since they both exhibit d-wave symmetry and evolve continuously into each other [4]. The doping leads to a nonzero conductivity in this region,
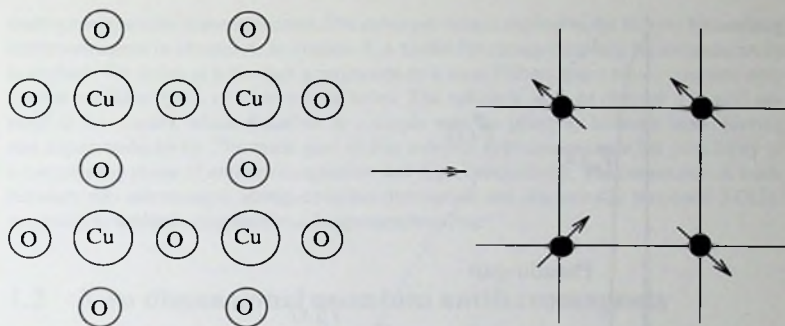
Figure 1-2. The CuO_2-plane has a square-lattice structure. At zero doping, the system has a half-filled Cu-band, giving one electron per Cu-site.

but its physics does not fit the Fermi liquid description of normal metals. Superconductivity sets in at $x \simeq 0.06$. The critical temperature $T_c(x)$ reaches its maximum at around $x = 0.15 - 0.2$ (optimal doping). The superconducting region to the left of the optimal doping is called underdoped, the region to the right overdoped. The normal state in the overdoped region is more like a normal metal, with Fermi liquid properties.

In doped La_2CuO_4, there is an anomaly at the doping $x = \frac{1}{8}$, where the system becomes an insulator under certain conditions. This is related to the formation of stripes, a form of collective charge and magnetic order, which is discussed in section 1.5. There are recent claims of a coexistence phase of antiferromagnetism and superconductivity in the regime $x \leq \frac{1}{8}$ [7].

It has been argued [8] that the physics of the CuO_2 planes can be captured by the single-band Hubbard model electrons in the CuO_2-planes are tightly bound to the Cu-atoms. Electrons can tunnel between neighboring copper sites. In addition, the model contains repulsive charge-charge interaction between electrons on the same site. It is given by

$$\mathcal{H} = t \sum_{<i,j>} \sum_{\sigma=\uparrow\downarrow} \left(c_{i\sigma}^\dagger c_{j\sigma} + c_{j\sigma}^\dagger c_{i\sigma} \right) + U \sum_i n_{i\uparrow} n_{i\downarrow} - \mu \sum_i (n_{i\uparrow} + n_{i\downarrow}), \quad (1.1.1)$$

where the summation $\sum_{<i,j>}$ runs over the bonds of a square lattice. Second quantization-notation is used. The fermion-operators $c_{i\sigma}^\dagger$ create an electron with spin σ at the Cu-site i. They satisfy the anticommutation relations

$$\begin{aligned} \{c_{i\sigma}, c_{j\tau}^\dagger\} &= \delta_{ij}\delta_{\sigma\tau}, \\ \{c_{i\sigma}, c_{j\tau}\} &= 0. \end{aligned} \quad (1.1.2)$$

The number operator $n_{i\sigma} = c_{i\sigma}^\dagger c_{i\sigma}$ measures the occupation of the (i, σ)-state.
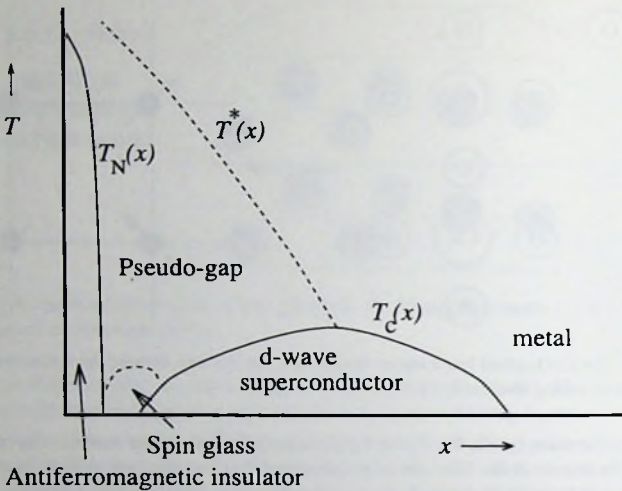
Figure 1-3. The generic phase-diagram of the cuprate materials.

The first term in the Hubbard model describes the hopping of electrons between nearest-neighbor Cu-sites. The second is an on-site Coulomb repulsion between electrons. The chemical potential is included to fix the electron-density in the planes.

The interactions in this model are highly simplified. The use of models of this kind relies on the principle of universality: microscopically very different models can yield the same physics at long wavelengths, or low energies. The Hubbard model is an appropriate description of the system, if the additional interactions which must be included to obtain a realistic Hamiltonian are irrelevant at the length scales of interest. Despite the apparent simplicity of the model, its physics is far from trivial and remains poorly understood.

The models which are considered in this thesis contain an additional simplification, which results from a projection to a low-energy sector of the Hilbert space. This projection reduces the number of degrees of freedom in the model and makes it bosonic. In the next section, it is discussed how the Hubbard model at half-filling (which describes an antiferromagnetic Mott insulator) can be mapped onto a Heisenberg spin model through such a projection. In chapter 2 a similar procedure is used for the charge ordered stripe state, yielding a spatially anisotropic Heisenberg spin model. Using this model, the spin-sector in an ordered stripe state is analyzed. The results provide a connection between the behavior in the magnetic sector and the charge-properties of the stripe phase. In chapter 3, a new type of coherent state is introduced. This state is especially suited for the semi-classical description of bosonic systems with a finite number of degrees of freedom per site which

undergo a quantum phase transition. The coherent state is applied to the bilayer Heisenberg antiferromagnet in chapter 4. In chapter 5, a model for strong-coupling superconductivity is studied. We arrive at it through a projection to a local Hilbert space which contains only nearest-neighbor pairs of electrons or holes. The coherent state of chapter 3 is also applied to this model, which describes in a simple way the interplay between spin-ordering and superconductivity. The main goal of this analysis is to demonstrate the possibility of a coexistence phase of antiferromagnetism and superconductivity. The connection is made between this microscopic strong-coupling description and the recently proposed $SO(5)$-approach to antiferromagnetism and superconductivity.

1.2   Two dimensional quantum antiferromagnets

1.2.1   The large U limit of the Hubbard model.

The low-energy sector of the Hubbard model simplifies significantly for the case of half-filling and large $\frac{U}{t}$. In the absence of the kinetic term, every site is singly occupied in the groundstate. Switching on t, one finds that any hop involves the creation of an on-site singlet at an energy cost U. The half-filled system is therefore an insulator, with a gap of order U towards charge excitations. This type of interactions-induced insulator is called a Mott-Hubbard insulator. The only low-energy degrees of freedom left in the system are the spins of the localized electrons.

Virtual excitations across the charge gap induce an effective interaction between the spins. Since electrons can only hop onto sites where the spin is anti-parallel to their own, neighboring electrons can lower the kinetic energy of the system by anti-aligning their spins.

Indeed, the Hubbard model at half-filling can be mapped onto the antiferromagnetic Heisenberg spin model by integrating out the charge-excitations. The resulting Hamiltonian acts on the projected Hilbert space, where double site-occupancy is forbidden.

$$\mathcal{H} \;=\; J \sum_{<i,j>} \left(\vec{S}_i \cdot \vec{S}_j - \frac{1}{4} n_i \right) + \mathcal{O}(\frac{t^3}{U^2}). \tag{1.2.1}$$

The exchange-constant J is given by $\frac{2t^2}{U}$. The spin operators $\vec{S}$ read

$$S^\alpha = \frac{1}{2}(c_\uparrow^\dagger, c_\downarrow^\dagger)\, \sigma_\alpha \begin{pmatrix} c_\uparrow \\ c_\downarrow \end{pmatrix}, \tag{1.2.2}$$

where σ_α is a Pauli spin-matrix.

$$\sigma_x = \begin{pmatrix} 0 & 1 \\ 1 & 0 \end{pmatrix} \;;\; \sigma_y = \begin{pmatrix} 0 & -i \\ i & 0 \end{pmatrix} \;;\; \sigma_z = \begin{pmatrix} 1 & 0 \\ 0 & -1 \end{pmatrix}. \tag{1.2.3}$$

As the half-filled system has every site singly occupied, the operator n_i in eq. (1.2.1) can by replaced by one. It contributes a shift in the groundstate energy.

The above procedure can also be followed at lower fillings. Away from half-filling, it becomes possible for charges to move without causing double occupancy. The effective Hamiltonian on the projected Hilbert space therefore contains both spin-spin interactions and hopping-terms. A much-studied model of this type is the $t - J$ model:

$$\mathcal{H}_{t-J} = t \sum_{<ij>} \sum_{\sigma=\pm\frac{1}{2}} \left((1 - n_{i,-\sigma}) c_{i,\sigma}^{\dagger} c_{j,\sigma} + (1 - n_{j,-\sigma}) c_{j,\sigma}^{\dagger} c_{i,\sigma} \right)$$
$$+ J \sum_{<ij>} \vec{S}_i \cdot \vec{S}_j - \mu \sum_i n_i . \tag{1.2.4}$$

The projection-operators in the hopping-term ensure that no doubly occupied states are created. A derivation of this Hamiltonian from the Hubbard model in the large U limit yields an additional term: a combination of a spin-spin interaction and a hopping process. For reasons of simplicity, this term is usually omitted. A model of the $t - J$ type is discussed in chapter 5.

1.2.2 Spontaneous symmetry breaking, Goldstone modes

The Heisenberg Hamiltonian has a global rotational symmetry. On the classical level, this means that the Hamiltonian is invariant under global rotations of the spin-vectors $\vec{S}_i$. For the quantum system, it implies that $\mathcal{H}$ commutes with the generators of global $SU(2)$ transformations S_{tot}^{α}. If a spin-ordering transition occurs at some critical temperature, the rotational symmetry is spontaneously broken. Spontaneous symmetry breaking is a feature specific to systems with an infinite number of degrees of freedom. We give a definition of the process, focusing specifically on the case of the Heisenberg antiferromagnet [3].

Consider the Heisenberg Hamiltonian on a finite lattice in a staggered magnetic field:

$$\mathcal{H} = J \sum_{<i,j>}^{N} \vec{S}_i \cdot \vec{S}_j - \sum_i^{N} (-1)^{i_x + i_y} H S_i^z . \tag{1.2.5}$$

The staggered magnetic field explicitly breaks the $SU(2)$ rotational symmetry of the Hamiltonian. Sending H to zero before taking the thermodynamic limit results in an infinite-N groundstate which is $SU(2)$-symmetric. This is not necessarily the case when the order of the limits is reversed. The system is said to exhibit spontaneous symmetry breaking if

$$\lim_{H \to 0} \lim_{N \to \infty} \frac{1}{N} \sum_i^{N} (-1)^{i_x + i_y} \langle S_i^z \rangle \neq 0. \tag{1.2.6}$$

Consequently, the symmetry-broken state is characterized by an order-parameter which becomes non-zero. In this case, it is the spontaneous staggered magnetization:

$$\vec{M} = \frac{1}{N} \sum_i^N \vec{m}_i = \frac{1}{N} \sum_i^N (-1)^{i_x+i_y} \langle \vec{S}_i \rangle . \tag{1.2.7}$$

Due to the rotation invariance of the model, the order-parameter can be chosen in any direction by changing the orientation of the symmetry-breaking field. This freedom to rotate the order parameter gives rise to low-energy collective modes which involve spatial modulations of $\langle \vec{S}_i \rangle$: the Goldstone modes. These modes have a vanishing energy at the ordering wave-vector, where the modulation of $\langle \vec{S}_i \rangle$ amounts to a global rotation of the order-parameter. Goldstone modes appear in all systems which exhibit spontaneous breaking of a global continuous symmetry [2].

For quantum systems, two types of symmetry-breaking need to be distinguished: exact and non-exact. Exact symmetry-breaking occurs if the symmetry-breaking field commutes with the Hamiltonian. The ordered state which results is an eigenstate of the Hamiltonian. The elementary excitations for these systems have a quadratic dispersion. An example of this type of spontaneous symmetry breaking is the ordered ferromagnet. In systems with non-exact symmetry breaking, the ordered state is not an eigenstate of the Hamiltonian, but can instead be thought of as a superposition of a number of low-energy eigenstates which become degenerate in the thermodynamic limit. Their Goldstone modes have a linear dispersion. The Heisenberg antiferromagnet exhibits symmetry breaking of this type. Another example is the breaking of translational symmetry in a crystal, which gives rise to acoustic phonons.

The Goldstone modes dominate the low-energy physics of the ordered states. Occupation of the Goldstone excitations results in a reduced value of the order-parameter. There is a theorem due to Mermin and Wagner [5], which states that, for the case of 1 and 2 dimensions, the Goldstone modes completely disorder the symmetry-broken state at any finite temperature. Spontaneous breaking of a continuous symmetry in a model with short-range interactions is therefore not possible at non-zero temperatures in 1 and 2 dimensions. This theorem also holds for the case of classical systems. As we shall discuss in section 1.3, the $T = 0$ one-dimensional quantum Heisenberg model can be mapped onto a finite T two-dimensional classical Heisenberg model. It follows that spontaneous rotational symmetry breaking in 1 dimension is not possible even at $T = 0$.

The Mermin-Wagner theorem implies that the two-dimensional antiferromagnet can only have long-range order at $T = 0$. The model eq. (1.2.1) therefore cannot reproduce the finite-temperature Néel order that is seen in the cuprates at half-filling. To achieve this, it is necessary to take into account the magnetic coupling between the perovskite planes, as well as the spin-anisotropies caused by the interstitial rare-earth atoms [9]. These additional interactions introduce 3-dimensionality and break the $SU(2)$-invariance of the Hamiltonian.

---

[2]If the interactions are 'sufficiently' short-ranged.

Since these contributions are very small, it is possible to include them in a mean-field manner, subsequent to a more accurate treatment of the two-dimensional, $SU(2)$-symmetric degrees of freedom. This problem is addressed in chapter 2.

1.2.3   The large S expansion

The general-S formulation of the Heisenberg model provides us with a convenient computational tool: the large S expansion. For $S \to \infty$, the quantum antiferromagnet becomes equivalent to its classical counterpart –this will be demonstrated below for the $T = 0$ case. Since the classical system has perfect Néel order at zero temperature, the same must be true for the quantum antiferromagnet in the large S limit. The Néel state can therefore be used as a zeroth order approximation in a semi-classical expansion in $\frac{1}{S}$.

The $\frac{1}{S}$-expansion is conveniently derived using the Holstein-Primakov boson representation for the spin-operators [6]:

$$
\begin{aligned}
S^z &= S - b^\dagger b, \\
S^+ &= \sqrt{2S}\sqrt{1 - \frac{b^\dagger b}{2S}}\, b, \\
S^- &= b^\dagger \sqrt{2S}\sqrt{1 - \frac{b^\dagger b}{2S}}.
\end{aligned}
\tag{1.2.8}
$$

In this representation, the maximally polarized state $m^z = S$ plays the role of a vacuum. The boson-operator $b^\dagger$ creates excitations on this vacuum, which represent the states with lower m^z. Since the number of states in a multiplet is finite, it is necessary to impose a constraint on the number of bosonic excitations: $n_b \leq 2S$. This constraint can be implemented by augmenting the Hamiltonian with projection operators. However, as long as $\langle n_b \rangle \ll 2S$, the constraint will have no effects on the results and the projection operators can be omitted. In practice, the $\frac{1}{S}$-expansion only works inside the ordered state, where this condition is indeed satisfied.

Since we are considering antiferromagnetic ordering, it is necessary to introduce two spin-sublattices A and B. On sublattice A, the preferred spin direction is up, on sublattice B it is down. Performing the $SU(2)$ transformation $S_i^z \to -S_i^z$, $S_i^y \to -S_i^y$ on the B sublattice and expanding the Hamiltonian to second order in the boson-operators (next-leading order in $\frac{1}{S}$), one obtains

$$
\mathcal{H} = -dNJS^2 + \frac{1}{2}SJ \sum_{<ij>} \left(b_i^\dagger b_i + b_j^\dagger b_j + b_i^\dagger b_j^\dagger + b_j b_i \right).
\tag{1.2.9}
$$

Note that the lowest order term is indeed the energy of an ordered Néel state. After a transformation to momentum space, the Hamiltonian can be diagonalized by the Bogoliubov

transformation for bosons. This introduces the quasi-particles

$$a_k^\dagger = \cosh(u_k)b_k^\dagger + \sinh(u_k)b_{-k}, \tag{1.2.10}$$

which are called antiferromagnons. They are the quantized Goldstone modes of the anti-ferromagnet. The parameter u_k is fixed by the diagonalization condition

$$\tanh(2u_k) = \gamma_k \equiv \frac{1}{d}\sum_{\alpha=1}^{d}\cos(k_\alpha). \tag{1.2.11}$$

In terms of the new quasi-particles, the Hamiltonian is given by

$$\mathcal{H} = -dNJS(S+1) + \sum_{k>0}\omega_k\left(a_k^\dagger a_k + \frac{1}{2}\right), \tag{1.2.12}$$

where ω_k is the spin-wave dispersion

$$\omega_k = 2dJS\sqrt{1-\gamma_k^2} = 2\sqrt{d}JS\left(k + \mathcal{O}(k^2)\right). \tag{1.2.13}$$

To this order in S (the Gaussian level), the antiferromagnons are freely propagating particles, with velocity $c_s = 2\sqrt{d}JS$. Spin-wave interactions show up in the higher order terms.

The antiferromagnetic order-parameter is reduced by the Gaussian fluctuations. At $T = 0$ ($\langle n_a \rangle = 0$), the reduction is given by

$$\delta S = \langle b_k^\dagger b_k \rangle = \frac{1}{2}\int_k \frac{d^d k}{(2\pi)^d}\left(\frac{1}{\sqrt{1-\gamma_k^2}} - 1\right). \tag{1.2.14}$$

For $d = 1$, the integral in eq. (1.2.14) diverges, signalling the instability of $T = 0$ Néel order in one dimension. For $d = 2$, one finds $\delta S = 0.197$. This suggests that $S = \frac{1}{2}$-antiferromagnetism can exist in two dimensions at zero temperature.

On the face of it, it might appear unjustifiable to apply the results of an expansion in $\frac{1}{S}$ to the case $S = \frac{1}{2}$. Some justification for this procedure can be found by considering the higher order terms in the expansion. A calculation to order $\frac{1}{S^2}$ has been carried out by Igarashi [10]. This work addresses the value of the order-parameter and the spin-wave velocity, as well as that of the spin-stiffness ρ_s and the perpendicular susceptibility $\chi_\perp$. These two quantities determine the long-wavelength dynamics of the quantum antiferromagnet. The spin-stiffness is related to the energy cost of twisting the order-parameter along one of the crystal axes. The susceptibility measures the induced magnetization by a uniform magnetic

field applied perpendicular to the spin-ordering vector. They are related to the spin-wave velocity by $\rho_s = \chi_\perp c_s^2$. Igarashi obtained the following results.

$$
\begin{aligned}
M &= S - 0.19660 + \frac{0.0035}{(2S)^2}, \\
c_s &= 2\sqrt{2}JS\left(1 + \frac{0.1579}{2S} + \frac{0.0215(\pm 0.0002)}{(2S)^2}\right), \\
\rho_s &= JS^2\left(1 - \frac{0.235}{2S} - \frac{0.041(\pm 0.003)}{(2S)^2}\right), \\
\chi_\perp &= \frac{1}{8J}\left(1 - \frac{0.551}{2S} + \frac{0.065(\pm 0.001)}{(2S)^2}\right).
\end{aligned}
\tag{1.2.15}
$$

Notice that the prefactors of the order $\frac{1}{S^2}$ terms are small as compared to the lowest order corrections, although not negligible. This suggests that the main correction to the zeroth order term comes from the non-interacting spin-waves. Although $\frac{1}{S}$ is not itself a small parameter for $S \sim 1$, an expansion in this parameter apparently still provides a way to organize the quantum-corrections into more and less important ones. As a result, the prefactors of the higher order terms become rapidly smaller, providing convergence even for $S = \frac{1}{2}$. This assumption appears to be confirmed by the good agreement between the above spin-wave results and recent high-precision Monte Carlo simulations by Kim and Troyer [11] (table 1-1).

The above spin-wave results will be used as input for a finite-temperature analysis in chapter 2. In chapter 3, a technique closely related to the spin-wave expansion is applied to the problem of two coupled two-dimensional Heisenberg antiferromagnets.

1.3 The quantum non-linear sigma model

1.3.1 Relation to the Heisenberg antiferromagnet

At long wavelengths, the quantum Heisenberg antiferromagnet can be described by an effective continuum-theory: the quantum non-linear sigma model (QNLS). This model was

	spin-wave	Quantum Monte Carlo	Difference	$\mathcal{O}\left(\frac{1}{S^2}\right)$ contribution
Z_ρ	0.724	0.713	0.012	-0.041
Z_χ	0.514	0.524	-0.01	0.065
Z_c	1.179	1.167	0.012	0.022

Table 1-1. Comparison between spin-wave and Monte Carlo-results for the renormalization-factors of ρ_s, $\chi_\perp$ and c_s ($\rho_s = Z_\rho JS^2$, etc.), for the square lattice $S = \frac{1}{2}$ antiferromagnet [10] [11]

introduced by Chakravarty, Halperin and Nelson (CHN) in 1988 [12], as a generalization of the classical non-linear sigma model (CNLS), The latter had its origin in QCD, but had already been applied successfully to the description of classical Heisenberg spin systems, and to the quantum Heisenberg antiferromagnet at zero temperature [15]. The QNLS can be used to describe two-dimensional quantum antiferromagnets at non-zero temperatures, where the system has no long-range order and spin-wave theory breaks down.

We will use the QNLS in its path-integral formulation. In this formalism, a classical statistical mechanics problem is quantized by adding one extra dimension, the imaginary time direction, on which periodic boundary conditions are imposed. At non-zero temperatures, the extend of this dimension becomes finite, $\sim \frac{\hbar}{k_B T}$. For systems in which the time and space-dimension enter in the same way, i.e. systems with dynamical critical exponent $z = 1$, quantum mechanics at finite temperatures becomes equivalent to classical statistical mechanics in a constrained volume. A discussion of this formalism can be found in the book of Fradkin [13] and in ref [14].

To obtain the QNLS, it is assumed that Néel order is well established at short distances. An order parameter $\vec{n}_i$ can then be defined locally, as a spatial average of the staggered magnetization over one unit cell. The deviations from the local average, which give rise to longitudinal fluctuations of the order-parameter, are integrated out. One is left with an effective action for the low-energy transversal fluctuations of $\vec{n}_i$. This action is called the lattice rotor model. It describes the physics of rotors with a fixed length on a lattice. The QNLS is obtained by taking the lattice spacing to zero. This coarse graining procedure is discussed in the next section. In chapter 4, it is performed for the bilayer antiferromagnet, and in chapter 5 for an $SO(5)$ symmetric model.

The partition function of the QNLS is given by

$$\mathcal{Z} = \int D\vec{n} \prod_i \delta(\vec{n}_i^2 - 1) e^{-S/\hbar}. \tag{1.3.1}$$

with the action[3]

$$S = \frac{1}{2} \int_0^{\beta\hbar} d\tau \int d^d x \left[\chi_\perp^0 \left(\frac{\partial \vec{n}}{\partial \tau} \right)^2 + \rho_s^0 (\nabla \vec{n})^2 \right]. \tag{1.3.2}$$

which is subject to periodic boundary conditions in the spatial and the imaginary time direction. The δ-function in the measure fixes the length of $\vec{n}_i$, which does not change under transversal fluctuations. It is this constraint which introduces non-linearity into the model. The unconstrained version of eq. (1.3.2) is called the sigma model. It describes a collection of non-interacting spin-waves.

The two parameters that appear in the action are the bare spin-stiffness and perpendicular susceptibility: in other words ρ_s and $\chi_\perp$ defined at the lattice scale. The long-wavelength,

---

[3]We have taken the continuum limit, lattice-spacing to zero, in the action.

or renormalized parameters are the ones actually measured in experiments (see table 1-1). They can be obtained from the QNLS in a renormalization-group calculation, using the bare parameters as input. This calculation is carried out in the appendix to chapter 2.

Haldane derived the non-linear sigma model from the Heisenberg model in the semi-classical large-S limit [15]. He obtained the following values for the bare stiffness and susceptibility

$$\rho_s^0 = JS^2a^{2-d} \quad ; \quad \chi_\perp^0 = \frac{a^{-d}}{4Jd}, \tag{1.3.3}$$

where a is the lattice spacing of the related Heisenberg model. These are just the lowest-order term in the spin-wave expansions for ρ_s and $\chi_\perp$, or their mean-field values.

It should be noted that there is no way to accurately derive the bare parameters for, say, a QNLS describing an $S = \frac{1}{2}$ system. The form of the QNLS is dictated by the fact the Heisenberg antiferromagnet is a vector model which has an acoustic mode. It will therefore be the same for a small S system as for the large S case derived by Haldane. The bare parameters entering the QNLS are however more or less phenomenological. Nevertheless, certain dependencies which are found in the large S limit , like $\rho_s \propto J$ and $\chi_\perp \propto \frac{1}{J}$, are probably true also for the actual bare parameters.

Finally, notice that the QNLS indeed reproduces the acoustic spin-wave mode of the ordered antiferromagnet. This is easily checked by noting that the QNLS action can be interpreted as describing a set of coupled harmonic oscillators, where ρ_s^0 plays the role of a spring-constant and $\chi_\perp^0$ that of a mass. Its saddle-point equations therefore describes propagating 'sound-waves', with a velocity $c_s^0 = \sqrt{\rho_s^0/\chi_\perp^0}$.

1.3.2 The classical non-linear sigma model

In the high-temperature limit, the QNLS must become equivalent to the CNLS. For $T \gg \rho_s^0$, the size of the integration domain along the time-direction, $L_\tau = \beta\hbar$, becomes very small. Since the partition function is dominated by configurations which vary slowly, we can expand in L_τ

$$\begin{aligned}
\vec{n}(L_\tau, \vec{x}) &= \vec{n}(0, \vec{x}) + L_\tau \frac{\partial \vec{n}}{\partial \tau} + \mathcal{O}(L_\tau^2) \\
&= \vec{n}(0, \vec{x}),
\end{aligned} \tag{1.3.4}$$

where the last equivalence is due to the periodic boundary conditions. Hence, the dominant configurations are τ-independent in the high-temperature limit. Eq. (1.3.1) then becomes

$$\mathcal{Z}_{\text{CNLS}} = \int D\vec{n} \prod_i \delta(\vec{n}_i^2 - 1) e^{-\beta \int d^dx \frac{1}{2}\rho_s^0 (\vec{\nabla}\vec{n}(x))^2}, \tag{1.3.5}$$

which is indeed the partition function for a classical continuum model.

1.3.3 Cross-over diagram

The number of parameters in the action can be reduced by one. Let us rescale the space and the time coordinates in the following way:

$$\vec{x} \rightarrow \Lambda \vec{x},$$
$$\tau \rightarrow x_0 = c_s^0 \Lambda \tau, \tag{1.3.6}$$

where $\Lambda \propto \frac{1}{a}$ is a cut-off in momentum space. All coordinates are now dimensionless. The QNLS action takes the Lorentz-invariant form

$$S = \frac{\hbar}{2g_0} \int_0^{\beta \hbar c_s^0 \Lambda} dx_0 \int d^d x \left[\sum_{\alpha=0}^{d} \left(\frac{\partial \vec{n}}{\partial x_\alpha} \right)^2 \right], \tag{1.3.7}$$

where $g_0 = \frac{\Lambda^{d-1}}{\sqrt{\chi_\perp^0 \rho^0}}$. The Lorentz-invariance of the model ensures that the dynamical critical exponent z is equal to one.

The dimensionless coupling constant g_0 tunes the amount of quantum-fluctuations in the system. In the large S limit, it is given by (Λ is taken to be $\frac{1}{a}$) [15]

$$g_0 = \frac{2\sqrt{d}}{S}. \tag{1.3.8}$$

The coupling constant vanishes in the classical $S \rightarrow \infty$ limit[4]. In the following, we focus on the case $d = 2$.

As a function of g_0 and temperature, the QNLS has three distinct regimes with qualitatively different behavior: the renormalized classical (RC), quantum disordered (QD) and quantum critical (QC) regime. These regimes are shown in the cross-over diagram figure 1-4. This diagram can be obtained from a momentum-shell renormalization analysis of the QNLS [12]. The details of this analysis are discussed in the appendix to chapter 2.

There is an intuitive argument for understanding the various regions in this diagram, [12] [16]. It is based on comparing the spatial length-scales in the problem with L_τ. Since it relies on the Lorentz-invariance of the system, it is only strictly valid close to the critical point.

First, let us consider the action eq.(1.3.7) at zero-temperature. The imaginary time integration extends to infinity. Since $z = 1$, $\mathcal{Z}$ is in this case just the partition function of a *classical* non-linear sigma model in $d + 1$ dimensions, at a dimensionless temperature g_0 (compare equations (1.3.5) and (1.3.7)). For the two-dimensional case, the zero-temperature problem is therefore equivalent to that of a classical Heisenberg antiferromagnet in three dimensions. This system undergoes a phase-transition to a Néel ordered state at a critical

---

[4]For $d \rightarrow \infty$, g_0 diverges, but its critical value (fig. 1-4) diverges faster, so this is also a classical limit.
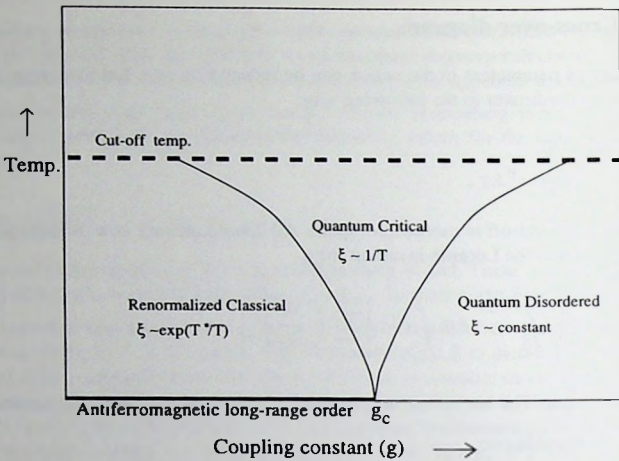
Figure 1-4. cross-over diagram of the d=2 quantum non-linear sigma model

temperature. The $T = 0$ quantum system therefore exhibits an order-disorder transition at some finite $g_0 = g_c$.

As the temperature is increased from zero, the problem becomes that of a classical Heisenberg system in 2+1 dimensions, where one of the dimensions is compactified to a circle with circumference L_τ. The system is no longer strictly three-dimensional and therefore cannot have true long-range order. In the region $g_0 < g_c$, the correlation length for Néel order becomes finite at non-zero temperatures. One finds an exponential scaling of the correlation length with L_τ: $\xi \propto \exp[2\pi\rho_s^0\beta]$. Since quantum fluctuations are small for these values of g_0, it is possible to integrate out the imaginary time-dependence on the Gaussian level and obtain an effective 2d CNLS with a renormalized stiffness [12]. This motivates the designation 'renormalized classical' for this region of the cross-over diagram.

In the disordered region $g_0 > g_c$, the $T = 0$ correlation length is much shorter than L_τ, so little will change as the temperature is increased from zero. Consequently, the correlation length only has a very weak dependence on temperature. This is the quantum disordered regime.

The cross-over from the quantum disordered to the quantum critical region occurs when the correlation length and L_τ become of the same order. The system enters a region where L_τ is the only relevant length-scale, since it is the shortest and acts as a cut-off. This leads to highly universal behavior. The correlation-length is given by $\xi \propto L_\tau \propto \frac{1}{T}$.

The cross-over from the renormalized classical to the quantum critical regime is found by comparing L_τ to the characteristic length in the ordered Néel state, the Josephson correla-

tion length $\xi_J = \frac{\hbar c_s}{\rho_s}$. This is the length-scale which separates long-wavelength Goldstone fluctuations from short-wavelength critical fluctuations.

The quantum critical region ends at a high-temperature cut-off, where the correlation length is of the order of one lattice spacing and a continuum-description breaks down. This occurs roughly at $k_B T = \rho_s^0$.

1.3.4 The quantum antiferromagnet at finite temperatures

A one-loop renormalization calculation yields the following results for the zero-temperature renormalized stiffness and susceptibility [12]

$$
\begin{aligned}
\rho_s &= \rho_s^0 \left(1 - \frac{g_0}{g_c}\right), \\
\chi_\perp &= \chi_\perp^0 \left(1 - \frac{g_0}{g_c}\right),
\end{aligned}
\tag{1.3.9}
$$

where $g_c = 4\pi$ is the critical value of g_0, where both the stiffness and the susceptibility vanish. The spin-wave velocity undergoes no renormalization, $c_s = c_s^0$. Note that ρ_s and $\chi_\perp$ are renormalized by the same factor. Comparing these results with those stated in table 1-1, it becomes clear that the $S \to \infty$ expressions for the bare parameters are not very accurate. Since the renormalized values of the parameters *are* know with some accuracy (from spin-wave theory and Monte Carlo simulations), it is possible to work backwards: determining the bare parameters from their renormalized values. CHN use the following expression

$$
\frac{g_0}{4\pi} = \frac{1}{1 + 4\pi \chi_\perp c_s / \Lambda},
\tag{1.3.10}
$$

which follows from eq. (1.3.9) and the definition of g_0. They take $\Lambda a = 2\sqrt{\pi}$, which ensures that the spherical Brillouin zone used for the QNLS has the same surface as the square Brillouin zone of the lattice antiferromagnet. With this choice of Λ, the spin-wave results for the renormalized stiffness and susceptibility yield $g_0/4\pi = 0.72$. Consequently, the $S = \frac{1}{2}$ antiferromagnet is still well within the ordered region.

With the bare parameters fixed, the QNLS can now be used to analyze the physics at non-zero temperatures. The model has been successfully applied to the case of La_2CuO_4 [12]. It also yields accurate fits to Quantum Monte Carlo simulations of the square lattice antiferromagnet [11]. The renormalized classical regime is clearly observed. Unfortunately, it is found that the $S = \frac{1}{2}$ system is still too well-ordered to exhibit quantum critical behavior. The lattice cut-off is reached before the cross-over to the QC regime can occur. This has motivated the search for microscopic systems in which the parameter g_0 can be tuned through its critical value. All systems discussed in the following chapters have this property, and this is a main underlying theme of this thesis.

1.4 Spin coherent state path integral

1.4.1 Spin coherent states

The quantum non-linear sigma model discussed in the previous section can be obtained in a semi-classical approach. In this section, the spin path-integral is formulated and the QNLS is extracted. The spin coherent state formalism provides a convenient framework in which to perform the semi-classical analysis.

The spin coherent state is given by [18] [13]

$$|\hat{n}\rangle = e^{i\theta(\cos\phi S^y - \sin\phi S^x)}|S, S\rangle, \tag{1.4.1}$$

where $\hat{n} = (\sin\theta\cos\phi, \sin\theta\sin\phi, \cos\theta)$ [5]. This state is constructed to reproduce the degrees of freedom of a classical spin. The reference state $|S, S\rangle$ is maximally classical in the sense that it minimizes the uncertainty in the Casimir operator:

$$\langle S, S|\vec{S}^2|S, S\rangle - \langle S, S|\vec{S}|S, S\rangle^2 = S(S+1) - S^2 = S. \tag{1.4.2}$$

To obtain the coherent state, the $SU(2)$ transformation $R(\hat{n}) = e^{i\theta(\cos\phi S^y - \sin\phi S^x)}$ is performed on the reference state. The property eq. (1.4.2) is conserved under R. The $SU(2)$ transformation is parametrized in such a way that states with a different $\hat{n}$ are physically distinct, i.e. they differ by more than a phase-factor. This implies

$$|\langle\hat{n}|\hat{n}'\rangle|^2 = 1 \Rightarrow \hat{n} = \hat{n}', \tag{1.4.3}$$

but *not* $\langle\hat{n}|\hat{n}'\rangle = 0$ for $\hat{n} \neq \hat{n}'$. The coherent states are non-orthogonal.

Taking the expectation-value of the spin-operator with respect to the coherent state, we obtain a classical spin (a vector) of size S

$$\langle\hat{n}|\hat{S}|\hat{n}\rangle = S\hat{n}. \tag{1.4.4}$$

As a result, the expectation-value of a quantum spin-Hamiltonian with respect to a product wavefunction of these states yields the corresponding classical Hamiltonian.

$$\left(\prod_i \langle\hat{n}|_i\right) J \sum_{<ij>} \vec{S}_i \cdot \vec{S}_j \left(\prod_i |\hat{n}\rangle_i\right) = J S^2 \sum_{<ij>} \hat{n}_i \cdot \hat{n}_j. \tag{1.4.5}$$

---

[5]This is a proper definition of the coherent state for all values of $\hat{n}$ except at the south-pole, where the ϕ-dependence should disappear. Taking $|S, -S\rangle$ as the reference state, this problem is shifted to the north-pole. It is possible to use the definition eq. (1.4.1) for the northern- and the alternative definition for the southern hemisphere, patching the two coherent states together at the equator. In the following, small deviations of $\hat{n}$ from a preferred direction are considered and this problem does not play a role.
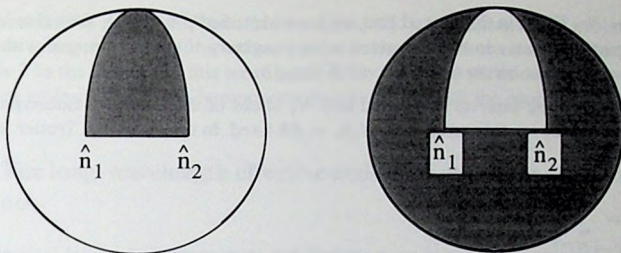
Figure 1-5. The spherical triangle spanned by $\hat{n}_1$, $\hat{n}_2$, and the north pole. Its area can be defined in two ways, shown left and right.

The spin coherent states form an overcomplete basis on the spin Hilbert space. It is possible to resolve the unity operator in terms of these states

$$1 = \frac{2S+1}{4\pi} \int d\hat{n} |\hat{n}\rangle\langle\hat{n}| . \tag{1.4.6}$$

In a multi-spin Hilbert space, the prefactor acquires a power N (the number of spins) and the integration runs over all configurations $\{\hat{n}\}$.

Due to the overcompleteness of the coherent state basis, the overlap between different coherent states is non-zero. It is given by

$$\langle\hat{n}_1|\hat{n}_2\rangle = \left(\frac{1 + \hat{n}_1 \cdot \hat{n}_2}{2}\right)^S e^{iS\Phi(\hat{n}_1,\hat{n}_2)} , \tag{1.4.7}$$

where $\Phi(\hat{n}_1, \hat{n}_2)$ is the area of the spherical triangle spanned by $\hat{n}_1$, $\hat{n}_2$ and the north pole (fig. 1-5). Note that the definition of this area is ambiguous, since 'inside' and 'outside' cannot be properly defined on a sphere. The two definitions of the area are related by $\Phi' = 4\pi - \Phi$, giving rise to a phase-difference $e^{i4\pi S}$ in the overlap between both possibilities. This should not have any observable consequences. This is indeed the case, since S is either integer or half-integer due to spin-quantization.

1.4.2   The coherent state path-integral

The partition function of quantum statistical mechanics is given by

$$\begin{aligned}
Z &= \text{Tr} e^{-\beta\mathcal{H}} \\
&= \text{Tr} e^{i\mathcal{H}t/\hbar} ,
\end{aligned} \tag{1.4.8}$$

where $\beta = (k_B T)^{-1}$. In the second line, we have identified $\beta \hbar = -it$. With this identification, the partition sum can be interpreted as an imaginary-time path-integral with periodic boundary conditions on the time interval of size $\beta \hbar$.

The imaginary time interval is divided into N_τ slices of thickness δ_τ. Subsequently, the limit $N_\tau \to \infty$, $\delta_\tau \to 0$ is taken with $N_\tau \delta_\tau = \beta \hbar$ fixed. In this limit, the Trotter formula is applied [13]

$$\mathcal{Z} = \lim_{\substack{N_\tau \to \infty \\ \delta_\tau \to 0}} \left(e^{-\delta_\tau \mathcal{H}} \right)^{N_\tau}. \tag{1.4.9}$$

The resolution of the identity eq. (1.4.6) is inserted between every two time-slices

$$\mathcal{Z} \propto \lim_{\substack{N_\tau \to \infty \\ \delta_\tau \to 0}} \left(\prod_{j=1}^{N_\tau} \int d\{\hat{n}_j\} \right) \left(\prod_{j=1}^{N_\tau} \langle \{\hat{n}_j\} | e^{-\delta_\tau \mathcal{H}} | \{\hat{n}_{j+1}\} \rangle \right). \tag{1.4.10}$$

The configurations satisfy $\hat{n}_0 = \hat{n}_{N_\tau}$ because of the periodic boundary conditions. Assuming that the configurations are smooth as a function of imaginary time, eq. (1.4.10) can be expanded in δ_τ. Using $\langle \{\hat{n}_j\} | \mathcal{H} | \{\hat{n}+j+1\} \rangle = \langle \{\hat{n}_j\} | \mathcal{H} | \{\hat{n}_j\} \rangle + \mathcal{O}(\delta_\tau)$, we obtain

$$\mathcal{Z} \propto \lim_{\substack{N_\tau \to \infty \\ \delta_\tau \to 0}} \left(\prod_{j=1}^{N_\tau} \int d\{\hat{n}_j\} \right) \prod_{j=1}^{N_\tau} \left(\langle \{\hat{n}_j\} | \{\hat{n}_{j+1}\} \rangle - \delta_\tau \langle \{\hat{n}_j\} | \mathcal{H} | \{\hat{n}_j\} \rangle \right). \tag{1.4.11}$$

The second term just yields the classical Heisenberg Hamiltonian eq. (1.4.5). The first term is the overlap between states on different time-slices, which follows from eq. (1.4.7). After expanding in δ_τ, it becomes

$$\langle \{\hat{n}_j\} | \{\hat{n}_{j+1}\} \rangle = 1 + iS \sum_{i=1}^{N} \delta_\tau \bar{\Phi}(\hat{n}_i(\tau_j)) + \mathcal{O}(\delta_t^2), \tag{1.4.12}$$

where $\delta_\tau \bar{\Phi}(\hat{n}_i(\tau_j))$ is the infinitesimal area $\Phi(\hat{n}_i(\tau_j), \hat{n}_i(\tau_{j+1}))$ on the unit sphere.

Exponentiating and taking the time-continuum limit, the path-integral is obtained

$$\mathcal{Z} = \int D\hat{n} e^{-S_E[\hat{n}]}, \tag{1.4.13}$$

with the Euclidean action

$$-S_E[\hat{n}] = \int_0^{\beta \hbar} d\tau \left[iS \sum_i \bar{\Phi}(\hat{n}_i(\tau)) - JS^2 \sum_{\langle ij \rangle} \hat{n}_i(\tau) \cdot \hat{n}_j(\tau) \right]. \tag{1.4.14}$$

The first term in the action is a Wess-Zumino term [13]. It is a phase-factor, which is given by the area traced out on the unit sphere by the circle-segment connecting $\hat{n}_i(\tau)$ and the north-pole [6] In the absence of this term, eq. (1.4.13) is just the partition sum of a classical Heisenberg system. The Wess-Zumino term therefore drives all the quantum effects.

1.4.3   The long-wavelength effective action for quantum antiferromagnets

On the classical level, antiferromagnets and ferromagnets in zero magnetic field are effectively the same. The Hamiltonian of the classical antiferromagnet can be transformed into that of a ferromagnet by staggering the spins. For Heisenberg spin-operators, the commutation relations are not invariant under $S^\alpha \rightarrow -S^\alpha$ and this transformation is not possible. Hence, the fact that these two types of magnetism have different properties is a pure quantum effect. In the path-integral formulation, this effect should have its origin in the Wess-Zumino term. This is indeed the case. Staggering the spins simply transforms $J \rightarrow -J$ in the potential part of the action, such that it becomes the potential energy of a ferromagnet. In the Wess-Zumino term, however, it induces a staggering. This is different from what the term looks like in the action of a ferromagnet, where it has the same sign on every site.

Below, we derive a long-wavelength action for quantum *anti*ferromagnets starting from the spin path-integral. For simplicity, we focus on the one-dimensional case, adding some remarks regarding higher dimensions. We use the method described in ref [17], which becomes particularly simple for the case of one dimension.

The derivation starts from the assumption that there is Néel ordering at least at distances of the order of a couple of lattice spacings. The spin-chain is divided into two-spin unit cells, labelled by the index x. In each unit cell, a Néel moment $\vec{m}_x$ and an average spin $\vec{l}_x$ is defined.

$$
\begin{aligned}
\vec{m} &= \frac{1}{2}\left(\hat{n}_1 - \hat{n}_2\right), \\
\vec{l} &= \frac{1}{2}\left(\hat{n}_1 + \hat{n}_2\right).
\end{aligned}
\tag{1.4.15}
$$

The assumption of local Néel order implies $l \ll 1$. Using the identity $\vec{m}^2 + \vec{l}^2 = 1$, the unit vectors $\hat{n}_1$ and $\hat{n}_2$ can be expressed in terms of the normalized Néel moment $\vec{m}$ and the

---

[6]In real time (i.e. not imaginary), the single spin path integral can be interpreted as that of a charged particle with vanishing mass $S\delta_\tau/2$, which moves on the surface of a sphere. At the centre of the sphere is a monopole with magnetic charge S. In this interpretation, S_{WZ} is the Aharanov-Bohm phase of the particle, which is related to the magnetic flux through the area enclosed by the particle's world-line. The ambiguity in the definition of this area, which was discussed earlier, then imposes the quantization condition on the magnetic charge S. The Dirac string of the monopole can be thought of as leaving the sphere at the south-pole. This causes a divergence of the monopole vector potential at the south-pole, which, in the spin-picture, is related to the fact that the coherent state is ill-defined at this point.

average spin.

$$\begin{aligned}
\hat{n}_1 &= \hat{m}\sqrt{1-l^2}+\vec{l}, \\
\hat{n}_2 &= -\hat{m}\sqrt{1-l^2}+\vec{l}.
\end{aligned} \tag{1.4.16}$$

Inserting this into the action and expanding to lowest relevant order in $\vec{l}$, we obtain, up to a constant

$$\begin{aligned}
-S_{\mathrm{E}} &= \int_0^{\beta\hbar} d\tau \sum_x \Big[2i S \vec{l}_x \cdot \partial_\tau \hat{m}_x \times \hat{m}_x \\
&\quad + J S^2 \Big(2\vec{l}_x \cdot (\hat{m}_{x+1} - \hat{m}_x) + \frac{1}{2}(\hat{m}_{x+1} - \hat{m}_x)^2 + 4\vec{l}_x^2 \Big) \Big].
\end{aligned} \tag{1.4.17}$$

In the continuum-limit, the differences $\hat{m}_{x+1} - \hat{m}_x$ can be replaced by gradients $2a\partial_x \hat{m}(x)$, where a is the lattice constant.

The fields $\vec{l}(x)$ are integrated out, yielding an effective action for the Néel moments. Since eq. (1.4.17) is Gaussian in $\vec{l}$, this can be done simply by solving $\vec{l}$ from the Euler-Lagrange equations. We find

$$\vec{l} = \frac{-i}{4JS}\partial_\tau \hat{m} \times \hat{m} - \frac{a}{2}\partial_x \hat{m}, \tag{1.4.18}$$

inserting this in eq. (1.4.17) yields

$$S_{\mathrm{Eff.}} = \int_0^{\beta\hbar} d\tau \int dx \left[i\frac{S}{2}\vec{m} \cdot \partial_\tau \hat{m} \times \partial_x \hat{m} + \frac{1}{2}\left(\chi_\perp (\partial_\tau \hat{m})^2 + \rho_s (\partial_x \hat{m})^2 \right) \right]. \tag{1.4.19}$$

The second term in eq. (1.4.19) is the quantum non-linear sigma model eq. (1.3.2). The bare stiffness and susceptibility are given by

$$\rho_s = JS^2 a \; ; \; \chi_\perp = \frac{1}{4Ja}. \tag{1.4.20}$$

The results for general dimensions were given in eq. (1.3.3).

As is discussed in the book of Fradkin [13], the first term in the action is related to the topology of the spin-configurations. In one dimension, it can be written as $2\pi S Q$, where the integer Q is a winding number . Such a winding number can be assigned to all smooth configurations $\{\hat{m}(x, \tau)\}$ with a finite action –which implies that $\hat{m}$ converges to a constant value at $|(x, \tau)| \to \infty$. Since configurations with an infinite action are exponentially suppressed, they need not be considered. The path-integral can therefore be written as a sum over the path-integrals for configurations with a particular winding-number, weighted by a phase-factor $e^{i2\pi QS} = (-1)^{2QS}$. For integer S, this phase-factor is always equal to 1 and the action reduces to the quantum non-linear sigma model. For half-integer S, however,

the phase-factor is 1 for even and -1 for odd winding-numbers and the QNLS-description breaks down.

From this property of the topological term, Haldane [15] conjectured that all integer-spin chains have short-range correlations and a gapped spectrum, while all half-integer spin chains are qualitatively similar to the $S = \frac{1}{2}$ chain and have a critical mode and quasi long-range spin correlations.

In dimensions higher than 1, the topological term seems not to play a role even for the case of half-integer spins. In a derivation of the effective action along the lines shown above for $d = 1$, this term is killed by local cancellations between different rows. This cancellation seems to hold also at large length scales, since the long-wavelength behavior of the two-dimensional $S = \frac{1}{2}$ quantum antiferromagnet can be successfully described using a QNLS without the topological term [12] [19].

This statement also holds for the case of even-leg spin-ladders, where the same cancellation occurs. From a QNLS perspective, it would therefore seem that even-leg spin-ladders and integer-spin chains are qualitatively similar, since they can both be described by a 1d QNLS. And indeed, both systems form incompressible spin-liquids, meaning that they have a gapped spectrum and no apparent long-range order.

Analytical and numerical calculations, however, show that the $S = 1$ chain and the two-leg $S = \frac{1}{2}$ ladder are in two different phases, separated by a critical point [20]. At this critical point, the spin-gap, which is present in both phases, closes. This phenomenon can be understood from the work of den Nijs and Rommelse [21], who performed an analysis of the spin-1 chain which did not rely on a mapping to a semi-classical continuum model. They showed that this system has 'hidden order'. This order is most easily visualized by going to a path-integral description of the spin-1 chain where the degree of freedom on every space-time point is the spin-component S^z, which can take the values 1, 0 or -1. The configuration on a single time-slice is then given by a sequence of these three numbers. In a system with perfect hidden order, removing all the zeroes in this sequence yields the antiferromagnetic configuration 1,-1,1,-1,.... It is possible to define a non-local order parameter for this phase. The order parameter is nonzero for the spin-1 chain, but zero for even-leg spin ladders, which implies that these two systems are qualitatively different, and should indeed be separated by a phase transition.

Nothing like hidden order appears in the continuum QNLS description, and it therefore does not capture all the physics of the integer-S spin chains. However, the QNLS does seem applicable to the even-leg spin ladders and to higher dimensional systems.

1.5 Stripes and superconductivity

The problems which are discussed in chapters 2 and 5 are related to the existence of stripe-order. This type of order is briefly introduced here and some of the properties of stripes are discussed.

$$\uparrow \downarrow \uparrow \circ \downarrow \uparrow \downarrow \circ \uparrow \downarrow \uparrow$$
$$\downarrow \uparrow \downarrow \circ \uparrow \downarrow \uparrow \circ \downarrow \uparrow \downarrow$$
$$\uparrow \downarrow \uparrow \circ \downarrow \uparrow \downarrow \circ \uparrow \downarrow \uparrow$$
$$\downarrow \uparrow \downarrow \circ \uparrow \downarrow \uparrow \circ \downarrow \uparrow \downarrow$$
$$\uparrow \downarrow \uparrow \circ \downarrow \uparrow \downarrow \circ \uparrow \downarrow \uparrow$$
$$\downarrow \uparrow \downarrow \circ \uparrow \downarrow \uparrow \circ \downarrow \uparrow \downarrow$$
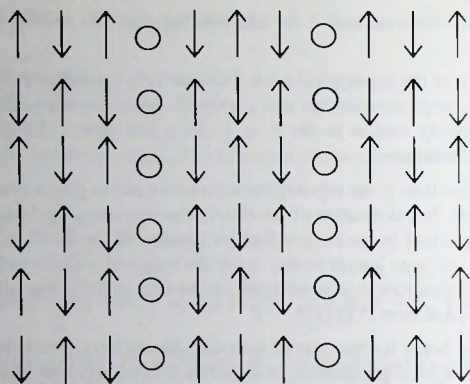
Figure 1-6. An ordered stripe state.

Stripes are structures which result from a collective ordering of holes and spins. They were first observed by Tranquada and coworkers, who performed neutron-scattering experiments on the spin-1 insulator $La_{2-x}Sr_xNiO_4$, a sister compound of the cuprate superconductors [22]. They found magnetic and charge peaks at incommensurate wave-vectors. This fits with a 'stripe' structure such as shown in fig. 1-6. The holes form lines which are anti-phase domain walls for the antiferromagnetic order of the spins. The spin-modulation has twice the period of the charge modulation, which gives the ratio 1:2 for the discommensuration vectors.

These structures had been predicted by Zaanen and Gunnarson in 1989 from a Hartree-Fock analysis of the Hubbard model [23]. Similiar calculations were performed by other groups [24]. The hole densities obtained from the Hartree-Fock analysis are more spread out than has been drawn in figure 1-6, but they are indeed centered on sites, and there indeed is a total density of one hole per site along the stripes. The stripe state in the nickelates is an insulator. These various features of the nickelate stripes can be understood quite well from the Hartree-Fock analysis.

To get a feeling for why such structures might form, consider the case of a single hole in a Néel ordered antiferromagnet (fig.1-7). If the hole moves away from its original position, it creates a string of ferromagnetic bonds, which costs exchange energy. The resulting string-potential confines the hole to the neighborhood of its original position. In a stripe-structure, the lines of holes can move without creating ferromagnetic bonds, because of the phase-change of the antiferromagnetic order across the stripes. This results in a lower kinetic energy for the stripes than for a system with uniformly distributed holes. In addition, there is the fact that a single hole breaks four antiferromagnetic bonds, while the holes in a stripe only break two each. This yields a lower potential energy for the stripe-state than for the
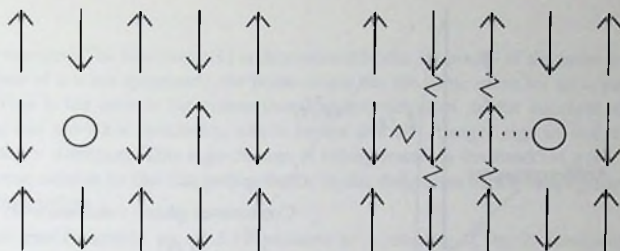
Figure 1-7. A moving hole in an antiferromagnetic background creates a string of broken bonds.

uniform configuration.

In the cuprate superconductors, neutron scattering measurements reveal dynamical stripe-correlations in the underdoped region. The stripes are stabilized at the commensuration point $x = \frac{1}{8}$, where the spacing between stripes is precisely four lattice constants. The cuprate stripes are different from those in the nickelates. They have a filling of half a hole per site and the behavior of the magnetic sector suggests that they are centered on the bonds rather than on the sites [41]. Recent elastic neutron scattering experiments show *static* stripe correlations at dopings close to $x = \frac{1}{8}$ (fig.1-8) [27], while muon-scattering experiments suggest that low-temperature static stripe order occurs throughout the super-conducting region for $x \leq \frac{1}{8}$ [7].

The cuprate stripes can be stabilized by inducing a buckling in the perovskite plane, which acts as a pinning potential. This is done by replacing La-atoms by Eu or Nd, which causes a transition from low-temperature orthogonal (LTO) to low-temperature tetragonal (LTT) order for the lattice. In the LTT phase, stripes are stable over a range of dopings. The LTT deformation can be varied by varying the Eu or Nd doping. Also stripes stabilized by this mechanism seem to coexist with superconductivity for $x \leq \frac{1}{8}$ [28]. The superconductivity has a low T_c, but is remarkably robust with respect to large magnetic fields. This suggests that one is not dealing with weak-link superconductivity, where there is a phase-separation between stripe-ordered regions and superconducting regions, but rather with true micro-scopic coexistence.

Quantum fluctuations play a more important role in the cuprates than in the nickelates and the cuprate stripes are not well described by the Hartree-Fock theory. Scalapino and White find stripes in density matrix renormalization group calculations of the t-J model which are closer to what is seen in the cuprates [25]. The DMRG-stripes are bond-centered and, near the doping $x = \frac{1}{8}$, half-filled. Furthermore, the holes are found to form short-range d-wave pairs at low densities before ordering into a stripe phase at higher densities, which may be related to the observation of coexisting stripe order and superconductivity.

The microscopic origin of the stripe phase is not addressed in this thesis. However, much insight can be gained by a Ginzburg-Landau analysis, which relies on an expansion of the
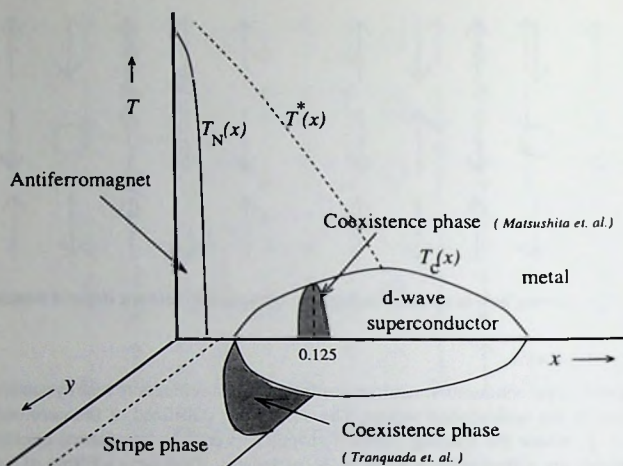
Figure 1-8. Proposed topology of the phase diagram for $La_{2-x-y}Sr_xEu_yCuO_4$ [67]. In the shaded areas, elastic neutron scattering experiments have revealed stripe-order in a superconducting sample. Muon scattering experiments suggest that there is coexistence at low temperatures in the entire superconducting region for $x \leq 0.15$

free energy in terms of the charge- and the spin order parameter of the stripe phase. Such an expansion is valid close to the onset temperature for stripe-order, where these order parameters are small. Zachar, Emery and Kivelson have performed a mean field analysis of this type , in which gradients of the order-parameter fields are not included. Their results are discussed in the first section of chapter 2.

To describe the stripes in the cuprates, the order-parameter for superconductivity has to be included in the Ginzburg-Landau analysis. This order-parameter is related to a spontaneous breaking of the symmetry under global phase-transformations $(U(1))$

$$
\begin{aligned}
c_{i\sigma}^\dagger &\rightarrow e^{i\phi}c_{i\sigma}^\dagger \\
c_{i\sigma} &\rightarrow e^{-i\phi}c_{i\sigma}
\end{aligned} \Rightarrow \mathcal{H} \rightarrow \mathcal{H} . \tag{1.5.1}
$$

The above symmetry implies that every term in the Hamiltonian has the same number of creation and annihilation operators. It is therefore related to the conservation of particles. In the superconducting state, the phase ϕ orders in a preferred global direction, and particle number is no longer conserved. The order-parameter

$$
\Delta^* = \frac{1}{N} \sum_k g(k) \langle c_{k\uparrow}^\dagger c_{-k\downarrow}^\dagger \rangle = |\Delta|e^{i\phi} \tag{1.5.2}
$$

becomes nonzero. The function $g(k)$ is determined by the symmetry of the order-parameter. For the case of s-wave symmetry, the phase-angle has the same value for all k-vectors and $g(k)=1$. This is the case in the conventional superconductors. In the cuprates, the order-parameter has a d-wave symmetry, which means that $e^{i\phi}$ changes sign as one turns from the x to the y direction. This sign-change is incorporated in the function $g(k)$, which is in that sense similar to the staggering-factor in the definition of the order-parameter for antiferromagnetism.

The phase-transformation eq. (1.5.1) amounts to a rotation of the 2-component vector $(\text{Re}(\Delta), \text{Im}(\Delta))$. The transition to the superconducting phase therefore belongs to the universality class of the XY-model. The broken $U(1)$ rotational symmetry gives rise to acoustic Goldstone modes, which carry current. It is these excitations with a vanishing energy at long wavelengths which cause the phenomena of superconductivity.

The proposed zero-temperature phase-diagram as a function of x and y, which is shown in figure 1-8, is based on an extension of the mean field Landau theory for stripe formation with a coupling to the order parameter of superconductivity [67]. The order-parameter expansion is in this case used to analyse zero temperature phase transitions. Since the zero-temperature quantum system corresponds to a classical system in a higher dimension, the mean-field theory becomes more reliable in this case.

A direct transition from an antiferromagnet, like the stripe state, to a superconductor is always first order, although the individual disordering transitions of antiferromagnetism and superconductivity are both second order. Neglecting for the moment the charge-ordering transition, it is easily seen that, if the spin and the phase sector are somehow decoupled, one has two second order transitions instead of one first order one, and an intermediary phase occurs which is either spin- and phase-disordered or a superconducting antiferromagnet. Including the charge order-parameter, the following scenarios are found for the case of a smooth transition from the paramagnetic superconductor to the stripe-antiferromagnet

paramagnetic superconductor	$\rightarrow$	superconducting stripe-paramagnet
	$\rightarrow$	superconducting stripe-antiferromagnet
	$\rightarrow$	stripe-antiferromagnet ,
paramagnetic superconductor	$\rightarrow$	superconducting stripe-paramagnet
	$\rightarrow$	stripe-paramagnet
	$\rightarrow$	stripe-antiferromagnet ,
paramagnetic superconductor	$\rightarrow$	superconducting stripe-antiferromagnet
	$\rightarrow$	stripe-antiferromagnet .

The parameter which is varied to tune the system through these transitions need not be the Eu doping, which induces LTT deformation. One could for instance also think of magnetic fields, or Zn doping, which disorder the superconductivity.

The first and the second scenario are of the kind discussed above, where the charge-ordering now gives rise to an additional intermediary phase. In the last scenario, the spin-spin coupling drives the formation of an antiferromagnetic anti-phase domain structure, while the charge-ordering on the domain walls follows parasitically. Spin- and charge ordering occur simultaneously, at a second order transition. This is the scenario which is shown in figure 1-8.

In general, a number of scenarios involving first order transitions are also possible, but especially the observation of quantum critical behavior in the magnetic sector of the underdoped superconductors [66] suggests that one has a smooth transition in the cuprates. This is discussed in more detail in the introduction of chapter 5.

A smooth transition gives rise to the possibility of a coexistence phase of antiferromagnetic stripe order and superconductivity (shaded areas in fig. 1-8). The coexistence of charge-order and superconductivity, of which the superconducting stripe paramagnet is an example, has been investigated in microscopic models by a number of authors [51]. A microscopic picture of the coexistence of antiferromagnetism and superconductivity has however not been available. In chapter 5, a t-J-like model is investigated which demonstrates the possibility of such a coexistence phase.

1.6   The SO(5) approach to high T_c superconductivity

The global $SO(3)$ invariance under spin-rotations and the $U(1)$-invariance under phase transformations play an important role in the physics of cuprate superconductors. Transversal spin fluctuations are for instance a crucial ingredient in the physics of the stripe phase (see chapter 2) and it has been argued that phase-fluctuations are responsible for the unconventional behavior in the pseudo-gap region [26]. For the model considered in chapter 5, it is found that these two symmetries can be viewed as deriving from a larger, $SO(5)$, symmetry. The $SO(5)$-symmetric point can be reached by fine-tuning the parameters entering the model. The idea to describe the physics of superconductivity and antiferromagnetism in terms of a 'unifying' $SO(5)$-symmetry was proposed by Zhang in 1997 [29]. Below, the nature of this symmetry is explained, as an introduction to the work presented in chapter 5. Some of the reasons for considering a description of the cuprates in terms of a long-wavelength action with a weakly broken $SO(5)$-symmetry, as proposed by Zhang, are discussed.

$SO(5)$ is the smallest group containing a $U(1)$ and $SO(3)$ subgroup which allows for the introduction of a 5-component order-parameter consisting of the 2-component order-parameter of superconductivity and the 3-component order-parameter of antiferromagnetism (fig. 1-9). This"superspin" is given by

$$\vec{N} = \left(\Delta^\dagger + \Delta, \, \bar{S}^x, \, \bar{S}^y, \, \bar{S}^z, \, -i(\Delta^\dagger - \Delta) \right) , \tag{1.6.1}$$
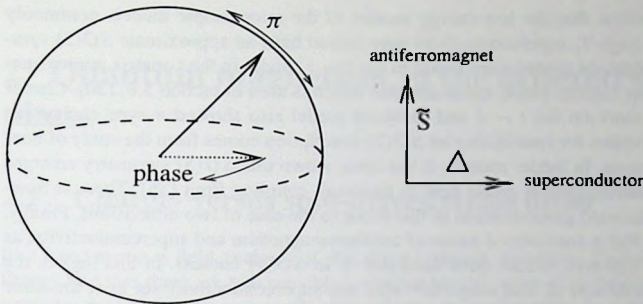
Figure 1-9. The $SO(5)$ superspin.

where

$$\Delta^\dagger = \sum_k g(k) c_{k\uparrow}^\dagger c_{-k\downarrow}^\dagger ,$$

$$\bar{S}^\alpha = \sum_k (c_{k+Q\uparrow}^\dagger, c_{k+Q\downarrow}^\dagger) \sigma^\alpha \begin{pmatrix} c_{k\uparrow} \\ c_{k\downarrow} \end{pmatrix} . \tag{1.6.2}$$

The function $g(k)$ describes a d-wave phasing of the Cooper-pairs. $\vec{Q} = (\pi, \pi, \pi)$ is the antiferromagnetic ordering vector and σ^α is a Pauli matrix.

The phase- and spin-rotations act on components 1 and 5 and 2 through 4 respectively. The rotations between the two superconductivity-components and the three antiferromagnetism-components are generated by the 6 π-operators, which are given by

$$\pi_\alpha^\dagger = \sum_k g(k)(c_{k+Q\uparrow}^\dagger, c_{k+Q\downarrow}^\dagger) \sigma^\alpha \sigma^y \begin{pmatrix} c_{-k\uparrow} \\ c_{-k\downarrow} \end{pmatrix} . \tag{1.6.3}$$

The π-operators are spin-1, charge 2 operators: they create and annihilate triplet electron-pairs.

In an $SO(5)$ symmetric model, a spontaneous breaking of the symmetry results in four Goldstone modes. If the superspin is pointing in the superconductivity-direction, these are one phase-mode and three π-modes; the AF phase has two spin-modes and two π-modes , while a mixed AF/SC phase yields one phase-mode, two spin modes and one π-mode. The π-modes are additional Goldstone modes which arise because of the higher symmetry that has been assumed. If the symmetry is weakly broken, they become quasi-Goldstone modes, with a small gap.

There are indications that the low-energy sectors of the microscopic models commonly used to describe high-T_c superconductivity may indeed have an approximate $SO(5)$ symmetry. Quasi Goldstone modes were found in the $t - J$ model in the t-matrix approximation (similar to the random phase approximation which is used in section 5.6) [30]. Cluster diagonalization work on the $t - J$ and Hubbard model also showed π-type excitations [31]. Other motivation for considering an $SO(5)$ description comes from the study of one-dimensional systems. In ladder models, it has been shown that $SO(5)$ symmetry emerges as a result of renormalization group flow in the weak coupling limit [36]. There is however no straightforward generalization of this result to the case of two dimensions. Finally, there is the fact that a coexistence phase of antiferromagnetism and superconductivity, as observed in the cuprates, occurs quite naturally in an $SO(5)$ context. In this regard, the finding of Matsushita *et al.* that magnetic-order and superconductivity set in at the same temperature for the $La_{2-x}Sr_xCuO_4$ sample with optimal magnetic order (fig. 1-8) is particularly striking.

The conjecture of an approximate $SO(5)$ symmetry has been used to derive a number of new results. It has for instance been predicted that the cores of the non-superconducting vortices which occur in a type-II superconductor in a magnetic field should be antiferromagnetic [32]. An '$SO(5)$ proximity effect' is predicted at the interface of an antiferromagnet and a superconductor [33]. In the ladder models, the occurrence of electron-like quasi-particles with non-Abelian exclusion statistics has been derived [34]. And recently, a mechanism for superconductivity has been proposed based on the energy-gain due to the π-fluctuations in the superconducting phase [35]. These various results remain to be tested.

2 Quantum magnetism in the ordered stripe phase

2.1 Charge- versus spin-driven stripe order

In a Landau mean field analysis of the stripe-ordering transition, Zachar, Kivelson and Emery find that there are two possible scenarios for the onset of stripe order [37]. In one scenario, the holes order as a result of the charge-charge coupling in a second order transition. The spins follow at a lower temperature and their transition is also second order. In the other scenario, the stripe-formation is driven by the coupling between charge and spin, and both order simultaneously in a first order transition. The two scenarios are called charge-driven and spin-driven.

Zachar *et al.* identify the spin-driven stripes with those which are found in Hartree-Fock calculations [23], while the charge-driven transition is identified with the mechanism of frustrated phase-separation, which was proposed by Emery and Kivelson [38].

As was discussed in section 1.5, holes have a disordering influence on the antiferromagnetic spin-order. If the exchange interaction of the spins is large enough with respect to the kinetic energy of the holes, this can lead to phase-separation, where, in the extreme case, all holes crowd together on one side of the sample and are in that way removed from the spin-system. This tendency to phase-separate is counteracted by the long-range Coulomb repulsion between charges, which favors a uniform state. In the frustrated phase-separation scenario, the stripes arise as a compromise between these two tendencies.

Both in the cuprates [22] and in the nickelates [39] the holes order at a higher temperature than the spins and both transitions are second order, in agreement with the charge-driven scenario. Zachar *et al.* therefore conclude that the stripes which are found in these systems are formed by frustrated phase separation.

Fluctuations have not been included in this mean field analysis. The important question is then whether they can change the above conclusion. In the following, it is argued that they do.

To appreciate this, it is important to make a distinction between the longitudinal and the transversal component of the spin order parameter. In order for the spin-driven stripe transition to occur, it is enough that the longitudinal component orders, since this is the one which couples to the charge in the Landau analysis. One therefore has $\frac{1}{N} \sum_i |\langle \vec{S}_i \rangle| \neq 0$ below this transition, but the average staggered magnetization $\frac{1}{N} \sum_i \eta_i \langle \vec{S}_i \rangle$ can still vanish because of the transversal fluctuations (η_i is a staggering-factor which takes into account the presence of the stripes). The transversal component then orders at a lower-temperature, in a second order transition.

If the charge order-parameter is commensurate with the underlying lattice, or pinned by quenched disorder, the Goldstone mode related to the spontaneous breaking of translational symmetry in the charge-ordering transition acquires a gap. The charge-fluctuations are in that case governed by a discrete symmetry. On the other hand, the spin order-parameter remains a three-component vector as long as spin-anisotropies can be neglected. Fluctuations will therefore affect the spins more strongly than the charges. In fact, if we assume that the system is completely two-dimensional (no spin-spin coupling between CuO_2-layers) and $SO(3)$ symmetric (no spin-anisotropies), then the spin-ordering transition should be suppressed all the way to zero temperature, since a continuous symmetry cannot be spontaneously broken at finite temperatures in two dimensions (Mermin-Wagner theorem). The charge-ordering breaks a discrete symmetry and *can* occur at finite temperatures. Clearly, fluctuations pull apart the two transitions in this case.

In the realistic case, the influence of weak three-dimensionality and spin-anisotropies has to be considered. Their influence can be estimated by comparing to the half-filled system. The hole-ordering transition occurs well below the temperature where antiferromagnetic order sets in at half-filling ($\sim$ 100 K versus 300 K). If the ordered holes have only a weak disordering influence, the spin-system below the charge-ordering temperature should be nearly equivalent to that at half-filling. Spin and charge would then still order simultaneously, even after the spin-fluctuations have done their work.

The zero-temperature staggered magnetization of the stripe antiferromagnet is roughly a factor two smaller than that for the antiferromagnet at half-filling. However, the magnetic ordering temperature is about a factor *ten* lower than at half-filling. In order for these observations to be explained in a spin-driven scenario, it is necessary for the disordering influence of stripes to be much more effective at finite temperatures than at $T = 0$.

In the following, this is investigated for the case of a specific, simple source of stripe-induced spin-disorder: the weakening of the antiferromagnetic spin-spin interactions across the stripes. It is found that the Néel temperature is indeed suppressed much stronger by this disorder than the zero-temperature magnetization. The reason for this is that the zero-temperature spin-system has an effective dimensionality of 3, while the finite temperature spin-system in the renormalized classical region is 2 dimensional. Any disordering influence is more effective in lower dimensions, explaining the different behavior of the two quantities.

2.2　Spin-only model for the static stripe phase

Castro-Neto and Hone (CH) proposed a simple spin-only model for the static stripe phase [40]. It assumes that the holes have completely frozen out in a static, regular stripe structure (fig. 2-1). The situation is then very similar to that of the Hubbard model at half-filling. The low-energy degrees of freedom of the system are the transversal fluctuations of the antiferromagnetic order parameter in the spin-domains. Virtual excitations across the stripe-deformation gap, i.e. spins hopping onto the holes and back, generate an effective
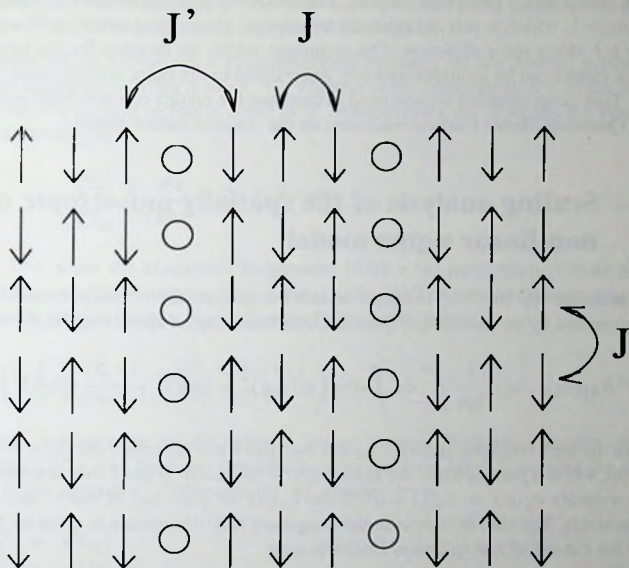
Figure 2-1. The charge-frozen stripe phase

antiferromagnetic interaction between the spins on different sides of the stripe. This interaction J' causes the antiphase-domain spin structure seen in fig. 2-1, which is one of the distinguishing features of the stripe phase. The reduction of J' with respect to J is the only way in which the charges affect the spin-sector in this model.

The weakness of the exchange interaction across the stripes has a disordering influence on the antiferromagnetism. This is immediately clear by considering the limiting cases. For $J' = J$, the spin-system is equivalent to that at half-filling and it should exhibit $T = 0$ long-range order. For $J' = 0$, it is effectively one-dimensional and long-range order cannot occur (Mermin-Wagner). The parameter $\alpha = J'/J$ tunes the spin-system between these two limits.

The low-energy physics of the frozen stripe phase is described by a coupled Heisenberg-ladder Hamiltonian

$$\mathcal{H} = J \sum_{\vec{i}} \vec{S}_{\vec{i}} \vec{S}_{\vec{i}+\delta_y} + J \sum_{i_x \neq pn_l, i_y} \vec{S}_{\vec{i}} \vec{S}_{\vec{i}+\delta_x} + \alpha J \sum_{i_x = pn_l, i_y} \vec{S}_{\vec{i}} \vec{S}_{\vec{i}+\delta_x}, \tag{2.2.1}$$

where $\vec{i} = (i_x, i_y)$ runs over a square lattice, $\vec{\delta}_x = (1, 0), \vec{\delta}_y = (0, 1)$. n_l measures the width

of the ladder and p counts the ladders. The following analysis focuses for simplicity on the case $n_l = 1$, which is just the spatially anisotropic Heisenberg model, with a reduced coupling αJ along the x-direction. The technique which we develop for the renormalization of this model can be straightforwardly generalized to the more realistic case of eq. (2.2.1) [41]. This generalization will be used to compare the results of a one-loop scaling analysis with Quantum Monte Carlo simulations on the coupled-ladder model.

2.3 Scaling analysis of the spatially anisotropic quantum non-linear sigma model

It is assumed that the Néel order parameter fluctuations in the charge ordered stripe phase are governed by an anisotropic quantum non-linear sigma model (AQNLS) [40][43],

$$S_{AQNLS} = \frac{1}{2g_0} \int_0^u d\tau \int d^2x \left(\alpha \left(\partial_x \hat{n} \right)^2 + \left(\partial_y \hat{n} \right)^2 + \frac{2}{1+\alpha} \left(\partial_\tau \hat{n} \right)^2 \right) , \quad (2.3.1)$$

where the bare coupling constant g_0 and the spin-wave velocity c are those of the isotropic system, while α parametrizes the anisotropy. In the classical limit, this describes spin waves with velocity $c_y(\alpha) = c\sqrt{(1+\alpha)/2}$ and $c_x(\alpha) = \sqrt{\alpha}c_y(\alpha)$ in the y- and x directions, respectively. The slab thickness in the imaginary time direction u is given by $\beta\hbar c\Lambda$, where Λ is the cut-off of our spherical Brillouin zone.

This model is derived by taking the naive continuum limit of a spatially anisotropic Heisenberg model. It was noted earlier that such a procedure does not actually give a very reliable result for the bare quantities. However, one can hope that the α-dependence obtained in this way is correct and that the inaccuracies only affect the bare value of g, which is taken as a phenomenological parameter in the model.

A momentum-shell renormalization group calculation of this model is performed. The details of such an analysis can be found in the appendix, section 2.6, where the case of the isotropic QNLS is reviewed.

The renormalization of the AQNLS has received some attention recently [40, 44]. We adopt here a variation on the procedure as proposed by Affleck[44]. The central observation is that this model contains two ultraviolet cut-offs. As a ramification of the anisotropy, the highest momentum states in the x-direction will have an energy E_x^{max} which is a factor $\sqrt{\alpha}$ smaller than that of the highest momentum states in the y direction. Therefore, the initial renormalization flow from E_y^{max} down to E_x^{max} is governed by one dimensional fluctuations. At E_x^{max} the resulting model can be rescaled to become isotropic, albeit with 'bare' parameters which are dressed up by the one dimensional high energy fluctuations.

Keeping the full model eq. (2.3.1), the one dimensional fluctuations are integrated out by neglecting the dispersions in the x direction entirely. This causes the anisotropy parameter α to become a running variable as well, which is always relevant. When the renormalized

$\alpha = 1$, the model has become isotropic. The main reason for using this procedure is that it simplifies greatly the finite-temperature analysis of the AQNLS.

The calculations which follow are a straightforward variation on the general procedure outlined in the appendix. Writing $\hat{n} = (\vec{\pi}, \sigma)$, where σ is the component of $\hat{n}$ in the direction of ordering, we expand to fourth order in $\vec{\pi}$. Subsequently, the $\vec{\pi}$-fields are Fourier-transformed according to

$$\vec{\pi}(\vec{x}, \tau) = \sum_{n=-\infty}^{\infty} \int \frac{d^2k}{(2\pi)^2} \vec{\pi}(\vec{k}, n) e^{i\vec{k}\cdot\vec{x} - i\omega_n \tau}, \tag{2.3.2}$$

where $\omega_n = 2\pi n/u$ are the Matsubara frequencies (with u the integration-domain along the time-direction, eq.(2.3.1), whose bare value is $\beta\hbar c\Lambda$). The momenta k are rescaled with Λ to become dimensionless. Separating the fields according to

$$\vec{\pi}(\vec{k}, n) = \begin{cases} \vec{\pi}_>(\vec{k}, n) & ; \quad e^{-l} < |k_y| < 1 \\ \vec{\pi}_<(\vec{k}, n) & ; \quad 0 < |k_y| < e^{-l} \end{cases}, \tag{2.3.3}$$

where l is small, we integrate out the fields $\pi_>$, using a square Brillouin zone for convenience (see figure 2-2). The fields are integrated out to one-loop level, following the same procedure as in the appendix [1]. Subsequently, we rescale

$$\begin{aligned} k_y' &= e^l k_y, \\ \pi'(\vec{k}, n) &= \zeta^{-1}\pi_<(\vec{k}, n), \end{aligned} \tag{2.3.4}$$

which yields

$$\begin{aligned} S'^{(2)} &= \frac{u_0}{2g_0} \sum_n \int \frac{dk_x dk_y'}{(2\pi)^2} e^{-l} \left(\alpha_0 k_x^2 + e^{-2l} k_y'^2 + \frac{2}{1+\alpha_0} \frac{4\pi n^2}{u^2} \right) \times \\ &\quad \times \left(1 + \frac{g_0}{u_0} I \right) \zeta^2 \left| \vec{\pi}'_{n,k} \right|^2 \\ &= \frac{u'}{2g'} \sum_n \int \frac{dk_x dk_y'}{(2\pi)^2} \left(\alpha' k_x^2 + k_y^2 + \frac{2}{1+\alpha'} \frac{4\pi^2 n^2}{u'^2} \right) \left| \vec{\pi}'_{n,k} \right|^2, \end{aligned} \tag{2.3.5}$$

where I is the one-loop contribution

$$I = u_0 l R(\alpha_0, u_0), \tag{2.3.6}$$

---

[1] Since we expanded to fourth order, we can only calculate the renormalization of the quadratic term in the action. As is pointed out in the appendix, this is sufficient, because there exists a Ward-Takahashi identity which limits the number of scaling parameters in the model. This identity ensures that the higher-order terms renormalize in the same way as the quadratic one. Since it relies on the invariance of the model under global rotations of the prefered direction in *spin*-space, it is not affected by the anisotropy of the action in *coordinate*-space and can still be applied.
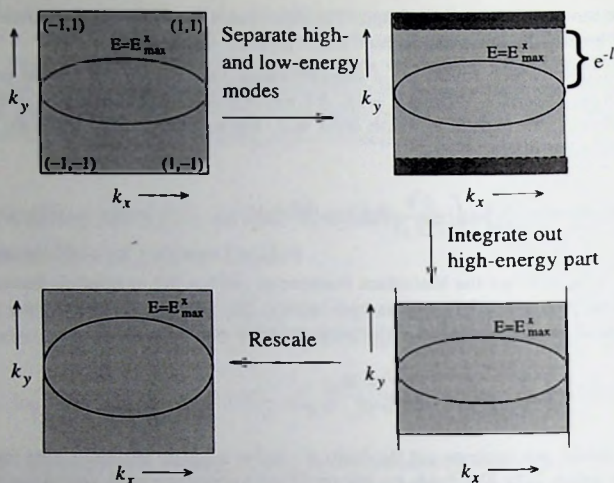
Figure 2-2. The procedure used here for integrating out the predominantly one-dimensional high-energy fluctuations in the square Brillouin zone. Note that the equipotential contour $E = E_{max}^x$ becomes more circular after the rescaling, which demonstrates that the effective action for the low-energy modes has a smaller spatial anisotropy than the original action. The procedure is iterated until the anisotropy vanishes. We then switch to a spherical Brillouin zone to perform the renormalization of the effective isotropic model.

with

$$R(\alpha_0, u_0) = \sqrt{\frac{1 + \alpha_0}{2}} \int_{-1}^{1} \frac{dk_x}{(2\pi)^2} \frac{\coth\left(\frac{u_0}{2} \sqrt{\frac{1 + \alpha_0}{2}} \sqrt{\alpha_0 k_x^2 + 1}\right)}{\sqrt{\alpha_0 k_x^2 + 1}} . \tag{2.3.7}$$

The last line in eq.(2.3.5) defines the renormalized parameters u', g' and α', which are given by

$$\alpha' = \alpha_0 e^{2l} , \tag{2.3.8}$$

$$u' = u_0 \sqrt{\frac{1 + \alpha_0}{1 + \alpha'}} e^{-l} , \tag{2.3.9}$$

$$\frac{u'}{g'} = \frac{u_0}{g_0} e^{-3l} \zeta^2 \left(1 + \frac{g_0}{u_0} I\right) . \tag{2.3.10}$$

Note that, contrary to the isotropic case, eq. (2.6.11), the spacing in the frequency direction

($\sim 1/u'$) now scales differently from the k_y-momentum (eq.(2.3.4)). This is due to the α-dependence of the spin-wave velocity in the y-direction.

The field-rescaling factor ζ is obtained by the procedure described in the appendix. It reads

$$\zeta = e^l \left[1 - \frac{g_0}{u_0} l \right]. \tag{2.3.11}$$

Iterating these results, the following flow-equations are obtained:

$$\alpha = \alpha_0 e^{2l}, \tag{2.3.12}$$

$$\frac{\partial g}{\partial l} = -\frac{\alpha g}{1 + \alpha} + g^2 R(\alpha, u), \tag{2.3.13}$$

$$\frac{\partial t}{\partial l} = t + t g R(\alpha, u), \tag{2.3.14}$$

where t is the dimensionless temperature, whose bare value reads $t_0 = k_B T / \rho_s^0$. The equation (2.3.9) for u after one renormalization step also holds for its value after a number of iterations. The same is the case for α (compare eq.(2.3.8) and eq.(2.3.12)). We find that α is a relevant variable, which implies that the anisotropy indeed scales away as the high-energy states are integrated out.

From eq. (2.3.12) it follows that $\alpha = 1$ corresponds with $l = l_1 = -\ln \sqrt{\alpha_0}$. At $T = 0$, the bare coupling constant of the effective isotropic model can be obtained by integrating eq. (2.3.13) up to $l = l_1$. This is most easily done by substituting $g = \bar{g} f$ and imposing that $\bar{g} \frac{\partial f}{\partial l}$ cancels the linear-order term. Eq. (2.3.13) then reduces to the set of equations

$$\frac{1}{f} \frac{\partial f}{\partial l} = -\frac{\alpha}{1 + \alpha}, \tag{2.3.15}$$

$$\frac{1}{\bar{g}^2} \frac{\partial \bar{g}}{\partial l} = f \sqrt{\frac{1 + \alpha}{2\alpha}} \frac{\text{arsinh}\sqrt{\alpha}}{2\pi^2}. \tag{2.3.16}$$

Eq. (2.3.15) is solved by $f(l) = (1 + \alpha)^{-1/2}$. Inserting this into eq. (2.3.16) we obtain for $g_1 = g(l_1)$

$$g_1 = g_0 / \left[\sqrt{\frac{2}{1 + \alpha_0}} - \frac{g_0}{2\pi^2} \left(\text{arsinh}(\sqrt{\alpha_0}) / \sqrt{\alpha_0} + \right.\right.$$
$$\left.\left. \ln(1 + \sqrt{1 + \alpha_0}) - \ln(\sqrt{\alpha_0}(1 + \sqrt{2})^2) \right) \right]. \tag{2.3.17}$$

This zero-temperature result can be used as long as $g_1 / t_1 \gg 1$. The bare dimensionless temperature of the effective isotropic model then follows from the equation for u (2.6.11)

$$g_1 / t_1 = (g_0 / t_0) \sqrt{\alpha_0 (1 + \alpha_0)/2} \tag{2.3.18}$$

Except for these altered bare quantities, the isotropic model is analyzed in the standard way [12], which is reviewed in the appendix.

Putting $g_1 = g_c = 4\pi$ and solving g_0, we find the critical bare coupling for the anisotropic model

$$g_c(\alpha_0) = 4\pi \sqrt{\frac{2}{1+\alpha_0}} / \left[1 + \frac{2}{\pi} \left(\mathrm{arsinh}(\sqrt{\alpha_0})/\sqrt{\alpha_0} + \ln(1 + \sqrt{1+\alpha_0}) - \ln(\sqrt{\alpha_0}(1 + \sqrt{2})^2) \right) \right]. \tag{2.3.19}$$

This result is the same within a couple of percents as the outcome of a direct one-loop renormalization group analysis of the anisotropic action eq.(2.3.1) [40]. The difference originates in an inaccuracy in our calculation. After using a square Brillouin zone to integrate out the high-energy 1-dimensional fluctuations, we switch to a spherical Brillouin zone for the analysis of the effective isotropic model. In the process, some states are thrown away, which introduces the small inaccuracy. The reason that we use here an approximate mapping to an effective isotropic model instead of doing a direct analysis of the AQNLS, is that it allows us to straightforwardly obtain the finite-temperature cross-over lines of the AQNLS, which are difficult to obtain otherwise.

For $\alpha_0 = 1$, the one-loop cross-over lines between the quantum-critical (QC) and the RC/QD regime are given by $t = \pm 2\pi(1 - g/4\pi)$. Taking (g_1, t_1) to lie on these lines and iterating the flow equations (2.3.13) and (2.3.14) backwards, we obtain the cross-over diagram for the anisotropic model, shown in fig. 2-3. Note that the anisotropy has a stronger effect on the t-dependence of the RC to QC line than on its g-dependence. This already indicates that the $T = 0$ properties will be less affected by the anisotropy than those at finite temperatures.

The one-loop mapping to an isotropic QNLS provides a simple way of calculating the correlation length in the anisotropic model. Noting that the correlation length in the y-direction scales as $\xi = \xi_0 e^{-l}$ under eq. (2.3.3), it immediately follows that $\xi^y(g_0, t_0) = e^{l_1} \xi_{\text{isotr.}}(g_1, t_1) = \alpha^{-\frac{1}{2}} \xi_{\text{isotr.}}(g_1, t_1)$ (while the correlation-length in the x-direction is simply $\xi_{\text{isotr.}}(g_1, t_1)$, so $\xi^x = \sqrt{\alpha}\xi^y$). We insert the 1-loop expression for $\xi_{\text{isotr.}}$ in the RC regime [12] and use equations (2.3.17) and (2.3.18) (the use of the $T = 0$ expression for g_1, eq.(2.3.17), is a good approximation if $g_1/t_1 \gg 1$). This yields

$$\xi^y(g_0, t_0) = \frac{0.9}{\sqrt{\alpha_0}} \frac{g_1}{2t_1} \exp\left[\left(1 - \frac{g_1}{4\pi} \right)/t_1 \right]$$
$$\simeq 0.9 \frac{g_0}{2t_0} \sqrt{\frac{1+\alpha_0}{2}} \exp\left[\sqrt{\alpha_0}\rho_s(0)/k_B T \right], \tag{2.3.20}$$

where the renormalized $T = 0$ stiffness is given by,

$$\rho_s(0) = \rho_s^0 \left(1 - \frac{g_0}{g_c(\alpha_0)} \right). \tag{2.3.21}$$
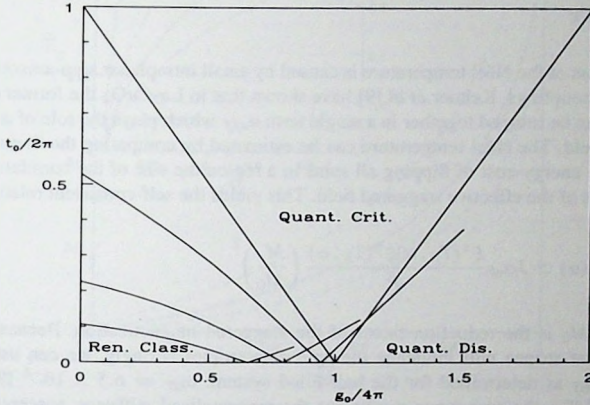
Figure 2-3. Cross-over diagram for the anisotropic QNLS. The lines are for $\alpha = 1, 0.4, 0.1$ and 0.025 from top to bottom. The end-points of the quantum-critical to quantum-disordered lines map onto $(g_1, t_1) = (8\pi, 2\pi)$. Note that when t_0 becomes larger than the crossover temperature from renormalized classical to quantum critical at $g_0 = 0$, one dimensional fluctuations are dominating for all values of g_0.

Eq.'s (2.3.20,2.3.21) are our central result. They show that the correlation length in the renormalized classical regime has a double *exponential* dependence on the anisotropy, both dependencies originating in the high frequency one dimensional fluctuations. As already pointed out by CH[40], the anisotropy causes g_c to decrease (e.g., fig. 2-3), leading to a reduction of ξ at a given temperature. However, we find an additional $\sqrt{\alpha}$ in the exponent which has been overlooked by CH, although it is included in the paper of Wang [45]. This is the specific way in which the greater effect of the thermal fluctuations, which we noted earlier, shows up in the renormalized classical regime. In fact, it shows that the basic invention of CHN is straightforwardly extended to the anisotropic case. The correlation length is given by the expression for the classical system, and quantum mechanics only enters in the form of a redefinition of the stiffness. However, for the classical correlation length expression one should use the one for the *anisotropic classical model*. Using the same procedure as for the quantum model, it is easy to demonstrate that the correlation length of the anisotropic classical $O(3)$ model in 2D behaves as $\xi \sim \exp(\sqrt{\alpha_0}\rho_s^0/k_B T)$,

and this explains the occurrence of the additional $\sqrt{\alpha_0}$ factor.[2]

2.4   Zero-temperature magnetization and Néel temperature

The finiteness of the Néel temperature is caused by small intraplanar spin-anisotropies and interplanar couplings. Keimer *et al* [9] have shown that in La_2CuO_4 the former dominate, and these can be lumped together in a single term α_{eff} which plays the role of an effective staggered field. The Néel temperature can be estimated by comparing the thermal energy $k_B T_N$ to the energy-cost of flipping all spins in a region the size of the correlation area in the presence of the effective staggered field. This yields the self-consistent relation

$$k_B T_N(\alpha) \simeq J\alpha_{\text{eff}} \frac{\xi^x(T_N, \alpha)\xi^y(T_N, \alpha)}{a^2} \left(\frac{M_s}{M_0}\right)^2 , \tag{2.4.1}$$

where M_s/M_0 is the reduction factor of the staggered magnetization. Because it is not expected that stripes will influence the spin anisotropies strongly, we can use the estimate for α_{eff} as determined for the half-filled system: $\alpha_{\text{eff}} = 6.5 \times 10^{-4}$ [9]. For the estimate of T_N, the spin-wave results for the renormalized stiffness, susceptibility and spin wave velocity are used (table 1-1) [10]. or $S = 1/2$, they are $\hbar c = 0.5897\sqrt{8}Ja$, $\chi_\perp(0) = 0.514\hbar^2/(8Ja^2)$, and $\rho_s = c^2\chi_\perp(0)$. The bare coupling constant is obtained from $(g_0/4\pi) = 1/(1 + 4\pi\chi_\perp c/\hbar\Lambda)$ [12], which yields $g_0 = 9.107$ for $\Lambda a = 2\sqrt{\pi}$. We notice that the 1-loop result for the temperature-dependence of the prefactor is not correct, but this is not very important as far as the reduction of the Néel temperature by the anisotropy is concerned.

Since our $T = 0$ results coincide with those obtained by CH[40], we use their expression for the zero temperature staggered magnetization [3],

$$\frac{M_s(\alpha)}{M_s(1)} = \sqrt{\frac{1 - g_0/g_c(\alpha)}{1 - g_0/4\pi}}, \tag{2.4.2}$$

---

[2]Following CHN , eq.'s (2.3.20,2.3.21) can also be obtained by integrating out all quantum fluctuations in the renormalized classical region to 1-loop order. This yields a 2d anisotropic classical non-linear sigma model, with effective dimensionless temperature

$$\frac{1}{t_0} = \frac{1}{k_B T} \left[\rho_s(0) + \frac{k_B T}{2\pi\sqrt{\alpha_0}} \ln \left(\frac{\hbar c\Lambda}{k_B T} \sqrt{\frac{1 + \alpha_0}{2}} \right) + \mathcal{O}(T^2) \right].$$

with $\rho_s(0)$ given by eq. (2.3.21), where $g_c(\alpha_0)$ is now precisely the critical coupling obtained by CH. Momentum-shell renormalization of this 2d model again yields eq.(2.3.20).

[3]Because of the neglect of topological terms, this expression yields a lower bound for the staggered magnetization.
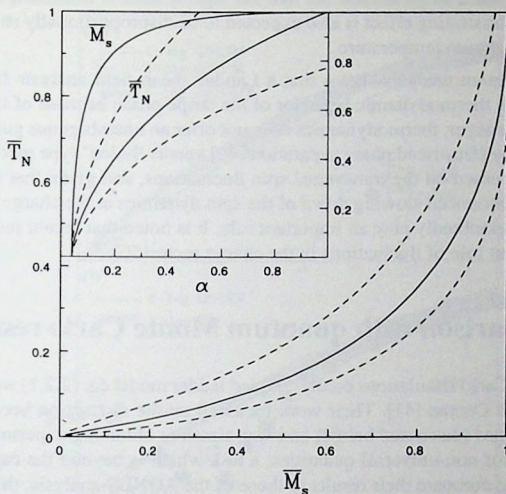
Figure 2-4. The Néel temperature versus the zero temperature staggered magnetization, with the anisotropy as implicit parameter. Both quantities are normalized with respect to their value in the isotropic system. The upper/lower dashed line gives $\tilde{T}_N$ for α_{eff} (Néel stabilizing field) a factor 10 larger/smaller than in the isotropic system. *Inset*: $\tilde{T}_N$ and $\tilde{M}_s$ as a function of the anisotropy parameter α.

and its anisotropy dependence is shown together with the results for the Néel temperature in the inset in fig. 2-4. To illustrate the effects of a different α_{eff} in the stripe phase (e.g., the inter-planar coupling may be much reduced due to frustration) we have also plotted the results for $\alpha_{\text{eff}}(\alpha < 1) = 10\alpha_{\text{eff}}(\alpha = 1)$ (upper dashed line) and for $\alpha_{\text{eff}}(\alpha < 1) = 0.1\alpha_{\text{eff}}(\alpha = 1)$ (lower dashed line). In Fig. 2-4 T_N is plotted versus M_s. As expected, the dependence of T_N on anisotropy is considerably stronger than that of M_s. A reduction of M_s by a factor of 2 due to a spin-wave anisotropy $\sim \sqrt{\alpha} \sim 1/4$ order is accompanied by a suppression of T_N by roughly an order of magnitude.

In the above we relate different experimentally accessible quantities (spatial- and spin anisotropies, Néel temperature, $T = 0$ staggered order, correlation length) and further[46, 47] experimentation is needed to unambiguously demonstrate that spatial anisotropy is the cause of the low spin ordering temperature. If the fluctuation behavior in the RC regime is indeed as general as suggested by the present analysis, other sources of stripe induced spin disorder could have similar consequences. For instance, local charge deficiencies in the stripes caused by quenched disorder would give rise to unscreened (by charge) pieces

of domain walls. Such stripe defects are like the dipolar defects discussed by Aharony *et al*, [48] and their frustrating effect is also expected to be disproportionally stronger at finite temperature than at zero temperature.

Above all, the present analysis shows that a Landau mean-field analysis falls short as a description for the thermodynamic behavior of the stripe phase because of the importance of fluctuations. Stronger, thermodynamics does not offer an unambiguous guidance regarding the microscopy (frustrated phase separation [49] versus 'holon' type mechanisms[23]). Here we have focussed on the transversal spin fluctuations, and given that there is ample evidence for a pronounced slowing down of the spin dynamics at the charge ordering temperature, these undoubtedly play an important role. It is noted that recent results point at a similarly important role of fluctuations in the charge sector[50].

2.5   Comparison with quantum Monte Carlo results

Quantum Monte Carlo simulations on the coupled ladder model eq. (2.2.1) were carried out by Tworzydlo and Osman [41]. Their work focussed on the distinction between site- and bond-ordered stripes (discussed below) and was aimed at obtaining experimentally verifiable predictions for non-universal quantities, a task which is beyond the capability of the QNLS. In order to compare their results to those of the AQNLS-analysis, they generalized the QNLS-description to the case of coupled ladders with a general number of legs. For two- and three-leg ladders, they obtain the following expressions for the spin-wave velocity in the x and y direction

$$c_x^2 = \alpha c_0^2 \begin{cases} \frac{(3+\alpha)}{2(1+\alpha)} & \text{for } n_l = 2 \\ \frac{9(7+3\alpha)}{2(1+2\alpha)(13+2\alpha)} & \text{for } n_l = 3 \end{cases} \tag{2.5.1}$$

$$c_y^2 = c_0^2 \begin{cases} \frac{(3+\alpha)}{4} & \text{for } n_l = 2 \\ \frac{3(7+3\alpha)}{2(13+2\alpha)} & \text{for } n_l = 3 \end{cases} \tag{2.5.2}$$

where c_0 is the spin wave velocity in the isotropic limit. The results of the AQNLS analysis can be formulated in terms of these spin-wave velocities. The renormalized spin-stiffness is given by

$$\rho_s(\alpha) = \rho \frac{c_x(1 - \frac{g_0}{g_c(\alpha)})}{c_y(1 - \frac{g_0}{g_c(1)})}, \tag{2.5.3}$$

where

$$g_c(\alpha) = 4\pi \sqrt{c_0/c_y} \left(1 + \frac{2}{\pi} (c_y \text{arsinh}[c_x/c_y]/c_x + \ln[c_y(1 + \sqrt{1 + c_x^2/c_y^2})/c_x/(1+\sqrt{2})^2]) \right), \tag{2.5.4}$$
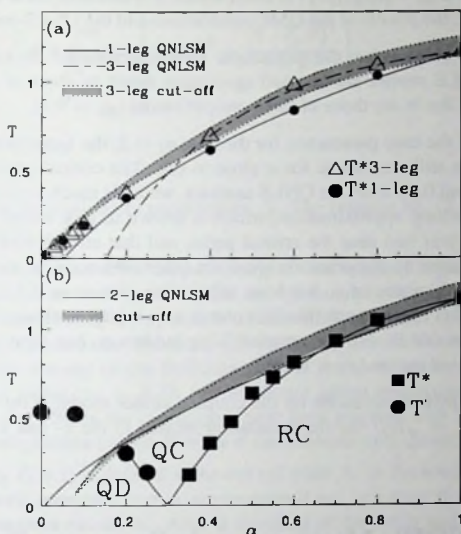
Figure 2-5. Crossover temperatures as a function of anisotropy α for the coupled three leg (a) and two leg (b) spin-ladder models. The lines and points refer to the analytical- and numerical results, respectively, for the various scales. Notice that the 1-leg 'cut-off' (1D-2D cross-over) follows closely the results for T^*.

and where ρ_s is the renormalized stiffness for the isotropic model.

As was discussed in section 1.4.3, the cases of coupled even-leg and odd-leg ladders are vitally different. For even-leg ladders, the topological term in the action gives no contribution and the QNLS is a good description. The $\alpha = 0$ state has a gap and no spin order. For odd-leg ladders, the topological term induces quasi long-range spin-order at $\alpha = 0$. As a result, this system has true long-range order for any non-zero value of α. This behavior is not captured by the QNLS. Nevertheless, a QNLS-description should be valid for this system as well if α is not to small, so close to the fully two-dimensional limit.

The QMC analysis focuses on the cross-over scales. The cross-over temperature from the QC to the RC regime is given by $T^* = 2\pi\rho_s(\alpha)$. That from the QC to the QD regime by $T' = \text{const}.\rho_s(\alpha)$ [4]. For the high-temperature cut-off, the expression $T_0 =$

---

[4] The constant depends on the choice of g^*, which is the value of g_0 for which $\xi(t_0 = 0, g_0) = a$ in the QD regime. See section 2.6.2. Since it cannot be determined from the one-loop analysis, it is taken as a fitting

$2\pi\rho_s c_x(g_0/(4\pi c_0) + (1 - g_0/g_c)/c_y)$ is used, which is reasonable for α close to its critical value. In figure 2-5, the results of the QMC simulations and the QNLS-analysis are plotted.

For the 1-leg case, which is just the anisotropic Heisenberg model discussed in the above, the QMC and QNLS results are in good agreement down to about $\alpha = 0.2$. The bare parameters used in the fit are those of the isotropic model ($g_0 = 9.1$).

With this choice of the bare parameters for the case $n_l = 2$, the agreement between QNLS and QMC results is still reasonable for α close to one. The critical value of α is however estimated to be about 0.08 from the QNLS analysis, which is much to small. Given the fact that we used a one-loop approximation, which is known to give incorrect results for the slope of the cross-over line near the critical point, and that effects such as the additional reduction of spin-order by dimerization were not taken into account, this is not very surprising. In fig. 2-5, the value of g_0 has been adjusted to give $\alpha_c = 0.3$ ($g_0 = 11.0$), while at the same time ρ_s^0 is chosen such that the correct $\alpha = 1$-limit is obtained. This procedure gives quite a reasonable fit. For the coupled 3-leg ladders g_0 has been adjusted to give a better fit in the high-α region ($g_0 = 10.5$).

Finally, in recent QMC-simulations on the coupled-ladder model, Kim *et al.* [42] indeed find the relation $\xi^x = \sqrt{\alpha}\xi^y$ for the correlation lengths in the x- and y-direction at low-temperatures.

2.6 APPENDIX: Momentum-shell renormalization of the quantum non-linear sigma model

2.6.1 Scaling

We review in some detail the momentum-shell renormalization of the QNLS, as set out in the papers of CHN and Nelson and Pelcovits (NP) [12] [52]. Since this introduces no additional complications, the case of general dimension d and number of order-parameter components n is considered. For notational convenience, the expressions in this section are in units where $\hbar = k_B = 1$.

Our starting point is the Lorentz-invariant form for the QNLS eq. (1.3.7). The unit vector $\hat{n}$ entering the action is decomposed in a component along the ordering direction, σ, and $n-1$ components perpendicular to it: $\vec{\pi}$. The σ-field is integrated out using the delta-function in the measure. The integrations over $\vec{\pi}$ are extended to the range $\langle -\infty, \infty \rangle$. We obtain

$$\mathcal{Z} = \int \prod_i \frac{d\vec{\pi}_i}{\sqrt{1 - \pi_i^2}} e^{-S[\vec{\pi}]},\tag{2.6.1}$$

parameter here.

with the action

$$S = \frac{1}{2g_0} \int \mathrm{d}^d x \int_0^{u_0} \mathrm{d}x_0 \left[(\partial_\mu \vec{\pi})^2 + \frac{(\vec{\pi} \cdot \partial_\mu \vec{\pi})^2}{1 - \vec{\pi}^2} \right], \tag{2.6.2}$$

where

$$u_0 = \frac{g_0}{t_0}, \tag{2.6.3}$$

and where t_0 is the dimensionless temperature $\frac{T}{\rho_s^0}$. The relation eq. (2.6.3) also holds for the renormalized quantities.

A lattice-regularization is used for the path-integral. The spatial integrations in the action therefore have a short-distance cut-off. This cut-off is implemented by transforming to momentum space and treating the system in a finite Brillouin zone. For convenience, this Brillouin zone is assumed to be spherical, with radius Λ. The radius is usually chosen in such a way that the volume of the Brillouin zone is the same as for the corresponding lattice model. This yields $\Lambda a = 2\sqrt{\pi}$ for the square lattice antiferromagnet (where a is the sublattice-spacing). Since the coordinates have been rescaled with Λ (eq. (1.3.6)), the dimensionless k-integrations extend over the d-dimensional unit sphere.

The bare action eq. (2.6.2) is defined at the cut-off scale Λ. In the renormalization procedure, the modes with momenta near Λ are integrated out, resulting in an effective action with a lower momentum cut-off Λ'. After a rescaling of the fields and the momenta, this effective action takes again the form eq. (2.6.2), but with renormalized values for g and t. This process is repeated, resulting in a flow of the scaling variables g and t. Certain physical properties of the model can be derived from studying these flows. In this section, the flow-equations are derived to one-loop order, which is the lowest non-trivial order in g_0.[5]

In the following, the action is expanded in $\vec{\pi}$ and only the lowest order terms are considered. There is a Ward-Takahashi identity due to Brézin and Zinn-Justin [53], which ensures that the higher order terms scale in the same way as the Gaussian one. This is necessary for the renormalized action to keep the form eq. (2.6.2) and for g and t to be the only scaling variables in the model.[6]

The square-root entering the measure in eq. (2.6.1) is a remnant of the integration over σ. It can be absorbed into the action, yielding an additional term

$$\rho \int \mathrm{d}^d x \int_0^{u_0} \mathrm{d}x_0 \left[-\frac{1}{2} \ln(1 - \vec{\pi}^2) \right]. \tag{2.6.4}$$

---

[5]Since we are applying it to the case of g_0 close to its critical value, which is 4π for $d = 2$, there might be some feeling of déjà vu : in section 1.2.2 a $\frac{1}{3}$-expansion was used to analyze an $S = \frac{1}{2}$-system. In fact, the $S \to \infty$ and the $g_0 \to 0$ limit refer to the same state. The 1-loop treatment is only strictly valid for $g_c \ll 1$, which is the case if the number of space-dimensions is close to $1 : d = 1 + \varepsilon$. However, since the flow of g is towards smaller values for $g_0 < g_c$, the flow-equations derived at the end of this section drive g towards the region where they become exact. Because of this property, these equations can be applied to the renormalized classical region in $d = 2$ with a greater accuracy than one would expect.

[6]The identity follows from the invariance of the QNLS-action on the choice of the preferred direction σ.

where ρ is the number of degrees of freedom per unit volume of the spherical Brillouin zone:

$$\rho = \int_{\text{Zone}} \frac{\mathrm{d}^d k}{(2\pi)^d} = \frac{S_d}{(2\pi)^d} \int_0^1 k^{d-1} \mathrm{d}k = \frac{S_d}{d(2\pi)^d}, \tag{2.6.5}$$

and where S_d is the surface of a sphere in d-dimensions. The ρ-term provides a potential for the $\vec{\pi}$-fields, which enforces the constraint $\vec{\pi}^2 < 1$.

We expand in the $\vec{\pi}$-fields and perform a Fourier transformation in both the space and the time variables:

$$\vec{\pi}(x) = \sum_{n=-\infty}^{\infty} \int_{\text{Zone}} \frac{\mathrm{d}^d k}{(2\pi)^d} \vec{\pi}(\omega_n, \vec{k}) e^{i\omega_n x_0 + i\vec{k} \cdot \vec{x}}. \tag{2.6.6}$$

Due to the finite range of the x_0 integration, the time Fourier-transformation introduces the discrete Matsubara frequencies $\omega_n = \frac{2\pi n}{u_0}$.

The $\vec{\pi}(\omega_n, \vec{k})$ are separated into slow modes, which are kept, and fast modes, which are integrated out.

$$\vec{\pi}(\omega_n, \vec{k}) = \begin{cases} \vec{\pi}_>(\omega_n, \vec{k}) & ; \quad e^{-l} < |\vec{k}| < 1 \\ \vec{\pi}_<(\omega_n, \vec{k}) & ; \quad |\vec{k}| < e^{-l} \end{cases}, \tag{2.6.7}$$

where $l \ll 1$. The separation is made in momentum- but not in frequency-space. This is related to the regularization procedure. We did not assume a short-time cut-off. As a result, the Matsubara-frequencies extend to $\pm\infty$ and all fall within the range $e^{-l}\omega_{\text{max}}$. The non Lorentz-invariance of the cut-off procedure has no consequences at the one-loop level.

The fast modes are integrated out. This calculation is dealt with in section 2.6.4. It results in an effective action for the low-momentum modes which has the following form (to Gaussian order)

$$S'^{(2)} = \frac{u_0}{2g_0} \sum_n \int \frac{\mathrm{d}^d k}{(2\pi)^d} \left(\vec{k}^2 + \frac{4\pi^2 n^2}{u_0^2}\right) \left(1 + \frac{g_0}{u_0} \hat{I}_{\text{loop}}\right) \left|\vec{\pi}_{n,k}\right|^2, \tag{2.6.8}$$

where I_{loop} is the one-loop contribution to the renormalization of the second order term, eq. (2.6.39).

Momenta and fields are rescaled according to

$$\begin{aligned} \vec{k} &\rightarrow \vec{k}' = e^l \vec{k}, \\ \vec{\pi} &\rightarrow \vec{\pi}' = \zeta^{-1} \vec{\pi}, \end{aligned} \tag{2.6.9}$$

which restores the radius of the Brillouin zone to 1. This yields

$$
\begin{aligned}
S'^{(2)} &= \frac{u_0}{2g_0} \sum_n \int \frac{d^d k'}{(2\pi)^d} e^{-dl} \left(\vec{k}'^2 e^{-2l} + \frac{4\pi^2 n^2}{u_0^2} \right) \left(1 + \frac{g_0}{u_0} I_{\text{loop}} \right) \zeta^2 \left| \vec{\pi}'_{n,k'} \right|^2 \\
&= \frac{u'}{2g'} \sum \int \frac{d^d k'}{(2\pi)^d} \left(\vec{k}'^2 + \frac{4\pi^2 n^2}{u'^2} \right) \left| \vec{\pi}'_{n,k'} \right|^2 .
\end{aligned} \tag{2.6.10}
$$

Comparing the first and the second line, one finds

$$
u' = u_0 e^{-l} , \tag{2.6.11}
$$

$$
\frac{u'}{g'} = \frac{u_0}{g_0} \zeta^2 e^{-(d+2)l} \left(1 + \frac{g_0}{u_0} I_{\text{loop}} \right) . \tag{2.6.12}
$$

Note that frequency and momentum scale in the same way: the spacing in the frequency-direction is rescaled by a factor e^l, as are the momenta. As a result, the spin-wave velocity c_s is *not* renormalized at the one-loop level.

The spin-rescaling factor ζ is still undetermined. From considering the scaling of the higher-order terms in S under eq. (2.6.9), it is clear that ζ must be of the form

$$
\zeta = e^{dl} \left(1 + \frac{g_0}{u_0} A \right) , \tag{2.6.13}
$$

where A is a one-loop contribution. This form ensures that all terms in the expansion of S scale in the same way at zero-loop, or tree-level. A can be obtained from a calculation of the one-loop contribution to $\left(\vec{\pi} \cdot \partial_\mu \vec{\pi} \right)^2$, which involves sixth- and eighth-order diagrams and is rather cumbersome.

A simpler approach is to introduce a small Néel-order stabilizing field into the action

$$
-\frac{h}{g_0} \int d^d x \int_0^{u_0} dx_0 \sigma(x) = -\frac{h}{g_0} \int d^d x \int_0^{u_0} dx_0 \left(1 - \frac{1}{2} \vec{\pi}^2 + \dots \right) . \tag{2.6.14}
$$

The renormalization of this term is considered in section 2.6.4. It yields

$$
\frac{h'u'}{g'} = \zeta^2 e^{-dl} \left[\frac{hu_0}{g_0} + \frac{1}{2} h(n-1) I_{\text{loop}} \right] . \tag{2.6.15}
$$

Since h represents a magnetic field, it must scale trivially as $(hu/g)' = \zeta hu_0/g_0$ [52]. One therefore has

$$
\zeta = e^{dl} \left[1 - \frac{g_0}{2u_0} (n-1) I_{loop} \right] . \tag{2.6.16}
$$

The renormalized couplings can now be used as input-parameters for a new round of integration and rescaling. From equations (2.6.11), (2.6.12) and (2.6.16) follow differential equations for the flow of t and g with l.

$$\frac{\partial g}{\partial l} = (1-d)g + \frac{S_d}{2(2\pi)^d}(n-2)g^2 \coth\left[\frac{g}{2t}\right] , \tag{2.6.17}$$

$$\frac{\partial t}{\partial l} = (2-d)t + \frac{S_d}{2(2\pi)^d}(n-2)gt \coth\left[\frac{g}{2t}\right] . \tag{2.6.18}$$

2.6.2   The flow diagram

For low temperatures, $\frac{t}{g} \ll 1$, the flow equations take the form

$$\frac{\partial g}{\partial l} = -g + \frac{g^2}{4\pi} , \tag{2.6.19}$$

$$\frac{\partial t}{\partial l} = \frac{gt}{4\pi} . \tag{2.6.20}$$

The equation for g has two fixed points: $g = 0$ and $g = g_c = 4\pi$. The stable $g = 0$ fixed point refers to the classical $S \to \infty$ state of the Heisenberg antiferromagnet, while the unstable fixed point at $g = g_c$ separates the ordered from the disordered $T = 0$ state. The dimensionless temperature t only has an unstable $t = 0$ fixed point. In the $g \downarrow 0$-limit, the flow-equation for t eq. (2.6.18) takes the form

$$\left.\frac{\partial t}{\partial l}\right|_{g\downarrow 0} = (2-d)t + \frac{S_d}{(2\pi)^d}(n-2)t^2 , \tag{2.6.21}$$

which indeed agrees with the result of NP for the classical non-linear sigma model in $2+\varepsilon$ dimensions [52].

Using the identity

$$\frac{g(l)}{t(l)} = \frac{g_0}{t_0}e^{-l} , \tag{2.6.22}$$

which follows from eq. (2.6.11), the differential equation (2.6.17) can be integrated. For $d = 2$ and $n = 3$, one obtains

$$g(l) = g_0 e^{-l}\left\{1 - \frac{t_0}{2\pi}\ln\left[\frac{\sinh\left(\frac{g_0}{2t_0}\right)}{\sinh\left(\frac{g_0}{2t_0}e^{-l}\right)}\right]\right\}^{-1} , \tag{2.6.23}$$

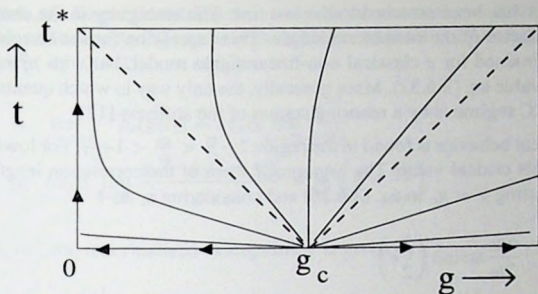$$t(l) = \frac{t_0}{g_0}e^l g(l) . \tag{2.6.24}$$

Figure 2-6. The one-loop flow-diagram for the QNLS. The dashed lines indicate the cross-over from the quantum critical to the renormalized classical and the quantum disordered regime.

The resulting flow-diagram is shown in figure 2-6.

From fig. 2-6, it is clear that there are three distinct low-temperature regimes. For $g < g_c$, the system flows first to small g and finally to high temperatures. This is the renormalized classical (RC) region (section 1.3.3). For $g \simeq g_c$, the flow is straight to high-temperature, with little change in g (the quantum critical (QC) region). And finally for $g > g_c$, the systems flows towards the strong coupling large g regime (quantum disordered (QD) region).

There is a simple procedure for calculating the (g,t)-dependence of the correlation-length from the flow-equations [12]. Since ξ has the dimension of a length, it scales trivially under the renormalization group transformation:

$$\xi(l) = \xi_0 e^{-l}. \tag{2.6.25}$$

Because of this property, the correlation length can be obtained by starting at the $\xi(l^*) = a$ line and integrating back to $\xi(g_0, t_0) = ae^{l^*}$. For the RC and QC region, it is assumed that $\xi = a$ at some temperature $t(l^*) = t^*$: the high-temperature cut-off of the QNLS. For the QD region, a cut-off g^* in the g-direction is assumed.

The value of ξ the RC and QC region follows directly from eq. (2.6.24)

$$\xi^{-1} = \frac{2t_0}{ag_0} \text{arsinh} \left[\sinh\left(\frac{g_0}{2t_0}\right) e^{-2\pi\left(\frac{1}{t_0} - \frac{1}{t^*}\right)} \right]. \tag{2.6.26}$$

The asymptotic behavior at low-temperatures in the RC and QC regime is now easily obtained. Assuming $t_0 \ll 1$, $\frac{g_0}{g_c} \ll 1 - \frac{t_0}{t^*}$ (deep RC), one obtains

$$\begin{aligned} \xi_{RC} &= \frac{ag_0}{t_0} e^{-2\pi/t^*} e^{2\pi\left(1 - \frac{g_0}{4\pi}\right)\frac{1}{t_0}} \\ &\simeq 0.9 \frac{\hbar c}{k_B T} e^{\rho_s^0\left(1 - \frac{g_0}{g_c}\right)/k_B T}, \end{aligned} \tag{2.6.27}$$

where $t^* = 2\pi$ has been assumed in the last line. The ambiguity in the choice of t^* only affects the prefactor of the correlation length. This expression for the correlation length is just the one obtained for a classical non-linear sigma model, but with $\rho_s^{()}$ replaced by its renormalized value eq. (2.6.32). More generally, the only way in which quantum mechanics enters in the RC regime is by a renormalization of the stiffness [12].

Quantum critical behavior is found in the region $1 - \frac{t_0}{t^*} < \frac{g_0}{g_c} < 1 + \frac{t_0}{t^*}$. For low temperatures, g_0 is close to its critical value. The asymptotic form of the correlation length is therefore obtained by setting $g = g_c$ in eq. (2.6.26) and considering $t_0 \ll 1$

$$
\begin{aligned}
\xi_{QC} &= \frac{ag_0}{2t_0}\mathrm{arsinh}\left(\frac{1}{2}e\right) \\
&\simeq 1.4\frac{\hbar c}{k_B T}.
\end{aligned}
\tag{2.6.28}
$$

As was discussed in section 1.3.3, this type of scaling with inverse temperature is in fact expected to occur on general grounds, related to the Lorentz-invariance of the model.

For the QD region $\frac{g_0}{g_c} > 1 + \frac{t_0}{t^*}$, the correlation-length is obtained by integrating back from $g = 2g_c$. This yields

$$
\xi_{QD} \simeq \frac{ag_0/2}{(g_0 - g_c) + 2t_0\exp\left[-2(g_0 - g_c)/t_0\right]}.
\tag{2.6.29}
$$

The very weak dependence on temperature is an indication of the presence of a spin-gap $\Delta \sim g_0 - g_c$ in the quantum disordered state.

2.6.3 Renormalized stiffness and susceptibility

In section 1.3.4, the renormalized values of ρ_s and $\chi_\perp$ in the $T = 0$ Néel state were used to make the connection between spin-wave and QNLS results. These values are derived here.

The stiffness can be obtained by noting that ρ_s defines a length-scale, the Josephson correlation length, through

$$
\xi_J = \frac{\hbar c_s}{\rho_s}.
\tag{2.6.30}
$$

This is the length-scale which separates the short-wavelength critical fluctuations from the long-wavelength Goldstone modes. It is at this length that the system begins to find out that it is no longer at the critical point (which means, of course, that ξ_J diverges at the critical point). The Josephson correlation length again scales as $\xi_J(l) = e^{-l}\xi_J(0)$. Since c_s is not renormalized at the one-loop level, ρ_s satisfies

$$
\rho_s(g_0) = \rho_s[g(l)]e^{-l}.
\tag{2.6.31}
$$

In the Néel phase, the large l limit takes the system to the classical $g = 0$, or $S \to \infty$ state. In this limit, the stiffness $\rho_s[g(l)]$ can be replaced by its bare value $\rho_s^0 = \hbar c_s \Lambda / g(l)$. Using the $t_0 = 0$-limit of eq. (2.6.23), one obtains

$$
\begin{aligned}
\rho_s(g_0) &= \lim_{l \to \infty} e^{-l} \rho_s[g(l)] = \hbar c_s \Lambda \lim_{l \to \infty} \frac{e^{-l}}{g(l)} \\
&= \hbar c_s \Lambda \lim_{l \to \infty} \frac{g_c - g_0(1 - e^{-l})}{g_c g_0} = \rho_s^0 \left(1 - \frac{g_0}{g_c} \right).
\end{aligned}
\tag{2.6.32}
$$

Since $\chi_\perp = \rho_s / c^2$, the renormalized susceptibility is given by

$$
\chi_\perp = \chi_\perp^0 \left(1 - \frac{g_0}{g_c} \right).
\tag{2.6.33}
$$

2.6.4 Integration over fast modes

The high-momentum modes are integrated out in a perturbative procedure. To this end, the action S is split into a Gaussian part S_0 and an anharmonic part S_I. The partition function can be written in the following form:

$$
\begin{aligned}
\mathcal{Z} &= \int D\vec{\pi}\, e^{-S_0[\vec{\pi}_<] - S_0[\vec{\pi}_>] - S_I[\vec{\pi}_<, \vec{\pi}_>]} \\
&= \int D\vec{\pi}_<\, e^{-S_0[\vec{\pi}_<]} \int D\vec{\pi}_>\, e^{-S_I[\vec{\pi}_<, \vec{\pi}_>]} e^{-S_0[\vec{\pi}_>]} \\
&\propto \int D\vec{\pi}_<\, e^{-S_0[\vec{\pi}_<]} \left\langle e^{-S_I[\vec{\pi}_<, \vec{\pi}_>]} \right\rangle_{0>} \\
&= \int D\vec{\pi}_<\, e^{-S'[\vec{\pi}_<]},
\end{aligned}
\tag{2.6.34}
$$

where S' is an effective action for the low-momentum modes. The $\langle \ldots \rangle_0$ brackets indicate an average with respect to the Gaussian action S_0. A factor $\mathcal{Z}_0$ has been omitted in the third line, since it only contributes a constant to the effective action.

The average is evaluated using the following identity:

$$
\begin{aligned}
\langle e^{S_I} \rangle &= \exp\left[\langle e^{-S_I} \rangle_c - 1 \right] \\
&= \exp\left[-\langle S_I \rangle_c + \frac{1}{2!} \langle S_I^2 \rangle_c + \ldots \right]
\end{aligned}
\tag{2.6.35}
$$

where $\langle S_I^a \rangle_c$ is the a-th cumulant of S_I. Since S_0 is Gaussian, all odd moments of the action are zero. The even moments can be expressed in terms of the variance using Wick's theorem for bosons,

$$
\langle \pi_1^* \pi_2^* \pi_3 \pi_4 \rangle_0 = \langle \pi_1^* \pi_3 \rangle_0 \langle \pi_2^* \pi_4 \rangle_0 + \langle \pi_1^* \pi_4 \rangle_0 \langle \pi_2^* \pi_3 \rangle_0,
\tag{2.6.36}
$$

(a) $\frac{1}{2\,g_0}$ + $\frac{1}{2\,g_0}$ + $\frac{1}{2}\rho$

+ $\frac{1}{4}\rho$

(b) $\frac{1}{2\,g_0}$

(c) $\frac{1}{2\,g_0}$ + $\frac{h}{8\,g_0}$ + $\frac{h}{8\,g_0}$

+ $\frac{1}{2}\rho_>$

Figure 2-7. (a) Diagrams for the lowest-order terms in the action. (b) One-loop contribution to the recursion relation for the $\left(\partial_\mu \vec{\pi}(x)\right)^2$-term. (c) Contributions to scaling of the magnetic field.

and similarly for higher moments. The expansion eq. (2.6.35) can therefore be cast into a form where all $\pi_>$ are contracted into second moments of S_0. Each pair yields a contribution

$$\langle \pi^{\alpha\,*}(\omega_n, \vec{k}) \pi^{\alpha'}(\omega'_n, \vec{k}') \rangle_0 = \frac{g_0}{u} \frac{(2\pi)^d}{\vec{k}^2 + \omega_n^2} \delta_{n,n'} \delta^d(\vec{k} - \vec{k}') \,. \tag{2.6.37}$$

The integration over the short-wavelength modes is conveniently performed in a diagrammatic approach. The diagrams entering the lowest orders of the action S are show in figure 2-7(a). The prefactors are those for the action in space-time, not in Fourier-space. External lines indicate low-momentum fields $\pi^\alpha_<$, while internal lines represent contracted pairs of $\pi^\alpha_>$. Slashes indicate space-time derivatives. Dotted lines separate pairs of fields with a common index α.

Each internal line contributes a propagator eq. (2.6.37). Closed lines yield a factor $n - 1$. Slashed lines have an extra factor $(\omega_n, \vec{k})$ due to the space-time derivative. All diagrams have conservation of total momentum. In figure 2-7(b), the diagrams for the lowest-order terms in the action are shown. The ρ-terms are a remnant of the δ-function in the measure of the QNLS, as discussed in section 2.6.1.

The graphs contributing to a certain term in the effective action are obtained by considering all possible contractions of graphs in the expansion eq. (2.6.35) which give the correct

structure for the external lines. To one-loop order, only the graphs which have one closed loop are considered. Graphs with the same number of loops are of the same order in g_0 [7].

The only one-loop contribution to Gaussian term $\left(\partial_\mu \vec{\pi}\right)^2$ in the effective action comes from the graph shown in fig. 2-7(b). It yields

$$
\begin{aligned}
&\int_< \prod_{i=1,2} \left(\frac{\mathrm{d}^d k_i}{(2\pi)^d} \sum_{n_i}\right) \int_> \prod_{i=3,4} \left(\frac{\mathrm{d}^d k_i}{(2\pi)^d} \sum_{n_i}\right) (2\pi)^d \delta^d(\vec{k}_1 - \vec{k}_2 + \vec{k}_3 - \vec{k}_4) \\
&\times \ \frac{g_0}{u_0} \frac{(2\pi)^d}{k_3^2 + \omega_{n3}^2} \delta_{n_3,n_4} \delta^d(\vec{k}_3 - \vec{k}_4) \left(\vec{k}_1 \cdot \vec{k}_2 + \omega_{n1}\omega_{n2}\right) \vec{\pi}_1^* \cdot \vec{\pi}_2 \\
&= \ \frac{g_0}{u_0} I_{\text{loop}} \int_< \frac{\mathrm{d}^d k}{(2\pi)^d} \sum_n \left(\vec{k}^2 + \omega_n^2\right) |\vec{\pi}_{n,k}|^2 \ .
\end{aligned} \tag{2.6.38}
$$

where

$$
\begin{aligned}
I_{\text{loop}} &= \ \sum_n \int_> \frac{\mathrm{d}^d k}{(2\pi)^d} \frac{1}{\vec{k}^2 + \omega_n^2} = \frac{u_0}{2} \frac{S_d}{(2\pi)^d} \int_{e^{-l}}^1 \mathrm{d}k \, k^{d-2} \coth\left[\frac{u_0}{2}k\right] \\
&= \ -l \frac{u_0}{2} \frac{S_d}{(2\pi)^d} \coth\left[\frac{u_0}{2}\right] + \mathcal{O}(l^2) \ .
\end{aligned} \tag{2.6.39}
$$

The contributions to the scaling of the Néel-order stabilizing field h are shown in fig. 2-7(c). The last of these graphs refers to the $\rho\vec{\pi}^2$-term. Since the ρ-terms are of order 1, contractions of these diagrams do not contribute at the one-loop level. However, since the number of degrees of freedom per unit volume is reduced after integration and rescaling, their prefactor ρ does change. We write

$$
\rho = \rho_< + \rho_> = \int_< \frac{\mathrm{d}^d k}{(2\pi)^2} + \int_> \frac{\mathrm{d}^d k}{(2\pi)^2} \ . \tag{2.6.40}
$$

The $\rho_< \vec{\pi}^2$-term enters the effective action, while the term with prefactor $\rho_>$ is precisely cancelled by the first graph in fig. 2-7(c). The one-loop contribution to the scaling of h comes from the second and third graph. It yields

$$
\frac{1}{2}h(n-1)I_{\text{loop}} \sum_n \int \frac{\mathrm{d}^d k}{(2\pi)^d} |\vec{\pi}_{n,k}|^2 \ . \tag{2.6.41}
$$

---

[7]It is essential here that the graphs carry a prefactor g_0^{-1}. The situation is therefore somewhat different for the ρ-terms. Their renormalization however plays no role at the one-loop level, as is discussed below

3 Coherent states with tunable quantum correlations

In this chapter, a coherent state is introduced that is especially suited for the semi-classical description of certain systems with strong local quantum fluctuations, which have to be integrated out before the proper long-wavelength theory can be obtained. Such systems are considered in chapters 4 and 5, where the coherent state which is introduced here is applied.

3.1 Product wavefunction groundstates

As the first step in a semi-classical analysis, the lowest-order approximation to the $T = 0$ groundstate is obtained. For the quantum antiferromagnet, which was discussed in the introduction, this is the Néel state, with a wavefunction

$$| \text{Néel} \rangle = \prod_{i \in A} c_{i\uparrow}^{\dagger} \prod_{i \in B} c_{i\downarrow}^{\dagger} |\text{vac}\rangle \,, \tag{3.1.1}$$

where A and B denote the spin up and spin down sublattice, respectively. This state can be obtained from a Hartree-Fock variational analysis, or from mean-field theory. Wavefunctions of this type are constructed by specifying the state in each unit cell, and taking a product.

$$|\{\Omega_i\}\rangle = \prod_i Y^{\dagger}(\Omega_i)|\text{vac}\rangle \,, \tag{3.1.2}$$

where $Y^{\dagger}(\Omega_i)$ creates the state specified by Ω in cell i. For the Néel state, the unit cell contains two sites and the configuration $\{\Omega_i\}$ is uniform: $Y^{\dagger}(\Omega_i) = c_{A i \uparrow}^{\dagger} c_{B i \downarrow}^{\dagger}$.

Product wavefunctions contain no inter-cell correlations, since

$$\langle A_j A_{j'} \rangle - \langle A_j \rangle \langle A_{j'} \rangle = 0 \,, \tag{3.1.3}$$

for $j \neq j'$. Another way to say this: there is no quantum entanglement between different cells. Quantum mechanics stops at the cell boundary [1]. Wavefunctions of this type provide

---

[1] For the Néel state, there is no entanglement between different *sites*. A better example is perhaps the BCS wavefunction for superconductivity [54]

$$|\text{BCS}\rangle = \prod_k \left(u_k + v_k c_{k \uparrow}^{\dagger} c_{-k \downarrow}^{\dagger} \right) |\text{vac}\rangle \,, \tag{3.1.4}$$

where the decoupling now takes place in k-space.

a mapping from a configuration in phase-space to a state in Hilbert space. An arbitrary state in Fock space can be written as a superposition of product wavefunctions. In the path-integral formalism, the additional degrees of freedom which arise because of this are dealt with by mapping to a phase-space description in a space with one additional dimension, imaginary time. The product wavefunctions correspond to configurations which are uniform in the imaginary time direction.

Typically, uniform product wavefunctions like the Néel state eq. (3.1.1) are good zeroth-order groundstates for systems with a spontaneously broken symmetry, which are characterized by an order-parameter [55]. Examples of such systems are the antiferromagnet (broken spin-rotation symmetry), crystals (broken translational symmetry) and superconductors (broken phase-rotation symmetry). The fact that the Hartree-Fock groundstate has the same order-parameter as the true groundstate suggests that both states are adiabatically connected, that is: one can tune from the true groundstate to the zeroth-order state by continuously switching of the inter-cell correlations, without encountering a phase transition. For the antiferromagnet, this can be achieved by sending S to infinity. Another way is to increase the dimensionality of the system. For large d, every unit-cell is surrounded by a large number of other cells and it effectively sees just the average state of the system. Inter-cell correlations therefore disappear in this limit (mean-field theory becomes exact). The fact that a phase-transition does not occur implies that the true groundstate can in principle be reached in a perturbative procedure around the zeroth-order state.

Important corrections to the zeroth order state come from the low-energy Goldstone modes related to a broken continuous symmetry. The semi-classical approach amounts to a quantization of these modes. The coherent state formalism is especially suited for this purpose. If the coherent state has the form

$$|\vec{\Omega}_i\rangle = R(\vec{\Omega}_i)Y_i^\dagger|\text{vac}\rangle, \tag{3.1.5}$$

where $R(\vec{\Omega})$ contains the symmetry-transformations of the system, with $R(0) = 1$, and where $\prod_i Y_i^\dagger$ creates the Hartree-Fock groundstate, then the path-integral formulated in the basis of this coherent state will have a uniform saddle-point configuration ($\{\vec{\Omega}_i\} = 0$) which corresponds to the zeroth order groundstate. The Goldstone modes are long-wavelength fluctuations around this uniform configuration, which can be analyzed using a gradient expansion.

Requantizing the system in terms of these long wavelength fluctuations around the classical saddle point yields quite often a faithful representation of the physics of the system. This semi-classical procedure is the way in which quantum field theory appears in condensed matter physics.

Below, it is discussed what transformation R should be used in the construction of a coherent state. As a simple example, the XY-spin model is considered. Section 3.3 deals with the construction of an $SO(N)$ generalized coherent state. The generalized coherent states can be used for systems where the lowest order groundstate $\prod_i Y_i^\dagger|\text{vac}\rangle$ is 'maximally classical', for instance the antiferromagnet. The generalized spin-coherent states discussed

in section 1.4 are of this type. In section 3.4, this procedure is generalized to the case of systems which undergo a zero-temperature disordering transition. For these systems, the zeroth-order groundstate has a more general form, and additional degrees of freedom enter the coherent state.

3.2 Dynamical algebra and symmetry algebra

In section 1.4.3, a semi-classical description of the Heisenberg antiferromagnet was derived using an $SU(2)$ coherent state. The ordered state of the antiferromagnet exhibits spontaneous breaking of a global $SU(2)$ symmetry. This choice of coherent state therefore ensures that the parametrization of the path-integral is convenient for the description of the Goldstone modes in the ordered state, and hence for a semi-classical analysis. In general, however, a coherent state related to a *larger* symmetry group than the one expressing the invariance of the Hamiltonian should be used. The algebra which generates the transformations contained in the coherent state should be the dynamical algebra of the system, not the symmetry algebra [18]. This distinction is explained below for the simple case of an XY-spin model, where the symmetry algebra is $SO(2)$ (rotation of a 2-component vector), while the dynamical algebra is $SO(3)$ (rotation of a 3-component vector). Further on, we will argue that, for a system with an order-parameter symmetry $SO(N)$, the dynamical algebra is typically $SO(N+1)$. The results derived in the next section for the case of general N (with restrictions on the Hilbert space), are very similar to what we obtain here for $N = 2$ in a more straightforward way.

The XY-Hamiltonian reads

$$\mathcal{H}^{XY} = J \sum_{<ij>} \left(S_i^x S_j^x + S_i^y S_j^y \right) + H \sum_i S_i^z , \tag{3.2.1}$$

where the S^α are Heisenberg spin-operators. This model has a global SO(2) symmetry, related to spin-rotations in the XY-plane. The algebra generating these rotations has just one element: S^z. The XY-spin $\vec{N} = (S^x, S^y)$ transforms as a 2-vector under S^z:

$$[S^z, S^x] = i S^y ; \ [S^z, S^y] = -i S^x , \tag{3.2.2}$$

$\vec{N}$ therefore forms a vector representation of $SO(2)$.

One could think of using an $SO(2)$ coherent state for the description of this system:

$$|\phi\rangle = e^{-i\phi S^z} |S, S^x = S\rangle , \tag{3.2.3}$$

which gives

$$\langle \phi | \vec{N} | \phi \rangle = S(\cos\phi, \sin\phi) , \tag{3.2.4}$$

since the operator $e^{i\phi S^z}$ rotates the spin around the Z-axis. However, this state does not correctly describe the response to a magnetic field in the Z-direction, since $\langle\phi|S^z|\phi\rangle = 0$ for any ϕ. The requirement that the expectation-value of the quantum Hamiltonian with respect to $\prod_i |\phi_i\rangle$ yields the classical Hamiltonian (eq.(1.4.5)) is therefore not fulfilled.

The rotations from the XY-plane to the Z-direction are generated by the components of $\vec{N}$. The group which acts on the reference state must be extended to include these rotations. The resulting group is $SO(3)$. The $SO(3)$ coherent state is obtained by including a rotation about the Y-axis into eq. (3.2.4) (we take $S = 1$ to allow comparison with a result obtained in the next section, eq. (3.3.13))

$$
\begin{aligned}
|\theta, \phi\rangle &= e^{-i\phi S^z}e^{i\theta S^y}|S^x = 1\rangle \\
&= \frac{1}{2}(1 + \sin\theta)e^{i\phi}|S^z = 1\rangle + \frac{1}{\sqrt{2}}\cos\theta|S^z = 0\rangle \\
&\quad + \frac{1}{2}(1 - \sin\theta)e^{-i\phi}|S^z = -1\rangle,
\end{aligned}
\tag{3.2.5}
$$

where $\theta \in [-\frac{\pi}{2}, \frac{\pi}{2}]$ is the angle of the classical Heisenberg spin $\langle\vec{S}\rangle$ with respect to the XY-plane. The result in the last two lines is obtained by writing the transformations on the reference state as a Taylor expansion in ϕ and θ, respectively. It was noted in section 1.4.3 that coherent states with a different (ϕ, θ) should be physically distinct, that is: differ by more than a phase-factor. This is the reason why the rotations generated by S^x are not included in eq. (3.2.5). With the above definition of the coherent state, the condition is fulfilled for all (ϕ, θ) except at the north and south pole ($\theta = \pm\frac{\pi}{2}$).

The above coherent state could be written down just by considering the degrees of freedom it should contain, namely those of a classical Heisenberg spin. For the more general case of an $SO(N)$ coherent state, we have less intuition about what the degrees of freedom should be, and it is therefore best to construct these by starting out with the most general transformation on the reference state and then constraining it by the condition that states with different parameters should differ by more than a phase factor. This is done in the next section, where the above result is reproduced in this way.

The spin-spin interactions in the XY Hamiltonian eq. (3.2.1) are antiferromagnetic. It can be transformed into a ferromagnetic XY model by staggering the vector $\vec{N}$,

$$
\vec{N}_i \rightarrow (-1)^{\sum_{\alpha=1}^{d} i_\alpha}\vec{N}_i.
\tag{3.2.6}
$$

This transformation respects the $SO(3)$ commutation relations. A similar transformation is not possible for the Heisenberg antiferromagnet, since a staggering of all three components of $\vec{S}$ does not respect the $SO(3)$ commutation relations. As was stated in the discussion of the Heisenberg path integral, this implies that antiferromagnetism and ferromagnetism are qualitatively different for quantum Heisenberg models. They are not for quantum XY models.

Because of the above transformation, the local order parameter for an XY system can be defined on a single site as the expectation value of the XY spin $\vec{N}_i$. A coarse-graining procedure such as was used for the Heisenberg antiferromagnet in section 1.4.3 is not necessary.

Using the $SO(3)$ coherent state eq. (3.2.5) and going through the same procedure as in section 1.4.3, the kinetic term in the action is found to be

$$\Phi = iL \left(\hat{\bar{n}}^x \partial_\tau \hat{\bar{n}}^y - \hat{\bar{n}}^y \partial_\tau \hat{\bar{n}}^x \right) \tag{3.2.7}$$

where

$$L = \langle S^z \rangle \; ; \; \hat{\bar{n}} = \frac{\langle \vec{N} \rangle}{|\langle \vec{N} \rangle|} \, , \tag{3.2.8}$$

with the expectation values taken with respect to the coherent state. We find that the kinetic term arises from a coupling between the $SO(2)$-vector $\vec{N}$ and the $SO(2)$ algebra S^z. It is therefore essential to include the additional $SO(3)$ rotation into the coherent state eq. (3.2.5) to allow for a non-zero expectation value of S^z.

The semi-classical description of the $SO(2)$ symmetric XY-model requires the use of an $SO(3)$ coherent state. The relevant algebra for the construction of the coherent state is the dynamical algebra, which is the one containing the operators entering the Hamiltonian ($SO(3)$ in this case) and not the algebra generating the symmetry transformations of the model ($SO(2)$). Another way to say this: the coherent state must contain all the symmetry transformations at the 'most symmetric point' of the model. In this simple example, this corresponds with the $SO(3)$-symmetric Heisenberg point, which can be reached by switching on a spin-spin interaction between the Z-components and switching of the magnetic field.

Finally, let us show that the structure as illustrated above for the XY model is also present in the case of the Heisenberg antiferromagnet, which was discussed in section 1.4.3. The first step in deriving the QNLS from the spin path-integral is to divide the lattice into two-spin unit cells. In each cell, the order parameter $\vec{m}_i = (\hat{n}_{1i} - \hat{n}_{2i})/2$ and the average spin $\vec{l} = (\hat{n}_{1i} + \hat{n}_{2i})/2$ are defined. Modulo a factor one half, these two quantities are the expectation values of the following operators with respect to the spin coherent state eq. (1.4.1)

$$\begin{aligned} \vec{L} &= \vec{s}_1 + \vec{s}_2 \,, \\ \vec{N} &= \vec{s}_1 - \vec{s}_2 \,. \end{aligned} \tag{3.2.9}$$

$\vec{L}$ is an $S = 1$ spin-operator (for a spin-$\frac{1}{2}$ antiferromagnet), its components form a representation of the $SO(3)$ algebra. $\vec{N}$ is a vector-representation of this algebra: the operators L^α generate rotations of the vector $\vec{N}$

$$[L^x, N^y] = i N^z \,, \tag{3.2.10}$$

and cyclic. Taken together, $\vec{L}$ and $\vec{N}$ form an $SO(4)$ algebra. Its elements can be organized in a 4×4 matrix $\overset{\leftrightarrow}{l}$

$$\overset{\leftrightarrow}{l} = \begin{pmatrix} 0 & & & \\ N_1 & 0 & & \\ N_2 & -L_x & 0 & \\ N_3 & L_y & -L_z & 0 \end{pmatrix} \tag{3.2.11}$$

with $l_{ba} = -l_{ab}$. The indices a and b take the values 1 through 4. The operators satisfy the $SO(N)$ commutation relations

$$[l_{ab}, l_{cd}] = i(\delta_{ac}l_{bd} + \delta_{bd}l_{ac} - \delta_{ad}l_{bc} - \delta_{bc}l_{ad}). \tag{3.2.12}$$

From the structure of the matrix $\overset{\leftrightarrow}{l}$ and these commutation relations, it can be seen that the $SO(3)$ subalgebra $\vec{L}$ can be organized in a 3×3 matrix. The minus signs of L_x and L_z can be removed without affecting the $SO(3)$ commutation relations. The elements of an $SO(N)$ algebra can in general be organized in an antisymmetric $N \times N$ matrix.

The following relations hold between an $SO(N)$ algebra $\overset{\leftrightarrow}{L}$ and a vector-representation of this algebra, $\vec{N}$.

$$\begin{aligned} [L_{ab}, N_c] &= i(\delta_{ac}N_b - \delta_{bc}N_a), \\ [N_a, N_b] &= i L_{ab}, \end{aligned} \tag{3.2.13}$$

It follows from these commutation relations that, for any N, an $SO(N)$ algebra and the vector representation of this algebra together form an $SO(N+1)$-algebra, as is demonstrated in the above for $N = 3$ and $N = 2$.

The results of section 1.4.3 can be rederived by expressing the Hamiltonian in terms of the operators $\vec{N}$ and $\vec{L}$ and using an $SO(4)$ coherent state to obtain the path-integral. The kinetic term, eq. (4.4.8), is then of the same from as the one for the XY model, eq. (3.2.7). Again, it couples the $SO(3)$ algebra to the time-derivative of the $SO(3)$-vector.

3.3 $SO(N)$ generalized coherent states

Note that the Hilbert-space in the two-site unit cell is spanned by 4 states, while the relevant group is $SO(4)$. This is also the case for the model considered in the next chapter. In chapter 5, a model is considered where there are 6 states per unit cell and the dynamical algebra is $SO(6)$. We therefore discuss the general case of an $SO(N)$ coherent state in an N-dimensional local Hilbert space. The incorporation of local quantum fluctuations into the coherent state is discussed in the next section. The method which is used to construct the coherent states is set out in the book of Perelomov [18]. The application to this particular problem is, as far as I know, new.

The coherent state is constructed by letting an element of $SO(N)$ act on a reference state

$$|\vec{\Omega}\rangle = R(\vec{\Omega})|\psi_0\rangle\,. \qquad (3.3.1)$$

Since the local Hilbert-space has dimension N, one can take R to be an $N \times N$ orthogonal matrix with unit determinant. The corresponding representation of the $SO(N)$ algebra is given by the $N \times N$ antisymmetric matrices

$$(l_{ab})_{ij} = -i(\delta_{ai}\delta_{bj} - \delta_{aj}\delta_{bi})\,, \qquad (3.3.2)$$

which indeed satisfy the commutation relations eq. (3.2.12).

A general orthogonal matrix R has the form

$$R = \left(\hat{\alpha} \,\middle|\, \hat{\beta} \,\middle|\, \cdots \,\middle|\, \hat{\lambda} \right)\,, \qquad (3.3.3)$$

where the N real N-component unit vectors $\hat{\alpha}$ through $\hat{\lambda}$ are mutually orthogonal. The determinant of this matrix is given by

$$\det R = \varepsilon_{i_1 \cdots i_N}\alpha_{i_1} \cdots \lambda_{i_N}\,, \qquad (3.3.4)$$

where $\varepsilon_{i_1 \cdots i_N}$ is the fully antisymmetric Levi-Civita tensor. An orthogonal matrix has determinant ± 1. From the above expression, it is seen that the condition that R has determinant equal to 1 can be satisfied by correctly choosing the sign of one of the unit vectors.

For a generalized coherent state, the reference state $|\psi_0\rangle$ is chosen to be a maximally polarized eigenvector of one of the elements of the dynamical algebra [18] [2]. The maximally polarized states are optimally classical in the sense that they minimize the uncertainty in the Casimir $\sum_{a<b} l_{ab}^2$

$$\begin{aligned}
\sum_{a<b} \left(\langle l_{ab}^2 \rangle_{\text{max.pol.}} - \langle l_{ab}\rangle_{\text{max.pol.}}^2 \right) &= N - 1 - \sum_{a<b}\langle l_{ab}\rangle_{\text{max.pol.}}^2 \\
&= N - 2 = \text{minimal}\,, \qquad (3.3.5)
\end{aligned}$$

where the first step follows from the definition of the matrices l_{ab}, eq. (3.3.2), while the second is a consequence of the fact that the maximally polarized eigenstates of the matrices l_{ab} have an eigenvalue ± 1. Since the expectation-value of a matrix-operator with respect to any state is bounded by its highest and lowest eigenvalue, $\sum_{a<b}\langle l_{ab}\rangle^2$ is largest when the expectation value is taken with respect to a maximally polarized state, indeed ensuring that the variance of l_{ab} is minimized.

---

[2]For a normal (not generalized) bosonic coherent state, the reference state is the vacuum.

In eq. (3.2.5), the reference state $|S^z = 1\rangle$ is used for the spin 1 XY-model. For the spin-$\frac{1}{2}$ antiferromagnet, one can use the Néel state in the two-site unit cell: $|\uparrow_1\downarrow_2\rangle = |N^z = 1\rangle$. The variance of l_{ab} is invariant under $SO(N)$ transformations, so the coherent state constructed from an optimally classical reference state is itself optimally classical.

The antisymmetric matrix l_{21} has the maximally polarized eigenvectors

$$| \pm 1\rangle = \frac{1}{\sqrt{2}}(1, \pm i, 0, \ldots, 0). \tag{3.3.6}$$

Taking $|\psi_0\rangle = |+1\rangle$, one finds that $SO(N)$ transformations of the form $SO(2) \times SO(N-2)$,

$$D = \begin{pmatrix} \begin{array}{cc|c} \cos\phi & \sin\phi & 0 \\ -\sin\phi & \cos\phi & \\ \hline & & \\ 0 & & SO(N-2) \end{array} \end{pmatrix}. \tag{3.3.7}$$

simply amount to a multiplication of this reference state by a phasefactor $e^{i\phi}$. In order for coherent states with different parameters to be physically distinct, these transformations must be 'divided out'. This is done by multiplying the matrix R from the right with a matrix of the form D, where this transformation is chosen such that R reduces to the following form

$$R' = \begin{pmatrix} \begin{array}{cc|ccc} M_1 & & \gamma_1 & \cdots & \lambda_1 \\ & & \gamma_2 & \cdots & \lambda_2 \\ \hline \alpha_3 & \beta_3 & & & \\ \vdots & \vdots & & M_2 & \\ \alpha_N & \beta_N & & & \end{array} \end{pmatrix}. \tag{3.3.8}$$

where M_1 and M_2 are the triangular matrices

$$
\begin{aligned}
M_1 &= \begin{pmatrix} \alpha_1^{>} & 0 \\ \alpha_2 & \beta_2 \end{pmatrix}, \\[2mm]
M_2 &= \begin{pmatrix} \gamma_3^{>} & & & \\ \gamma_4 & \ddots & & 0 \\ \vdots & \ddots & \ddots & \\ \vdots & & \ddots & \varepsilon_{N-1}^{>} \\ \gamma_N & \cdots & \cdots & \varepsilon_N & \lambda_N \end{pmatrix}.
\end{aligned}
\tag{3.3.9}
$$

The label $>$ indicates that that matrix-element is restricted to values ≥ 0. Since R' is still an $SO(N)$ matrix, the elements α_i through λ_i again form an orthonormal set of N-vectors, and $\det R' = 1$. The above form is obtained by letting the $SO(2)$ transformation

in D rotate the 2-vector (α_1, β_1) into the positive $(1, 0)$-direction, while the $SO(N-2)$ transformation rotates $(\gamma_3, \ldots, \lambda_3)$ into the positive $(1, 0, \ldots, 0)$-direction, $(\gamma_4, \ldots, \lambda_4)$ into the half-plane spanned by $(1, 0, \ldots, 0)$ and $(0, 1, 0, \ldots)$ with the second component positive, etc. .

Note that R' can only be of the form D if it is the unit matrix. This implies that the 'gauge-fixing' procedure used here indeed removes the phase degree of freedom from the coherent state. This state is now given by

$$
\begin{aligned}
|SO(N)\rangle &= \frac{1}{\sqrt{2}} R'(1, i, 0 \ldots) \\
&= \frac{1}{\sqrt{2}}(\alpha_1^>, \vec{\alpha}_{2 \cdots N} + i\hat{\beta}_{2 \cdots N}),
\end{aligned}
\tag{3.3.10}
$$

where $\vec{\alpha}_{2 \cdots N} \cdot \hat{\beta}_{2 \cdots N} = 0$ and $\alpha_1^{>2} + \vec{\alpha}_{2 \cdots N}^2 = \hat{\beta}_{2 \cdots N}^2 = 1$.

For the case of $N = 3$, the following parametrization of R' can be used

$$
\begin{aligned}
\hat{\alpha} &= (\cos\theta, -\sin\theta\cos\phi, -\sin\theta\sin\phi), \\
\hat{\beta} &= (0, -\sin\phi, \cos\phi), \\
\hat{\gamma} &= (-\sin\theta, \cos\theta\cos\phi, \cos\theta\sin\phi),
\end{aligned}
\tag{3.3.11}
$$

where $\phi \in [0, 2\pi]$ and $\theta \in [-\frac{\pi}{2}, \frac{\pi}{2}]$, ensuring that $\alpha_1 \geq 0$. The $SO(3)$ coherent state is characterized by these two angles, which parametrize a point on the unit sphere. It reads

$$
\begin{aligned}
|\theta, \phi\rangle &= \frac{1}{\sqrt{2}}(\alpha_1^>, \alpha_2 + i\beta_2, \alpha_3 + i\beta_3) \\
&= \frac{1}{\sqrt{2}}(\cos\theta, -\sin\theta\cos\phi - i\sin\phi, -\sin\theta\sin\phi + i\cos\phi).
\end{aligned}
\tag{3.3.12}
$$

Transforming to the basis of S^z eigenstates, $|S^z = \pm 1\rangle = \pm\frac{1}{\sqrt{2}}(0, 1, \pm i)$ and $|S^z = 0\rangle = (1, 0, 0)$, we obtain,

$$
\begin{aligned}
|\theta, \phi\rangle &= \frac{1}{2}(1 + \sin\theta)e^{i\phi}|S^z = 1\rangle + \frac{1}{\sqrt{2}}\cos\theta|S^z = 0\rangle \\
&\quad + \frac{1}{2}(1 - \sin\theta)e^{-i\phi}|S^z = -1\rangle,
\end{aligned}
\tag{3.3.13}
$$

which is indeed the expression we obtained earlier for the spin-1 $SO(3)$ coherent state, eq. (3.2.5).

3.4 Local quantum fluctuations

In chapters 4 and 5, models are considered where local quantum fluctuations drive the system to a zero-temperature phase transition where the order parameter vanishes. For these models, the zeroth order approximation to the groundstate in the vicinity of the transition is not a product wavefunction of maximally polarized, 'most classical', states. To describe the long-wavelength physics of such systems, we introduce coherent states for which the local quantum fluctuations are incorporated into the reference state. A measure of the quantum fluctuations in a local state $|\psi_0\rangle$ is the quantity

$$\sum_{a<b} \langle \psi_0 | l_{ab} | \psi_0 \rangle^2 , \tag{3.4.1}$$

which determines the variance of l_{ab}, eq.(3.3.5). Taking for the reference state a superposition of the ± 1 maximally polarized states $\frac{1}{\sqrt{2}}(1, \pm i, 0, \ldots)$

$$|\chi\rangle = (\cos \chi, -i \sin \chi, 0, \ldots) , \tag{3.4.2}$$

where $\chi \in [0, \frac{\pi}{4}]$, one finds

$$\sum_{a<b} \langle \chi | l_{ab} | \chi \rangle^2 = \sin^2 2\chi . \tag{3.4.3}$$

For $\chi = \frac{\pi}{4}$, this reference state is maximally polarized, for $\chi = 0$, it is minimally polarized. The parameter χ tunes the amount of quantum fluctuations in the reference state, varying the uncertainty in the Casimir $\sum_{a<b} l_{ab}^2$ between its highest and its lowest possible value.

For $\chi < \frac{\pi}{4}$, the $SO(N)$ transformations which multiply this state by a phase-factor are of the form $(\pm 1_{2\times 2}) \times SO(N-2)$. These matrices are given by eq. (3.3.7) with $\phi = 0$ or π. The phase-factor by which $|\chi\rangle$ is multiplied is simply ± 1. Since D is more restricted in this case, there are additional degrees of freedom in R'. We now have

$$R' = \begin{pmatrix} \alpha_1^> & \beta_1 & \gamma_1 & \cdots & \lambda_1 \\ \alpha_2 & \beta_2 & \gamma_2 & \cdots & \lambda_2 \\ \alpha_3 & \beta_3 & & & \\ \vdots & \vdots & & M_2 & \\ \alpha_N & \beta_N & & & \end{pmatrix} , \tag{3.4.4}$$

where the constraint $\alpha_1 \geq 0$ eliminates the transformation $|\chi\rangle \rightarrow -|\chi\rangle$ from R.

The coherent state is given by

$$|\hat{\alpha}\hat{\beta}\chi\rangle = R'|\chi\rangle = \cos \chi \hat{\alpha} - i \sin \chi \hat{\beta} . \tag{3.4.5}$$

It can be checked that, for any choice of the unit vectors $\hat{\alpha}$ and $\hat{\beta}$ with $\hat{\alpha} \cdot \hat{\beta} = 0$ and $\alpha_1 \geq 0$, an $SO(N)$ matrix of the form R' can be constructed. There are therefore no additional constraints on these two vectors.

Eq. (3.4.5) is the most general parametrization of a state in an N-dimensional Hilbert space, given that this state should be normalized and that it should differ by more than a phase-factor for different values of the parameters. This is important because we only considered the uncertainty in one particular Casimir as a measure of the quantum fluctuations, while $SO(N)$ has more than a single Casimir for $N > 3$. One could think of the uncertainty in the various Casimirs being tuned independently, which would require the introduction of additional degrees of freedom into the coherent state. Since the state obtained here is the most general one for this type of system, that is not necessary.

It is convenient to parametrize the vectors $\hat{\alpha}$ and $\hat{\beta}$ in the following way

$$
\begin{aligned}
\hat{\alpha} &= (\cos\psi\cos\phi, \sin\psi\cos\phi\,\hat{n} - \sin\phi\,\hat{\bar{n}}), \\
\hat{\beta} &= (\cos\psi\sin\phi, \sin\psi\sin\phi\,\hat{n} + \cos\phi\,\hat{\bar{n}}),
\end{aligned}
\tag{3.4.6}
$$

where $\hat{n}$ and $\hat{\bar{n}}$ are mutually orthogonal unit $(N-1)$ component vectors and $\psi \in [0, \pi/2]$, $\phi \in [-\frac{\pi}{2}, \frac{\pi}{2}]$.

With this parametrization, the following identities hold

$$
\langle N_a \rangle = \sin 2\chi \cos\psi\,\hat{n}, \tag{3.4.7}
$$

$$
\langle L_{ab} \rangle = \sin 2\chi \sin\psi \left(\hat{\bar{n}}_a \hat{n}_b - \hat{n}_a \hat{\bar{n}}_n \right), \tag{3.4.8}
$$

$$
\hat{n}_a = -\frac{1}{\sin 2\chi \sin\psi} \sum_b \langle L_{ab} \rangle\,\hat{\bar{n}}_b, \tag{3.4.9}
$$

where $L_{ab} = l_{1+a,1+b}$ is an $SO(N-1)$-algebra and $N_a = l_{1+a,1}$ is the vector representation of this algebra.

If the system has a spontaneously broken $SO(N-1)$ global symmetry, $\langle N_a \rangle$ is its order-parameter. The angle χ describes the reduction of this order-parameter by local quantum fluctuations, $\hat{n}$ and ψ parametrize the response to an external field and the unit vector $\hat{\bar{n}}$ determines the direction of the order parameter.

In order to construct the path-integral, the unit-operator has to be resolved in terms of the overcomplete coherent state basis. This resolution is given by

$$
1 = \frac{2N}{S_N S_{N-1}} \int d\hat{\alpha} d\hat{\beta}\, \delta(\hat{\alpha} \cdot \hat{\beta})\, \Theta(\alpha_1)\, |\hat{\alpha}\hat{\beta}\chi\rangle\langle\hat{\alpha}\hat{\beta}\chi|, \tag{3.4.10}
$$

where S_N is the surface of a sphere in N-dimensions and Θ is a step-function

$$
\Theta(\alpha_1) = \begin{cases} 0, & \alpha_1 < 0 \\ 1, & \alpha_1 \geq 0 \end{cases} \tag{3.4.11}
$$

Note that this resolution works for any value of χ. Of course, one can add an integration $\int_0^{\pi/4} d\chi$ and multiply the prefactor by $4/\pi$, that way including the χ-fields as dynamical parameters in the path-integral.

The overlap between two coherent states satisfies, to lowest order in the difference between their parameters

$$\langle \hat{\alpha} \hat{\beta} \chi | \hat{\alpha}' \hat{\beta}' \chi' \rangle \;=\; 1 + i \sin 2\chi \left[\delta \phi + \frac{1}{2} \sin \psi \left(\hat{\bar{n}} \cdot \delta \vec{n} - \vec{n} \cdot \delta \hat{\bar{n}} \right) \right], \qquad (3.4.12)$$

where $\vec{n} = \sin \psi \, \hat{n}$.

Constructing the coherent state path-integral in the way discussed in section 1.4.2, one obtains the kinetic term from the overlap given above

$$
\begin{aligned}
S_{\text{kin.}} &= \int_0^{\beta \hbar} d\tau \sum_i \left(i \sin 2\chi_i \left[\partial_\tau \phi_i + \frac{1}{2} \sin \psi_i \left(\hat{\bar{n}} \cdot \partial_\tau \vec{n} - \vec{n} \cdot \partial_\tau \hat{\bar{n}} \right) \right] \right) \\
&= \int_0^{\beta \hbar} d\tau \sum_i \left(i \sin 2\chi_i \, \partial_\tau \phi_i + i \sum_{ab} \langle L_{ab} \rangle_i \, \partial_\tau \hat{\bar{n}}_i^a \hat{\bar{n}}_i^b \right).
\end{aligned}
\qquad (3.4.13)
$$

The second term has the same form as for the $SO(3)$ and $SO(4)$ generalized coherent states, eq.s (3.2.7) and (1.4.17). It describes the transversal dynamics of the order parameter. The reduction of the order-parameter enters this term through a prefactor $\sin 2\chi$. The first term describes the longitudinal dynamics of the order parameter. It couples χ to the time-derivative of ϕ: the additional parameter which enters this coherent state because of the non-maximally polarized reference state.

The coherent state introduced here is a generalization of the generalized coherent state for a system with N degrees of freedom per unit cell and a dynamical algebra $SO(N)$. It describes the reduction of the order-parameter by local quantum fluctuations as well as its rotational degrees of freedom. A coherent state of this type can have applications in systems which undergo quantum disordering transitions. In the next chapter, the long wavelength effective action for the Heisenberg bilayer model is derived with the aid of this coherent state. In chapter 5, it is used as part of the ansatz wavefunction in a variational Hartree-Fock analysis of a system with phase and spin degrees of freedom. In the same chapter, the coherent state with $N = 5$ is applied to the construction of a path-integral for an $SO(5)$ symmetric model.

4 The bilayer Heisenberg model

4.1 A two-dimensional spin liquid without frustration

The study of non-classical collective quantum states of matter is a central theme of modern condensed matter physics. Despite the successes in 1+1 dimensions, it has proven difficult to address these matters in higher dimensions. Either the minus-sign problem intervenes (as in, e.g., the t-J model and frustrated spin models), or the tendency towards classical order is too strong (e.g. unfrustrated spin models). The bilayer Heisenberg model is special in this regard. It consists of two antiferromagnetic Heisenberg spin-systems, coupled by an inter-layer antiferromagnetic interaction. The system undergoes a zero temperature spin-disordering transition as a function of the inter-layer to intra-layer spin-spin interaction ratio. This model is sign-free, and convincing numerical evidence exists showing that its long-wavelength behavior is governed by the $O(3)$ quantum non-linear sigma model (QNLS) with tunable bare coupling constant g [56].

The attempts to formulate a spin-wave type description of the bilayer transition have not been very successful [57]. Spin-wave theory predicts that the average spin reaches the QNLS critical value $S_c \simeq .26$ at an inter-layer to intra-layer coupling ratio of about 7, which is much larger than the 2.56 found from numerical work and series expansions [59][60]. A modified spin-wave analysis [58], which includes elements of the Schwinger-boson mean-field theory, finds a *first order* transition at a ratio of 4.24, while the transition described by the QNLS is second order. Approaching the transition from the disordered side, Millis and Monien find a second order transition at a critical ratio of 4.48 from a Schwinger boson mean field analysis [2].

Chubukov and Morr (CM) made the key observation that, in order to obtain a good saddle-point description, the severe local (interplanar) fluctuations have to be integrated out first [61]. Spin-wave theory treats these fluctuations on the same level as the higher-dimensional in-plane fluctuations, while the Schwinger-boson mean field theory and the modified spin-wave method deal with the tendency to form inter-layer singlet states only approximately. Already at the mean field level, the theory of CM yields a critical ratio of 4, showing that the interplanar fluctuations were indeed underestimated by the other methods.

Using a new type of coherent state, we derive a path-integral description for the bilayer model in which the mean field solution of CM appears as a uniform saddle-point configuration. Integrating out the fluctuations around this saddle-point, an effective long-wavelength action is obtained, which is a QNLS with a coupling constant that depends on the relative magnitude of the two spin-spin interactions. The coupling constant is found to diverge at the mean-field transition, which implies that transversal fluctuations push the transition to a smaller inter-layer interaction in any finite dimension. The dependence of the QNLS cou-
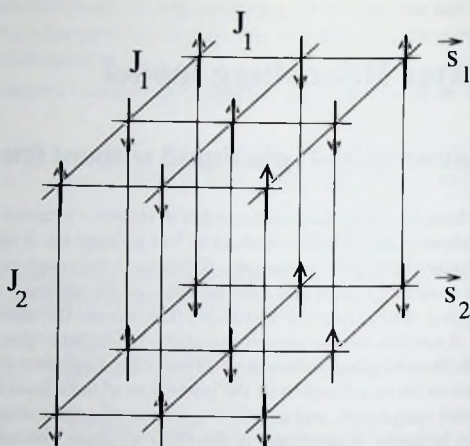
Figure 4-1. The bilayer system.

pling constant on the ratio of the two interactions is found to agree reasonable well with the results of an Ising series expansion [60].

4.2   The singlet-triplet basis

The bilayer model consists of two coupled square-lattice Heisenberg spin systems (fig. 4-1). It is a generalization of the two-leg spin-ladder to the case $d = 2$. In the following, the generalization to arbitrary dimensions is considered, although the terminology of the bilayer system is used (they will be called 'layers' rather than 'hypercubic lattices'). The $d \rightarrow \infty$ system corresponds to the classical limit at $T = 0$. This limit will be used to control the semi-classical expansion.

The bilayer Hamiltonian is given by

$$\mathcal{H} = J_1 \sum_{<ij>} (\vec{s}_{1i} \cdot \vec{s}_{1j} + \vec{s}_{2i} \cdot \vec{s}_{2j}) + J_2 \sum_i \vec{s}_{1i} \cdot \vec{s}_{2i} - \vec{H} \cdot \sum_i (\vec{s}_{1i} + \vec{s}_{2i}) . \qquad (4.2.1)$$

The summation $< ij >$ runs over the bonds in a single layer. The $S = \frac{1}{2}$ spins in layer one and two are denoted by $\vec{s}_{1i}$ and $\vec{s}_{2i}$. We focus on the case where both the inter-layer coupling J_2 and the intra-layer interaction J_1 are antiferromagnetic.

The zero-temperature, zero magnetic field phase diagram of this system is determined by the ratio $\alpha = \frac{J_2}{J_1 z}$, where $z = 2d$ is the coordination number. Note that we scale the ratio with the dimension of the 'layers'. With this scaling, the mean field transition occurs at $\alpha = 1$, giving the result $(J_2/J_1)_c = 4$ for the case of two dimensions, discussed above. The behavior at the two limiting values of α is easily understood. For $\alpha \downarrow 0$, the layers decouple. The system has a Néel ordered state in each layer, with the order parameter on the two planes antiparalel (fig. 4-1). In the $\alpha \rightarrow \infty$ limit, the different *sites* decouple and each spin-pair $(\vec{s}_{i1}, \vec{s}_{i2})$ forms a singlet state. This state is a simple example of a quantum spin liquid. It has a gapped spectrum and exhibits no spontaneous breaking of the global rotational symmetry of eq. (4.2.1). At some intermediate value of α, a phase transition has to occur from the Néel ordered state to the spin liquid.

As Chubukov and Morr pointed out, a correct semi-classical analysis of this model starts by integrating out exactly the dangerous zero-dimensional fluctuations between the layers. The Hamiltonian is then written in terms of the four local eigenstates of the $J_1 = 0$ system: the spin singlet $|A\rangle$ and the triplet $|1\rangle, |0\rangle, |-1\rangle$. This is done by introducing the total spin $\vec{S}$ and the Néel operator $\vec{\tilde{S}}$ for every pair $(\vec{s}_{1i}, \vec{s}_{2i})$

$$\vec{S}_i = \vec{s}_{i1} + \vec{s}_{i2} \; ; \; \vec{\tilde{S}} = \vec{s}_{i1} - \vec{s}_{i2} \, . \qquad (4.2.2)$$

These operators can be expressed in terms of the hard-core bosons creating/annihilating the two-spin states

$$
\begin{aligned}
A^\dagger &= \frac{1}{\sqrt{2}}(c_{1\downarrow}^\dagger c_{2\uparrow}^\dagger - c_{1\uparrow}^\dagger c_{2\downarrow}^\dagger) \, , \\
B_1^\dagger &= c_{1\uparrow}^\dagger c_{2\uparrow}^\dagger \, , \\
B_0^\dagger &= \frac{1}{\sqrt{2}}(c_{1\downarrow}^\dagger c_{2\uparrow}^\dagger + c_{1\uparrow}^\dagger c_{2\downarrow}^\dagger) \, , \\
B_{-1}^\dagger &= c_{1\downarrow}^\dagger c_{2\downarrow}^\dagger \, ,
\end{aligned}
\qquad (4.2.3)
$$

which satisfy the local constraint $A^\dagger A + \sum_m B_m^\dagger B_m = 1$ (half-filling). They are given by

$$
\begin{aligned}
S^z &= B_1^\dagger B_1 - B_{-1}^\dagger B_{-1} \, , \\
S^+ &= \sqrt{2}\left(B_1^\dagger B_0 + B_0^\dagger B_{-1} \right) \, , \\
\tilde{S}^z &= -A^\dagger B_0 - B_0^\dagger A \, , \\
\tilde{S}^+ &= \sqrt{2}\left(B_1^\dagger A - A^\dagger B_{-1} \right) \, .
\end{aligned}
\qquad (4.2.4)
$$

$\vec{S}$ acts as a spin-1 operator on the triplet sector. $\vec{\tilde{S}}$ generates singlet-triplet transitions. In terms of these operators, the Hamiltonian reads

$$\mathcal{H} = \frac{1}{2}J_1 \sum_{<ij>} (\vec{S}_i \cdot \vec{S}_j + \vec{\tilde{S}}_i \cdot \vec{\tilde{S}}_j) + \frac{1}{4}J_2 \sum_i \left(\vec{S}_i^2 - \vec{\tilde{S}}_i^2 \right) - \vec{H} \cdot \sum_i \vec{S}_i \, . \qquad (4.2.5)$$

where $\bar{S}_i^2 - \bar{\bar{S}}_i^2 = 1 - 4A_i^\dagger A_i$ measures the singlet-density at site i.

The Néel operator transforms as a vector under $\vec{S}$. The six operators $\vec{S}$ and $\vec{\bar{S}}$ form a representation of the $SO(4)$ algebra

$$[S^a, S^b] = i\varepsilon_{abc}S^c, \tag{4.2.6}$$

$$[\bar{S}^a, \bar{S}^b] = i\varepsilon_{abc}S^c, \tag{4.2.7}$$

$$[S^a, \bar{S}^b] = i\varepsilon_{abc}\bar{S}^c. \tag{4.2.8}$$

At the $J_2 = H = 0$ point (two decoupled layers) the system has a global $SO(4)$ invariance. It is broken for any finite J_2, leaving only an invariance under the $SU(2)$ subgroup generated by $\vec{S}$.

4.3   Mean field analysis

The Néel ordered phase is characterized by the order parameter $\vec{m} = \frac{1}{N} \sum_i \eta_i \langle \vec{\bar{S}}_i \rangle$, where η_i is the staggering-factor $(-1)^{\sum_{l=1}^d i_l}$. In the mean-field approximation, the Hamiltonian is reduced to a single-site form by replacing the environment of each site by a uniform state with staggered magnetization $\vec{m}$. The single-site Hamiltonian is diagonalized and $\vec{m}$ is solved from the self-consistency condition $\langle \vec{\bar{S}}_i \rangle = \eta_i \vec{m}$, where the average is taken with respect to the mean-field groundstate. This approximation becomes exact for $d \to \infty$ and in the limit of infinite range interactions [62], since in both these limits the two spins on a site are truly interacting with the average of the spins in the rest of the system.

We write $\vec{\bar{S}}$ as a sum of an order-parameter component and a fluctuating part, and neglect terms of the form (fluctuation)^2. The same is done for $\vec{S}$. For the moment we focus on $H = 0$, where $\vec{S}$ has no non-fluctuating component. Assuming the staggered magnetization to be polarized along the z-direction, we arrive at the mean field decoupling

$$\vec{\bar{S}}_i \cdot \vec{\bar{S}}_j \rightarrow \eta_i \bar{m} \left(\bar{S}_j^z - \bar{S}_i^z \right) + \bar{m}^2,$$

$$\vec{S}_i \cdot \vec{S}_j \rightarrow 0. \tag{4.3.1}$$

Note that the J_2-term is not decoupled, since it is already a single-site term in the singlet-triplet basis.

The resulting Hamiltonian is diagonalized. This yields

$$\mathcal{H}^{MF} = \frac{N}{4} \left(J_2 + J_1 z \bar{m}^2 \right) + \frac{1}{2} \sum_i \left(\left[-J_1 z \sin 2\chi \bar{m} - 2J_2 \cos^2 \chi \right] n_{Gi} \right.$$
$$\left. + \left[J_1 z \sin 2\chi \bar{m} - 2J_2 \sin^2 \chi \right] n_{Ei} \right), \tag{4.3.2}$$

where G and E are superpositions of the zero-magnetization hard-core bosons

$$
\begin{aligned}
G_i &= \eta_i A_i \cos \chi - B_{0i} \sin \chi , \\
E_i &= \eta A_i \sin \chi + B_{0i} \cos \chi ,
\end{aligned}
\tag{4.3.3}
$$

and where χ is fixed by the diagonalization condition

$$
J_1 z \bar{m} \cos 2\chi = J_2 \sin 2\chi .
\tag{4.3.4}
$$

The self-consistency requirement yields $\bar{m} = \sin 2\chi$. Inserting this into eq. (4.3.4), we obtain the condition

$$
\sin 2\chi (\cos 2\chi - \alpha) = 0 .
\tag{4.3.5}
$$

The spin-liquid phase has $\sin 2\chi = 0$. Its mean-field groundstate is given by $\prod_i A_i^\dagger |\text{vac}\rangle$, which is the exact $\alpha \to \infty$ state discussed before. The Néel ordered state has $\bar{m} = \sqrt{1 - \alpha^2}$. Its groundstate is a superposition of the spin singlet and the zero-magnetization triplet state.

$$
G_i = \eta_i \sqrt{\frac{1 + \alpha}{2}} A_i - \sqrt{\frac{1 - \alpha}{2}} B_{0i} .
\tag{4.3.6}
$$

At $\alpha = 0$, this gives a fully ordered Néel state on both layers. As α increases, the single-layer magnetization $\langle s_{1/2\,i}^z \rangle = \frac{1}{2}\bar{m}$ is reduced through an increase of the singlet component in the groundstate, but the Néel order remains. At $\alpha = 1$, a second-order transition occurs from the ordered state to the spin liquid.

The same analysis can be repeated in the presence of an external magnetic field perpendicular to the direction of ordering. One then allows for a non-fluctuating component $\langle S^x \rangle \neq 0$ of the total spin ($\langle S^z \rangle$ has to be zero since $\langle \vec{S} \rangle \perp \langle \vec{\bar{S}} \rangle$). In the small H limit, this calculation yields the mean field expression for the perpendicular susceptibility $\chi_\perp$

$$
\chi_\perp = \lim_{H \downarrow 0} \frac{\langle S^x \rangle}{H} = \frac{\bar{m}^2}{J_1 z \bar{m}^2 + 2 J_2 \langle n_A \rangle} = \frac{1 - \alpha}{J_1 z} .
\tag{4.3.7}
$$

For values of α close to the transition, the low-energy deformations of the spin-order are slow rotations of $\langle \vec{\bar{S}}_i \rangle$. The mean field stiffness for these fluctuations is given by [10]

$$
\rho_s = \frac{1}{2} J_1 |\langle \vec{\bar{S}} \rangle|^2 = \frac{1}{2} J_1 (1 - \alpha^2) ,
\tag{4.3.8}
$$

which yields for the spin-wave velocity

$$
c_s = \sqrt{\frac{\rho_s}{\chi_\perp}} = J_1 \sqrt{\frac{z}{2}(1 + \alpha)} .
\tag{4.3.9}
$$

Note that it is not correct to interpret the bilayer system as a single-layer antiferromagnet with $S = \frac{1}{2}\bar{m} < \frac{1}{2}$ and derive the transition in the presence of transversal spin-fluctuations from the critical spin-value $S_c \simeq \frac{1}{3}$ [57]. If this interpretation would hold, the mean-field perpendicular susceptibility should be independent of α, since it is independent of S for the single-layer system. Instead, one should compare the QNLS coupling constant $g = (\rho_s \chi_\perp)^{-1}$ to its critical value in order to find the transition. In section 1.4.3 we show this explicitly by mapping the bilayer model onto the QNLS.

To conclude, we note that the above mean-field groundstate becomes an exact eigenstates in the limit $d \to \infty$. To see this, we write $J_1 = \bar{J}_1 z$ and take the limit $d \to \infty$ while keeping $\bar{J}_1$ constant (this ensures a finite energy per site). The variation of the energy in the mean field groundstate is then given by

$$\langle \mathcal{H}^2 \rangle - \langle \mathcal{H} \rangle^2 = \Delta_0(J_1, J_2, \chi) + \mathcal{O}(d^{-1}). \tag{4.3.10}$$

Imposing $\Delta_0 = 0$ yields the mean field condition eq. (4.3.5), which therefore becomes the exact diagonalization condition for $d \to \infty$.

4.4   The bilayer path-integral

The spin-coherent state path integral eq. (1.4.13) is not a good starting point for the derivation of a QNLS from the bilayer model. In the basis used to derive this path-integral, the spin singlet state corresponds to a complicated space-time configuration of counter-precessing classical spins. As a result, the mean field groundstate in the Néel ordered phase, which interpolates between the $S = \frac{1}{2}$ Néel state and the spin singlet, does not correspond to a uniform, time-independent configuration. This makes it hard to identify and integrate out the fluctuations around the ordered state.

This problem is avoided when the coherent state constructed in chapter 3 is used. The parameter χ introduced there to tune the quantum correlations in the coherent state is the same as the χ appearing here in the mean-field groundstate. The bilayer model has a dynamical algebra $SO(4)$ and 4 states per unit cell. The appropriate coherent state is therefore given by eq. (3.4.5) with $N = 4$.

From eq. (3.4.9), we find that the coherent state indeed reproduces the mean-field degrees of freedom of the bilayer model

$$\begin{aligned}
\langle \vec{\bar{S}} \rangle &= \sin 2\chi \cos \psi \hat{\bar{n}}, \\
\langle \vec{S} \rangle &= \sin 2\chi \sin \psi \hat{n} \times \hat{\bar{n}}, \\
\langle n_A \rangle &= \cos^2 \psi (\cos^2 \chi \cos^2 \phi + \sin^2 \chi \sin^2 \phi),
\end{aligned} \tag{4.4.1}$$

where $\hat{\bar{n}}$ and $\hat{n}$ are mutually orthogonal 3-component vectors. The parameter χ determines the reduction of the magnitude of $\langle \vec{s}_{1i} \rangle$ and $\langle \vec{s}_{2i} \rangle$ by inter-layer quantum fluctuations. The

angle $\psi \in [0, \frac{\pi}{2}]$ fixes their relative orientation, which determines the ratio $|\langle \vec{\bar{S}} \rangle| / |\langle \vec{S} \rangle|$. It was noted in chapter 3 that the special choice for the reference state introduced an extra degree of freedom into the $SO(4)$ matrix R'. This degree of freedom is related to the transformation:

$$
\begin{aligned}
| \uparrow_1 \downarrow_2 \rangle &\rightarrow e^{i\phi} | \uparrow_1 \downarrow_2 \rangle, \\
| \downarrow_1 \uparrow_2 \rangle &\rightarrow e^{-i\phi} | \downarrow_1 \uparrow_2 \rangle.
\end{aligned}
\tag{4.4.2}
$$

For $\chi = \pi/4$, this transformation amounts to a multiplication of $|\psi_0\rangle$ by a phase-factor and we have to set $\phi = 0$. In the path-integral, the angle ϕ drives the dynamics of χ and vice-versa.

The bilayer path-integral can be written down by following the same procedure as in section 1.4.2). It is given by

$$
\mathcal{Z} = \int \left(\prod_i \frac{d\chi_i \, d^4\hat{\alpha}_i \, d^4\hat{\beta}_i}{\pi^4} \Theta(\alpha_i^1) \delta(\hat{\alpha}_i \cdot \hat{\beta}_i) \right) e^{-S_{\text{bilayer}}},
\tag{4.4.3}
$$

with the Euclidian action

$$
-S_{\text{bilayer}} = \int_0^{\beta\hbar} d\tau \, (i\Phi + \mathcal{V}).
\tag{4.4.4}
$$

The potential term $\mathcal{V}$ follows from the expectation-value of the bilayer Hamiltonian with respect to the coherent state, which can be obtained by using the results in eq. (4.4.1) on the Hamiltonian eq. (4.2.5)

$$
\begin{aligned}
\mathcal{V} = \; & \frac{1}{2} J_1 \sum_{\langle ij \rangle} \sin 2\chi_i \sin 2\chi_j \left(\vec{O}_i \cdot \vec{O}_j + \vec{\bar{n}}_i \cdot \vec{\bar{n}}_j \right) \\
& + \frac{1}{4} J_2 \sum_i \cos^2 \psi \, (\cos^2 \chi \cos^2 \phi + \sin^2 \chi \sin^2 \phi),
\end{aligned}
\tag{4.4.5}
$$

where

$$
\vec{O} = \frac{1}{\sin 2\chi} \langle \vec{S} \rangle = \vec{n} \times \vec{\bar{n}},
\tag{4.4.6}
$$

and where

$$
\vec{n} = \sin \psi \hat{n} \; ; \; \vec{\bar{n}} = \cos \psi \hat{\bar{n}}.
\tag{4.4.7}
$$

The kinetic term Φ follows from the overlap between coherent states on neighboring time-slices. It is given by eq. (3.4.13) with $N = 4$, which yields

$$
\Phi = -\sum_i \sin 2\chi_i \left(\partial_\tau \phi + \vec{O}_i \cdot \partial_\tau \hat{\bar{n}} \times \hat{\bar{n}} \right).
\tag{4.4.8}
$$

It is interesting to compare this expression to the one for the antiferromagnetic spin-chain, after expansion to lowest order in the average spin $\bar{l}$ eq. (1.4.17). Modulo factors 2, the Néel moment $\hat{m}$ is equivalent to $\bar{\bar{n}}$ here and the average spin to $\bar{O}$. The first feature we note is the absence of a coupling between the average spin and the gradient of the order-parameter in eq. (4.4.5). It is this coupling which gives rise to the topological term in the long-wavelength action for the antiferromagnetic spin-chain. Here, it is cancelled between the two layers. As was discussed in section 1.4.3, this is a well-known effect for two-leg ladders, which are described by the above action with $d = 1$. The existing analyses were in principle restricted to the case of weak inter-leg coupling. Here, the inter-leg quantum fluctuations are included exactly. We find that the cancellation still occurs at large J_2, because $\langle \vec{s}_{1i} \rangle$ and $\langle \vec{s}_{2i} \rangle$ are necessarily reduced by the same amount due to the inter-layer singlet formation.

The kinetic term in eq. (1.4.17) has the same form as eq. (4.4.8), except that here we have $\sin 2\chi$ instead of S and there is an additional term $\sin 2\chi \, \partial_\tau \phi$, which drives the dynamics of χ. The kinetic term therefore describes an antiferromagnet with a dynamic spin-size S.

4.5   Collective modes

To investigate the collective modes of the bilayer model, the action eq. (4.4.4) is expanded around the mean-field groundstate and the Euler-Lagrange equations are solved. For the case of the ordered state, we set

$$
\begin{aligned}
\vec{O}_i &= \varepsilon(\bar{O}_i^{xy}, \varepsilon\bar{O}_i^z), \\
\vec{\bar{n}}_i &= \eta_i\sqrt{1 - \vec{O}_i^2}(\varepsilon\bar{\bar{n}}_i^{xy}, \sqrt{1 - \varepsilon^2\bar{\bar{n}}_i^{xy\,2}}), \\
\cos^2\psi_i &= 1 - O_i^2,
\end{aligned}
\tag{4.5.1}
$$

where $\varepsilon \ll 1$ is the expansion parameter and where η_i is a staggering factor. The conditions $\vec{O} \cdot \vec{\bar{n}} = 0$ and $\vec{O}^2 + \vec{\bar{n}}^2 = 1$ are satisfied to lowest order in ε. Furthermore, we set $\chi = \chi_0(\alpha) + \varepsilon\bar{\chi}$ and $\phi = \varepsilon\bar{\phi}$. The action is expanded to second order in ε. The linear terms drop out, since the mean field state corresponds to a saddle point configuration of the action.

We find two sets of equations describing transversal and one describing longitudinal fluctuations. The transversal fluctuations satisfy (we have switched to real time)

$$
\begin{aligned}
\sin 2\chi_0\eta_i\partial_t\bar{\bar{n}}_i^x &= \frac{1}{2}J_1\sin^2 2\chi_0\left(z\bar{O}_i^y + \sum_\delta O_{i+\delta}^y\right) + 2J_2\cos^2\chi_0\bar{O}^y, \\
\sin 2\chi_0\eta_i\partial_t\bar{O}_i^y &= -\frac{1}{2}J_1\sin^2 2\chi_0\left(z\bar{\bar{n}}_i^x + \sum_\delta \bar{\bar{n}}_{i+\delta}^x\right),
\end{aligned}
\tag{4.5.2}
$$

where $\sum_\delta$ runs over all neighboring sites. The second set follows from $\bar{\bar{n}}^x \rightarrow \bar{\bar{n}}^y$, $\bar{O}^y \rightarrow -\bar{O}^x$.

The longitudinal modes follow from

$$\cos 2\chi_0 \partial_t \bar{\chi}_i = \cos 2\chi_0 J_2 \bar{\phi} , \tag{4.5.3}$$

$$\cos 2\chi_0 \partial_t \bar{\phi}_i = J_1 \left(z \sin^2 2\chi_0 \bar{\chi}_i - \cos^2 2\chi_0 \sum_\delta \bar{\chi}_{i+\delta} \right) + J_2 \cos 2\chi_0 \bar{\chi}_i .$$

The collective modes are obtained by a Fourier-transformation in the time and the space coordinates. Using $\cos 2\chi_0 = \alpha$ (ordered phase), we obtain

$$\omega_k^{\text{trans}} = \frac{\varsigma_1}{2} J_1 z \sqrt{(1 - \varsigma_2 \gamma_k)[(1 + \varsigma_2 \gamma_k) + 2\alpha + \alpha^2 (1 - \varsigma_2 \gamma_k)]} , \tag{4.5.4}$$

$$\omega_k^{\text{long}} = \varsigma_1 J_1 z \sqrt{1 - \varsigma_2 \alpha^2 \gamma_k^2} . \tag{4.5.5}$$

where

$$\gamma_k = \frac{1}{z} \sum_{\bar{\delta}} e^{i\vec{k} \cdot \bar{\delta}} = \frac{1}{d} \sum_{\bar{\delta} > 0} \cos(\vec{k} \cdot \bar{\delta}) , \tag{4.5.6}$$

and where $\varsigma = \pm 1$.

The spectrum in the disordered phase is obtained in a similar way by evaluating the equations of motion of the longitudinal sector with $\chi_0 = 0$. For the transversal sector, the expansion around the saddle-point configuration becomes different as compared to the ordered state, since there is no preferred direction for $\bar{\hat{n}}$ in the spin-liquid phase. However, the resulting spectrum is the same as for the longitudinal sector, since the disordered ground-state is $SO(3)$ symmetric,

$$\omega_k^{\text{liquid}} = \varsigma_1 J_1 z \sqrt{\alpha(\alpha - \varsigma_2 \gamma_k)} . \tag{4.5.7}$$

The mode-spectrum is shown in fig. 4-2.

In the ordered phase, the bilayer model has acoustic modes at $\vec{k} = (0, 0)$ and $\vec{k} = (\frac{\pi}{a}, \frac{\pi}{a})$ $(d = 2)$. These are the Goldstone modes of the system. Their dispersion $\partial \omega_k / \partial k$ is given by the mean-field expression for the spin-wave velocity eq. (4.3.9). A mode-softening occurs for $\alpha \downarrow 0$, where the Goldstone modes become two-fold degenerate due to the decoupling of the layers.

The longitudinal mode is dispersionless at the SO(4) symmetric point $\alpha = 0$. It has a large gap $\Delta = J_1 z$, which is the energy cost of flipping one $\vec{\bar{S}}$ in the ordered groundstate. As α increases, the mode acquires a dispersion. At the transition to the disordered state, its gap closes and the longitudinal and transversal modes become degenerate.

In the spin-liquid phase, the system has a gap $\Delta \propto \sqrt{\alpha - 1}$ and one, three-fold degenerate mode is found, corresponding to propagating triplet excitations.
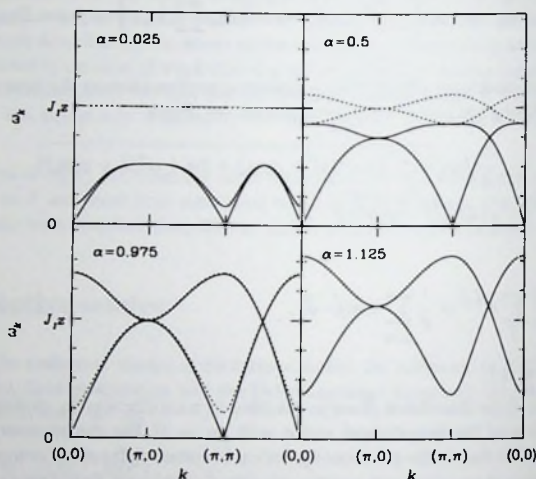
Figure 4-2. The mode-spectrum of the bilayer model. Dashed lines are longitudinal modes.

4.6 Long-wavelength effective action

In the vicinity of the order-disorder transition, the low-energy fluctuations of the ordered state are transversal fluctuations of the order-parameter $\langle \vec{S} \rangle$. The χ-fluctuations are gapped and do not couple to the transversal modes, we therefore omit them from the low-energy description. The ψ-fluctuations ($\langle \vec{S} \rangle \leftrightarrow \langle \vec{S} \rangle$) are at finite wavenumbers away from $(0,0)$ and (π, π). An effective low-energy action can be obtained by integrating out these fluctuations.

The procedure is very much the same as for the single-layer antiferromagnet (section 1.4.3). We assume that Néel order is established locally, which means that $|\vec{n}_i| \sim 1$, and $|\vec{O}_i| \ll 1$. This assumption *does not hold for* $\alpha \ll 1$, where the layers decouple. In that region, it is not correct to identify $\langle \vec{S} \rangle$ as the local order-parameter. Rather, the long-wavelength physics

should be described by two weakly coupled $S = \frac{1}{2}$ non-linear sigma models, where the order-parameters are defined in the planes. The present description is the correct one in the neighborhood of the order-disorder transition.

The parameters χ and ϕ are replaced by their saddle-point values, since their fluctuations are gapped. The fields $\hat{\bar{n}}_i$ are staggered: $\hat{\bar{n}}_i \rightarrow \eta_i \hat{\bar{n}}_i$. The action is expanded to second order in O_i and a term $(\vec{O}_i - \vec{O}_j)^2$, which acquires a prefactor a^2 in the continuum limit, is neglected. This yields

$$
S = \int_0^{\beta\hbar} \left[-i\sqrt{1-\alpha^2} \sum_i O_i \cdot \partial_\tau \hat{\bar{n}}_i \times \hat{\bar{n}}_i \right. \tag{4.6.1}
$$
$$
\left. + J_1(1-\alpha^2) \sum_{<ij>} \left(\frac{a^2}{4}(\partial_{i\rightarrow j}\hat{\bar{n}}_i)^2 + \vec{O}_i^2 \right) + \frac{1}{2}J_1 z\alpha(1+\alpha) \sum_i \vec{O}_i^2 + E_0 \right],
$$

where $a\partial_{i\rightarrow j}\hat{\bar{n}}_i = \hat{\bar{n}}_j - \hat{\bar{n}}_i$ and E_0 is the saddle-point energy. The $\vec{O}_i$ are integrated out by solving them from Euler-Lagrange equation

$$
\vec{O}_i = i\sqrt{\frac{1-\alpha}{1+\alpha}} \frac{\partial_\tau \hat{\bar{n}}_i \times \hat{\bar{n}}_i}{J_1 z}. \tag{4.6.2}
$$

Taking the continuum-limit $\sum_i \rightarrow a^{-d} \int d^d x$ and omitting constant terms, we obtain the QNLS action

$$
S = \frac{1}{2} \int_0^{\beta\hbar} \left[\chi_\perp^0 (\partial_\tau \hat{\bar{n}}(\vec{x},\tau))^2 + \rho_s^0 (\vec{\nabla}\hat{\bar{n}}(\vec{x},\tau))^2 \right], \tag{4.6.3}
$$

where the bare stiffness and susceptibility are given by

$$
\chi_\perp^0 = a^{-d} \frac{1-\alpha}{J_1 z},
$$
$$
\rho_s^0 = a^{2-d} \frac{1}{2} J_1(1-\alpha^2), \tag{4.6.4}
$$

which are the values of ρ_s and $\chi_\perp$ obtained from the mean field analysis, eq.s (4.3.7) and (4.3.8). The QNLS coupling constant is given by

$$
g_0 = \frac{1}{\sqrt{\chi_\perp \rho_s}} = \frac{2a^{d-1}\sqrt{d}}{(1-\alpha)\sqrt{1+\alpha}}, \tag{4.6.5}
$$

which is the central result of this chapter.

We find that the order-disorder transition of the bilayer model is in the universality-class of the O(3) QNLS, in agreement with the Monte Carlo results of Sandvick and Scalapino.
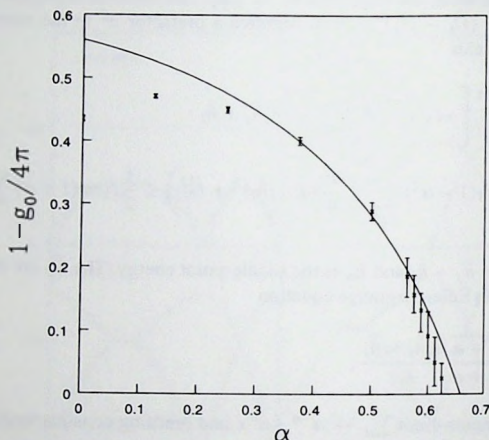
Figure 4-3. The reduction-factor $1 - \frac{g_0}{4\pi}$ versus α (this is the factor by which the bare stiffness and susceptibility get renormalized at the 1-loop level, eq. (1.3.9)). The crosses are results obtained from an Ising-expansion for the case two dimensions. The line is the mean-field estimate, fitted to agree with the Ising-expansion at $J_2 = 1.5J_1 \Rightarrow \alpha = 0.375$.

The coupling constant diverges at $\alpha = 1$. This implies that the transition to the disordered phase occurs at an $\alpha_c < 1$ in any finite dimension, since the mean field transition only coincides with the $g_0 = g_c$-point in the limit $d \rightarrow \infty$, where $\frac{g_c}{g_0(\alpha=0)} \rightarrow \infty$.

As was pointed out in section 1.3.4, the bare coupling constant obtained in the semi-classical approach is quite inaccurate for the case of small S and low dimensionality. One can however hope that the α-dependence of g_0 obtained in this way is still reasonable. To check this, the one-loop relation eq. (1.3.10) is used to calculate $g_0(\alpha)$ from the renormalized spin-wave velocity and perpendicular susceptibility. We use the Ising-expansion results of Zheng-Weihong [60] for these quantities.

As discussed above, the QNLS-action obtained here describes the bilayer at relatively large inter-layers couplings, where the low-energy physics is dominated by transversal fluctuations of $\hat{\vec{n}}$. The expression for g_0 is therefore not expected to be correct for small α. To compare the α-dependence found here to the results of the Ising-expansion, we multiply g_0

by a constant prefactor and fit it such that the resulting value of g_0 agrees with the expansion result at $J_2 = 1.5 J_1$, where the influence of the plane-decoupling at low-α seems to have disappeared. The result is shown in fig. 4-3. The error bars are those of the Ising-expansion results. The fit is not unreasonable, also considering the inaccuracies in the one-loop expression used to obtain g_0. The curvature of $1 - g_0/4\pi$ (which is the 1-loop renormalization factor of the spin stiffness and the perpendicular susceptibility, see eq. (1.3.9)) is underestimated, resulting in a critical coupling $\alpha_c \simeq 0.66$, instead of $\alpha_c \simeq 0.63$ obtained from the Ising-expansion.

In summary, we have presented a mapping from the bilayer model to the QNLS with a tunable coupling constant. This clarifies the origin of the order-disorder transition in this system. It shows that the mean field treatment of Chubukov and Morr, which deals exactly with the interlayer fluctuations, is the correct starting point for a semi-classical analysis of the transition. We expect the order-parameter structure of the bilayer to be quite common in the general context of quantum magnetism [63]. Our main result is the discovery of a new type of coherent state which allows for the requantization of such order-parameter structures.

5 Strong-coupling model for antiferromagnetism and superconductivity

5.1 The stripe/superconductor coexistence phase

As was discussed in the introduction, section 1.5, the possibility of a coexistence phase of stripes and superconductivity has been suggested by a number of authors. In measurements on Nd-doped $La_{2-x}Sr_xCuO_4$. Tranquada and coworkers find static stripe correlations in a superconducting sample [28]. The question of whether this is true coexistence or if the superconductivity is somehow spatially separated from the stripe-regions is still a matter of debate. More recently, static incommensurate magnetic order was found for Nd-free $La_{2-x}Sr_xCuO_4$ in the superconducting region around the doping $x = \frac{1}{8}$ [27].

Other indications for the presence of a coexistence phase come from the quantum-critical behavior which is reported for the spin-sector in the underdoped cuprate superconductors [64] [65] [66]. Aeppli *et al.* argue that this behavior is a result of the proximity (in parameter-space) to the ordered stripe-antiferromagnet. This state can either be reached by going to $x = \frac{1}{8}$ (Aeppli's suggestion) or by tuning an additional parameter which promotes stripe-order or suppresses superconductivity, like LTT-deformation or a magnetic field. This last possibility is attractive since quantum critical behavior is found throughout the underdoped region [67]. In order for quantum-criticality to arise as a result of the nearby spin-ordered state, the zero-temperature transition from the spin disordered superconductor to this state has to be smooth (one or more second order transitions). On the basis of an extension of the Landau theory for stripe formation of Zachar *et. al* [1] [37] which includes superconductivity , it has been argued that a direct transition is always first order, but a smooth transition can occur with the coexistence phase as an intermediary stage [67].

As was discussed at the end of section 1.6, the measurements on Nd-free $La_{2-x}Sr_xCuO_4$ are consistent with an $SO(5)$ interpretation of the coexistence phase. In this interpretation, one assumes that, for some reason, the system has an (approximate) $SO(5)$ symmetry at long wavelengths. This symmetry unifies the global $U(1)$ symmetry with respect to phase-transformations and the $SU(2)$-symmetry with respect to spin-rotations. There then exists a 5-component order-parameter related to the spontaneous breaking of this symmetry, which consists of the two-component order-parameter of superconductivity and the 3-component order-parameter of antiferromagnetism. If the coexistence phase indeed arises from a spontaneous breaking of such an $SO(5)$ symmetry, where the resulting order-parameter has components both in the antiferromagnetism and the superconductivity subspace, then the

---

[1]The Landau mean field theory is in this case applied to the effectively 3-dimensional $T = 0$ problem, where fluctuations play a less important role than at finite T (d=2). This considerably changes the discussion about the influence of fluctuations in section 2.1.

magnetic ordering and the superconductivity should be expected to set in at the same temperature. Near the optimum doping for the magnetic order ($x = 0.125$), this is indeed found within the accuracy of the measurement. This is of course only information from one particular quantity, the onset temperature, and relating the coexistence phase on the basis of this to $SO(5)$ ideas is very speculative. A more direct indication for the presence of an approximate $SO(5)$ symmetry near the doping $x = 0.125$ would be the observation of the pseudo-Goldstone modes related to the approximate higher symmetry of the system: the π-modes (see section 1.6). This has not been looked at yet. It should be noted that an application of $SO(5)$ ideas to this particular problem deviates in some sense from the 'standard' $SO(5)$ theory [29], where it is assumed that there is a symmetry relating the superconducting phase and the *half-filling* antiferromagnet.

To investigate the possibility of a coexistence phase, a simple strong-coupling model is proposed which describes the interplay between spin- and phase-order. The parameters entering this model are phenomenological. The phase-diagram is investigated in some detail for most of the parameter-values. A d-wave superconductor, an antiferromagnet, an insulating spin-liquid phase and a coexistence phase are found. It is seen that a smooth transition from the antiferromagnet to the superconductor is indeed only possible with this coexistence phase as an intermediary stage. Transversal spin-fluctuations are included to obtain the most important quantum-corrections to the phase-diagram. At finite temperatures, quantum-critical behavior occurs in the parameter region where these fluctuations destroy the magnetic order in the coexistence phase.

For specific values of the parameters, an $SO(5)$ symmetric point is found at the intersection of the superconductor, the antiferromagnet and the coexistence phase. An $SO(5)$ generalization of the bilayer QNLS is derived which describes the long-wavelength physics at this point.

The role of the large U limit (section 1.2.1), which explicitly breaks the $SO(5)$ symmetry, is studied. It is found that in this limit the π-modes are still present in the RPA mode-spectrum of the superconducting phase, but no longer in that of the antiferromagnet or the coexistence phase. As is the case for the $SO(5)$ symmetric ladder model [71], the π-mode in the superconducting phase continuously evolves from the triplet magnon mode of the spin liquid insulator. The π-mode in the antiferromagnetic phase becomes the longitudinal spin-mode seen in the bilayer model when U is tuned away from its value at the $SO(5)$-symmetric point.

5.2   The strong pairing limit

A special version of the Hubbard model (section 1.1) can be used to study the basic features of superconductivity in a simple setting. If the on-site energy U is taken to be negative, this term in the Hamiltonian describes an electron pairing interaction instead of a short-range Coulomb repulsion. The electron-pairing leads to superconductivity at low temperatures. There exists an exact mapping from this negative-U Hubbard model at arbitrary filling in

zero magnetic field, to the positive-U model at half-filling in a non-zero magnetic field [2]. This mapping demonstrates a number of analogies between superconductivity and antiferromagnetism [68].

In the large U limit, the half-filled Hubbard model becomes a pure spin system and can be described by a Heisenberg Hamiltonian. Similarly, the negative U model can be described by a pseudo-spin Hamiltonian in this limit. The correspondence is set out in table 5-1. It is based on the fact that for $U \ll -1$, all electrons are paired into on-site spin-singlet states. A site can therefore either be unoccupied (pseudo-spin down) or doubly occupied (pseudo-spin up). Following this mapping, it is seen that the strong-coupling superconducting state corresponds to an $S = \frac{1}{2}$ antiferromagnet in an external magnetic field. The XY Néel order in the plane perpendicular to the field corresponds to the phase-order in the superconducting state, the induced component along the field to the Cooper-pair density.

The magnitude of the antiferromagnetic moment in the positive U Hubbard model at half-filling depends on the ratio U/t. The moment in the half-filled cuprates is quite large, about one third, which suggests that the antiferromagnetism in these systems is close to the strong-coupling limit. The superconductivity in these materials seems to be in the intermediate coupling regime, with a coherence length of the order of 10 lattice spacings. However, it has been shown that the strong-coupling and the weak-coupling limits of superconductivity are adiabatically connected [69]: the system can be tuned from weak pairing to strong pairing without encountering a phase-transition. This implies that weak- and strong-coupling superconductivity are qualitatively similar.

Exploiting the adiabatic connectedness, we consider a simplified strong-coupling description of the coexistence phase. Our goal is to demonstrate the possibility of such a phase in a simple setting and to study its qualitative features.

The negative-U Hubbard model is not a good starting point, since on-site Cooper pairs are necessarily in a singlet state, which kills the spin degrees of freedom. Also, the superconductivity in this model is of s-wave type, while the phase-order found in the cuprates seems to be d-wave.

In the following, a model is therefore considered in which the building-blocks are nearest-neighbor Cooper pairs, or dimers. It can be viewed as the strong-coupling limit of a model describing Cooper-pair formation. We assume that the single-electron states have been integrated out, resulting in an effective Hamiltonian containing terms describing the charge-dynamics of the dimers and spin-spin interactions. In most of this work, we also assume

[2]In fact, the mapping is also possible with a non-zero magnetic field in the negative U Hubbard model, where the resulting positive-U Hamiltonian is away from half-filling.

$U \gg 1, n = 1$	$\uparrow$	$\downarrow$	S^z	S^+	H
$U \ll -1$	$\uparrow\downarrow$	o	$n_\uparrow n_\downarrow - \frac{1}{2}$	$c_\uparrow^\dagger c_\downarrow^\dagger$	μ

Table 5-1. Mapping from the spins in the large U Hubbard model at half-filling to the pseudo-spins in the strong-coupling negative-U Hubbard model.

that the doubly-occupied states are integrated out, which means that different dimers cannot overlap. The resulting model then has the form of a t-J model, where the particles are dimers instead of lower-Hubbard band electrons.

The proposed coexistence-phase in $La_{2-x}Sr_xCuO_4$ occurs at the interface of a paramagnetic superconducting phase and a charge-ordered antiferromagnetic phase, where the latter is either the LTT-stabilized stripe-phase, or the commensurate stripe-state at $x = \frac{1}{8}$. From the perspective of a strong-coupling description, the transition to the insulating phase would amount to an ordering transition of the Cooper pairs. It should be possible to include the appropriate interactions into the model and describe such a charge-transition. Indeed, White and Scalapino find that the stripes seen in density matrix renormalization group calculations on the t-J model can be viewed as an ordered state of short-range hole pairs [25].

However, instead of trying to describe stripe-formation as well as spin- and phase-ordering by this model, we will simplify the analysis by taking the half-filled antiferromagnet as the insulating state which borders the coexistence phase. This introduces complications if the model is formulated on a square lattice. At half-filling, there are many ways in which the square lattice can be completely covered by the dimers. Since all of these coverings should represent the same physical state, this introduces a large degeneracy into the description. This problem may not be present in the stripe phase. We therefore feel free to go to a different lattice, shown in figure 5-1, where the problem is avoided.

This type of lattice is known as the sparse, or $\frac{1}{5}$-depleted lattice [11]. We arrive at it by expanding each site of a square lattice to form a tilted square. The dimers are only allowed to sit on the bonds of the original square lattice. The dimer-Hamiltonian can now be thought of as describing the low-energy sector of a model defined on this lattice with a strong attractive nearest-neighbor interaction on the horizontal and vertical bonds. The half-filled state is well-defined in terms of the dimers.

An antiferromagnetic spin-spin interaction J is assumed along the horizontal and vertical bonds and a *ferromagnetic* interaction J_F along the diagonal bonds. This choice allows for an extension of the model to higher dimensions without introducing frustration into the spin system, making it possible to reach the $d \to \infty$ limit and check the mean field results there. For $J_F \gg J$, the half-filled system becomes equivalent to an $S = 2$ antiferromagnet on a square lattice. This property will be used to obtain an estimate of the quantum-corrections to the saddle-point results obtained in the next section.

Two hopping processes are introduced, with amplitudes t_1 and t_2. Both processes move a dimer from a horizontal (vertical) bond to a nearest-neighbor vertical (horizontal) bond. The t_1 process respects the spin-ordering, keeping the electrons which form the dimer on their original sublattice. The t_2 process moves the electrons from one sublattice to another, thereby frustrating Néel order.

Including a chemical potential μ, we arrive at the Hamiltonian

$$\mathcal{H} = \sum_i \left[\sum_{\sigma_1 \sigma_2} \left\{ t_1 \left(L_{i,\delta_x}^{\sigma_1 \sigma_2 \dagger} + L_{i,-\delta_x}^{\sigma_2 \sigma_1 \dagger} \right) \left(L_{i,\delta_y}^{\sigma_1 \sigma_2} + L_{i,-\delta_y}^{\sigma_2 \sigma_1} \right) \right. \right.$$
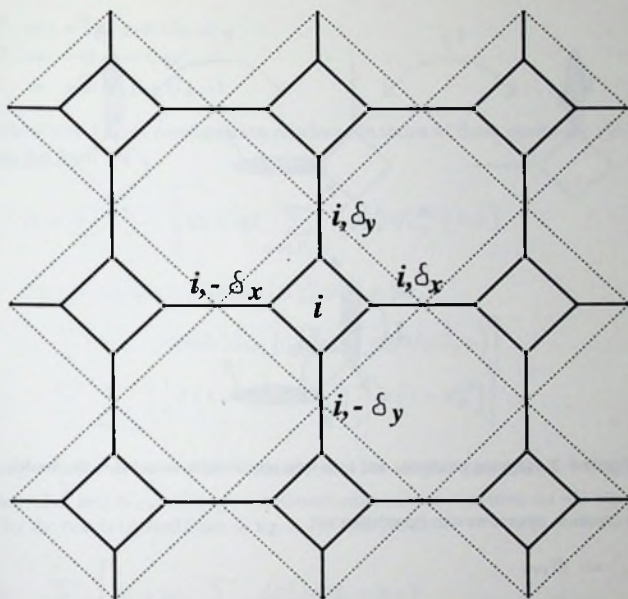
Figure 5-1. The sparse lattice. The dotted lines connect nearest-neighbor horizontal and vertical bonds.

$$
\begin{aligned}
&+ t_2 \left(L_{i,\delta_x}^{\sigma_1\sigma_2\,\dagger} + L_{i,-\delta_x}^{\sigma_2\sigma_1\,\dagger} \right) \left(L_{i,\delta_y}^{\sigma_2\sigma_1} + L_{i,-\delta_y}^{\sigma_1\sigma_2} \right) + \text{h.c.} \Big\} \\
&- J_F \left(\vec{s}_{1i,\delta_x} + \vec{s}_{2i,-\delta_x} \right) \cdot \left(\vec{s}_{1i,\delta_y} + \vec{s}_{2i,-\delta_y} \right) \\
&+ \sum_{\delta=\delta_x,\delta_y} \left(J \vec{s}_{1i,\delta} \cdot \vec{s}_{2i,\delta} - \mu n_{i,\delta} \right) \Bigg].
\end{aligned}
\tag{5.2.1}
$$

The dimers are created by the operators $L_{i,\delta}^{\sigma_1\sigma_2\,\dagger} = P c_{1i,\delta;\sigma_1}^{\dagger} c_{2i,\delta;\sigma_2}^{\dagger}$, where P projects out doubly occupied states. The electrons in the dimer are numbered from left to right and from bottom to top.

The Hilbert space on one horizontal/vertical bond is spanned by five states: unoccupied (V), spin-singlet (A) and spin-triplet $(1, 0, -1)$. The operators acting on this space are 5×5 matrices. Introducing the notation
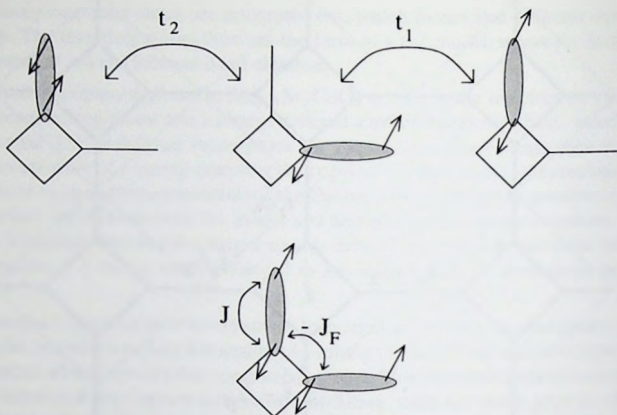
$$
(G_{ab})_{ij} = \delta_{i,a} \delta_{j,b},
\tag{5.2.2}
$$

Figure 5-2. Hopping processes and spin-spin interactions included in the model.

the dimer creation operators can be written as:

$$L^\dagger_{\uparrow\uparrow} = G_{1V},$$
$$L^\dagger_{\downarrow\downarrow} = G_{-1V},$$
$$L^\dagger_{\uparrow\downarrow} = \frac{1}{\sqrt{2}}(G_{0V} - G_{AV}),$$
$$L^\dagger_{\downarrow\uparrow} = \frac{1}{\sqrt{2}}(G_{0V} + G_{AV}). \tag{5.2.3}$$

These operators are the equivalent of the pseudo-spins which appear in the strong-coupling negative U Hubbard model. The operators $G_{\alpha V}$, $G_{V\alpha}$ and $\frac{1}{2}(n_\alpha - n_V)$ form an $S = \frac{1}{2}$ spin-algebra ($\alpha = 1, 0, -1, A$). Pseudo-spins with a different spin-index α do not commute. When studying the SO(5) symmetric point in section 5.5, the Hilbert space is expanded to include doubly occupied states. The operators (5.2.3) then become $S = 1$ pseudo-spins and operators with a different index α do commute in this case.

The spin degrees of freedom are the same as for the bilayer model in chapter 4. Again, it is convenient to introduce the total spin and the Néel moment on a dimer

$$\vec{S}_{i,\delta} = \vec{s}_{1i,\delta} + \vec{s}_{2i,\delta} \;\; ; \;\; \vec{\bar{S}}_{i,\delta} = \vec{s}_{1i,\delta} - \vec{s}_{2i,\delta}, \tag{5.2.4}$$

which are given by

$$S^z = G_{11} - G_{-1-1},$$

$$S^+ = \sqrt{2}(G_{10} + G_{0-1}),$$
$$\tilde{S}^z = -G_{A0} - G_{0A},$$
$$\tilde{S}^+ = \sqrt{2}(G_{1A} - G_{A-1}), \tag{5.2.5}$$

and which satisfy $SO(4)$ commutation relations. In terms of these operators, the Hamiltonian takes the form

$$\mathcal{H} = \sum_i \sum_{\substack{\delta_1 = \pm\delta_x \\ \delta_2 = \pm\delta_y}} \left[(t_1 + t_2) \sum_{\alpha=1,0,-1} \left(G_{\alpha V}^{i,\delta_1} G_{V\alpha}^{i,\delta_2} + \text{h.c.} \right) \right.$$
$$+ (t_1 - t_2)\,sign(\delta_1)sign(\delta_2) \left(G_{AV}^{i,\delta_1} G_{VA}^{i,\delta_2} + \text{h.c.} \right)$$
$$\left. - \frac{J_F}{4} \left(\vec{S}_{i,\delta_1} + sign(\delta_1)\vec{\tilde{S}}_{i,\delta_1} \right) \cdot \left(\vec{S}_{i,\delta_2} + sign(\delta_2)\vec{\tilde{S}}_{i,\delta_2} \right) \right]$$
$$+ \sum_i \sum_{\delta=\delta_x,\delta_y} \left[\frac{1}{4} J \left(1 - n_V^{i,\delta} - 4 n_A^{i,\delta} \right) - \mu \left(1 - n_V^{i,\delta} \right) \right]. \tag{5.2.6}$$

Absorbing a factor $\eta_i^\delta = (-1)^{i_x+i_y} sign(\delta)$ into the singlet-state $|A_{i,\delta}\rangle$, which induces a staggering of $\vec{\tilde{S}}$ and G_{AV} with η_i^δ, the Hamitonian can be rewritten on the square lattice formed by the bonds (dotted lines in fig. 5-1). This yields

$$\mathcal{H} \quad \sum_{<l,m>} \left[(t_1 + t_2) \sum_{\alpha=1,0,-1} \left(G_{\alpha V}^l G_{V\alpha}^m + \text{h.c.} \right) \right.$$
$$\left. + (t_1 - t_2) \left(G_{AV}^l G_{VA}^m + \text{h.c.} \right) - \frac{J_F}{4} \left(\vec{S}_l + \vec{\tilde{S}}_l \right) \cdot \left(\vec{S}_m + \vec{\tilde{S}}_m \right) \right]$$
$$+ \sum_l \left[\frac{1}{4} J \left(1 - n_V^l - 4 n_A^l \right) - \mu \left(1 - n_V^l \right) \right]. \tag{5.2.7}$$

5.3   Mean field analysis

A variational Hartree-Fock procedure is used for the mean-field analysis. In the Ansatz-wavefunction, the Néel-vector is fixed in the z- and the total spin in the x-direction ($\langle \vec{S} \rangle \cdot \langle \vec{\tilde{S}} \rangle = 0$). The pseudo-spin degrees of freedom of the charge/phase sector are described by an $S = \frac{1}{2}$ spin coherent state (eq. (1.4.1))

$$|\theta, \psi, \vec{\Omega}\rangle = \sin\theta e^{-i\psi}|V\rangle + \cos\theta|\vec{\Omega}\rangle. \tag{5.3.1}$$

The state $|\vec{\Omega}\rangle$ contains the spin degrees of freedom of the dimer

$$|\vec{\Omega}\rangle = e^{-i\vec{\phi}^y \tilde{S}^y} (\cos\chi|A\rangle - \sin\chi|0\rangle). \tag{5.3.2}$$

This is just the bilayer coherent state, eq. (3.4.5) with $N = 4$, which yields the expectation values listed in eq. (4.4.1), where the spin-orientation has been fixed and where the angle ϕ is set to zero.

We list the expectation-value of a number of quantities with respect to the variational state

$$
\begin{aligned}
n &= 1 - \langle n_V \rangle = \cos^2 \theta, \\
\langle G_{\alpha V} \rangle &= \sqrt{n(1-n)} e^{-i\psi} \langle \vec{\Omega} | \alpha \rangle, \\
\langle \vec{S} \rangle &= \hat{e}^x n \sin 2\chi \sin \bar{\phi}^y, \\
\langle \vec{\tilde{S}} \rangle &= \hat{e}^z n \sin 2\chi \cos \bar{\phi}^y, \\
\langle n_A \rangle &= n \cos^2 \chi \cos^2 \bar{\phi}^y,
\end{aligned}
\tag{5.3.3}
$$

where $\alpha = 1, 0, -1, A$. The relative magnitude of $\langle \vec{S} \rangle$ and $\langle \vec{\tilde{S}} \rangle$ is determined by $\bar{\phi}^y$, their total magnitude by χ. ψ represents the phase that orders in the superconducting state. θ fixes the dimer-density.

The variational energy is given by

$$
E_{\text{var.}}(\{\theta_l, \psi_l, \vec{\Omega}_l\}) = \langle \{l\} | \mathcal{H} | \{l\} \rangle,
\tag{5.3.4}
$$

where

$$
|\{l\}\rangle = \prod_l |\theta_l, \psi_l, \vec{\Omega}_l\rangle.
\tag{5.3.5}
$$

Taking $\vec{\Omega}_l$ and θ_l to be uniform, and assuming that $\psi_l = \psi^H (\psi^V)$ for horizontal (vertical) bonds, we arrive at the following mean field energy

$$
\begin{aligned}
E_{\text{MF}} = N &\left(\sin^2 2\theta (t_1 + t_2 - 2t_2 \cos^2 \chi \cos^2 \bar{\phi}^y) \times \right. \\
&\times \cos(\psi^H - \psi^V) - \frac{1}{2} J_F \cos^4 \theta \sin^2 2\chi \\
&\left. - \frac{1}{4} J \cos^2 \theta (1 - 4 \cos^2 \chi \cos^2 \bar{\phi}^y) - \mu \cos^2 \theta \right),
\end{aligned}
\tag{5.3.6}
$$

phase	n	$\cos 2\chi$	$\cos \phi^y$
Spin-liquid	1	1	1
Néel dSC	$\dfrac{-J - 4\mu - 16t_1 - 8Jt_2 + 64t_2^2}{4(1 - 8t_1 + 16t_2^2)}$	$\dfrac{J + 8t_2(n-1)}{2n}$	1
Singlet dSC	$\dfrac{4\mu + 16(t_1 - t_2) + 3J}{32(t_1 - t_2)}$	1	1
Triplet dSC	$\dfrac{J - 4\mu - 16(t_1 + t_2)}{4 - 32(t_1 + t_2)}$	0	0
AF	1	$\dfrac{J}{2}$	1

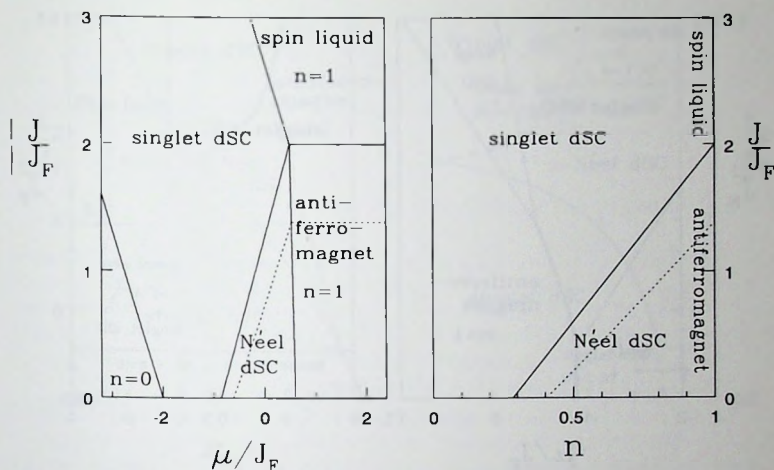Table 5-2. Mean-field results for the various phases.

Figure 5-3. Mean field phase diagram of J versus μ and n, for $t_1 > t_1^*$ ($t_1 = 0.4J_F$, $t_2 = -0.1J_F$). The dotted line indicates the quantum corrections if transversal spin-fluctuations are taken into account.

where N denotes the number of bonds. Minimizing eq. (5.3.6), a variety of mean-field groundstates is obtained as a function of the various parameters. The results are summarized in figures 5-3-5-5 and in table 5-2. We focus here on the case $t_1 > 0$, for which the superconducting state is of the d-wave type ($\psi^H - \psi^V = \pi$). The same phase-diagrams result for $t_1 \to -t_1$ and $t_2 \to -t_2$, but with s-wave instead of d-wave phase-order. Below, we discuss briefly the role that the various parameters play. For simplicity, J, t_1, t_2 and μ are expressed in units of J_F from here on.

The antiferromagnetic spin-spin interaction J tunes the singlet density in the groundstate at half-filling. For $J \ll 1$, the system has full Néel order with $\langle n_A \rangle = \frac{1}{2}$, $|\langle \vec{S} \rangle| = 1$. The singlet density increases linearly with J up to $\langle n_A \rangle = 1$ at $J = 2$, where the staggered magnetization vanishes in a second order transition to a dimerized spin state (fig. 5-3). This is just the bilayer order-disorder transition discussed in the previous chapter.

The value of the hopping amplitude t_1 determines the nature of the transition from the antiferromagnet to the singlet superconductor. For small t_1, the transition is first order as a
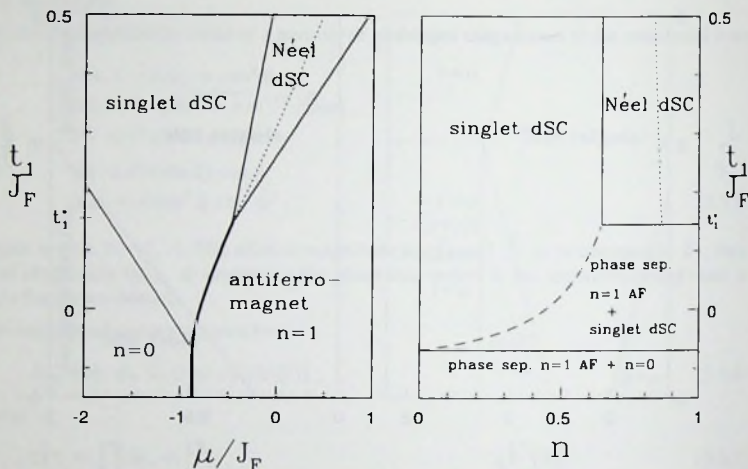
Figure 5-4. Mean field phase diagram of t_1 versus μ and n, for $J < 2J_F$ and $t_2 < t_1$ ($J = J_F$, $t_2 = -0.1 J_F$). The dotted line indicates the quantum corrections if transversal spin-fluctuations are taken into account. Bold lines represent first-order phase transitions.

function of μ, giving rise to a region of antiferromagnet/ superconductor phase separation in the $t_1 - n$ phase-diagram (fig. 5-4). At $t_1 = t_1^* = \frac{1}{8} + 2t_2^2$, the first order line splits into two second order lines and a coexistence region opens up. This is the Néel superconductor (NSC) phase, which has both Néel spin order and superconductivity. Since all electrons are paired in this model, superconductivity sets in as soon as the density n is decreased from its half-filling value of 1.

There are three processes which suppress the spin order-parameter in the NSC phase. One is simply the dilution of the spin system by doping it with hole-pairs. Another is the fact that the inter-dimer spin-spin interaction J_F scales with the dimer-density squared, while the intra dimer spin-spin interaction J scales linearly with n. As a result, the ferromagnetic interaction is suppressed by a factor n relative to J, which pushes the ratio J/J_F closer to its critical value. Finally, the hopping process t_2 frustrates the Néel order, provided that $sign(t_2) = -sign(t_1)$ (the other case is discussed below). The increase of the singlet density per dimer due to the last two processes results in a transition to the singlet superconductor at $n = n_c = \frac{J-8t_2}{2-8t_2}$.
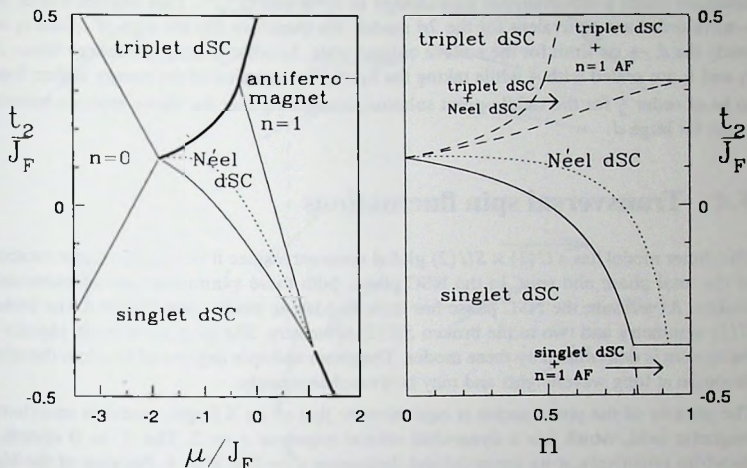
Figure 5-5. Mean field phase diagram of t_2 versus μ and n, for $J < 2J_F$ and $t_1 > (4+J^2)/32$ ($t_1 = 0.4J_F$, $J = J_F$). The dotted line indicates the quantum corrections if transversal spin-fluctuations are taken into account. Bold lines represent first-order phase transitions.

Since the t_2 process amounts to a t_1-type hop with an additional interchange of the two electrons forming the dimer, it picks up a minus-sign when acting on a dimer in the anti-symmetric spin-singlet state. Suppose that t_1 and t_2 have the same sign. A singlet-dimer, through the t_2-process, then frustrates the phase-ordering as favored by the t_1-hop. To reduce this frustration, the singlet content of the dimers is suppressed as t_2 is increased, enhancing the spin-ordering in the NSC phase. Eventually, a first order transition occurs to a ferromagnetically ordered triplet superconductor phase, where the singlet-density is reduced to zero (fig.5-5).

If t_1 and t_2 have opposite sign, the *triplet* component is suppressed through the same process, and the t_2-hop reduces the spin-order in the NSC phase. Note that t_2 causes a positive shift of the critical value t_1^* regardless of its sign. One always has $t_1 \geq |t_2|$ in the NSC phase, where the equal sign occurs only for $t_2 = -\frac{1}{4}$.

As was done for the bilayer model, it should be verified that the saddle-point solution becomes exact in the limit $d \to \infty$. To reach this limit, the model has to be formulated in

arbitrary dimension. The d-wave phase order then posses a problem, since it is not readily generalized to dimensions higher than 2. The Hamiltonian of the 2d system is however invariant under a simultaneous sign-change of t_1, t_2 and $G^{i, \pm \delta_i}_{\alpha V}$. This implies that d- and s-wave order are equivalent for the 2d model. We therefore flip the sign of t_1 and t_2 and study the $d \rightarrow \infty$ limit for the s-wave ordered state. In order to keep the energy finite, J_F, t_1 and t_2 are scaled with $\frac{1}{d}$ while taking the limit. The variation of the energy is then found to be of order $\frac{1}{d}$ for the saddle-point solution, confirming that the above analysis becomes exact for large d.

5.4   Transversal spin fluctuations

The dimer model has a $U(1) \times SU(2)$ global symmetry, since it is invariant under rotations of the total phase and spin. In the NSC phase, both these symmetries are spontaneously broken. As a result, the NSC phase has three Goldstone modes, one related to the broken $U(1)$ symmetry and two to the broken $SU(2)$ symmetry. The long-wavelength physics of the system is determined by these modes. The phase and spin degrees of freedom therefore decouple at long wavelenghts and may be treated separately.

The physics of the phase sector is equivalent to that of an XY-spin model in an external magnetic field, which has a dynamical critical exponent $z = 2$. The $T = 0$ system is therefore effectively at its upper critical dimension $d = 2 + z = 4$. Because of the high effective dimensionality, phase-fluctuations only give small correction to the mean field results for the insulator-superconductor transition [70].

The long-wavelength behavior of the spin-sector in the NSC phase can be described by a $z = 1$ QNLS action. The spin-sector therefore has an effective dimension 3 and the corrections to the mean field results from transversal spin fluctuations can be quite large. Based on what was found for the bilayer model, the bare coupling constant of the QNLS is expected to diverge both at the transition from the half-filling antiferromagnet to the spin liquid phase and at the transition from the NSC to the singlet superconductor. These transitions will therefore shift significantly if the fluctuations are included.

It was found for the bilayer model that the mean-field expressions for the stiffness and the susceptibility can be used as an estimate for the bare stiffness and susceptibility in the effective QNLS. These two quantities are derived for the present model.

The susceptibility is easily obtained by adding a magnetic field term to the mean field energy eq. (5.3.6).

$$H \sum_l \langle S^x \rangle = N H \cos^2 \theta \sin 2 \chi \sin \bar{\phi}^y. \tag{5.4.1}$$

Minimizing the energy, we obtain

$$\chi_\perp = \lim_{H \to 0} \frac{\frac{1}{2} \langle S^x \rangle}{H} = \frac{(1 - \cos 2 \chi) n}{2J - 16 t_2 (1 - n)}. \tag{5.4.2}$$
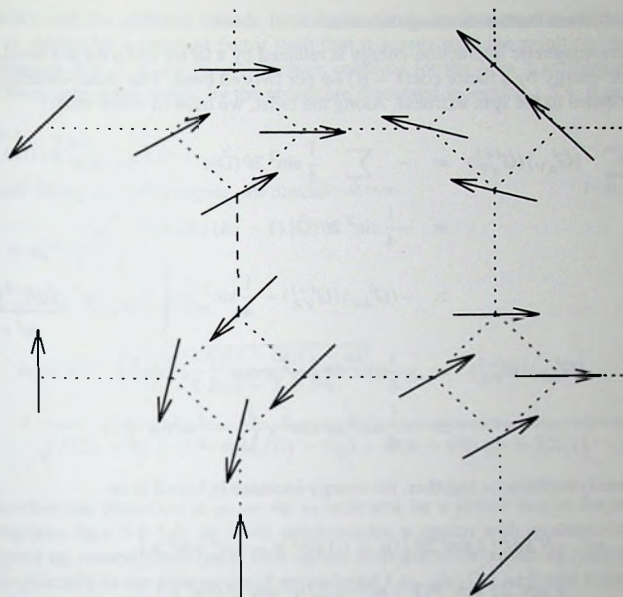
Figure 5-6. A spin-configuration with a twist along the $x + y$-direction.

This susceptibility vanishes at the transitions to the spin liquid and the singlet superconductor phase ($\chi \to 0$). It has a divergence at $n = 1 - \frac{J}{8t_2}$, which is related to the transition to the triplet superconductor (fig. 5-5). For $n = 1$ and $J_F \gg J$, eq. (5.4.2) becomes independent of J_F. It reduces to the susceptibility of a square lattice $S = 2$ antiferromagnet in this limit, apart for a numerical constant, which is due to the fact that $\chi_\perp$ was defined in terms of the $S = \frac{1}{2}$ spins on the sparse lattice.

To determine the spin stiffness, the configuration shown in fig. 5-6 is considered. It has a slow twist in the spin order parameter along the $x + y$-direction. The stiffness is given by the lowest-order correction to the groundstate energy due to this twist [10].

At each antiferromagnetic bond along the direction of the twist, the spins have been rotated over an angle $\alpha \, \delta\phi$ in the XZ-plane, at each ferromagnetic bond over an angle $(1 - \alpha) \, \delta\phi$. This configuration is described by the variational state eq. (5.3.1), where the spin-part is given by

$$e^{i \, l \, \delta\phi \, S^y} |\vec{\Omega}\rangle = e^{i \, l \, \delta\phi \, S^y} e^{-i \frac{1}{2} \alpha \, \delta\phi \, \bar{S}^y} \left(\cos \chi |A\rangle - \sin \chi |0\rangle \right) . \tag{5.4.3}$$

The index l labels the bonds along the twist.

The antiferromagnetic interaction-energy is reduced by a factor $\cos\alpha\,\delta\phi$ per bond, the ferromagnetic energy by a factor $\cos(1-\alpha)\,\delta\phi$ per twisted bond. The phase-ordering energy also contributes to the spin stiffness. Along the twist, we have (d-wave order)

$$
\begin{aligned}
\sum_{\alpha=1,0,-1}\langle G^l_{\alpha V}\rangle\langle G^{l+1}_{\alpha V}\rangle &= -\sum_{\alpha=1,0,-1}\frac{1}{4}\sin^2 2\theta\langle\vec{\Omega}|e^{-i\,l\,\delta\phi\,S^y}|\alpha\rangle\langle\alpha|e^{i\,(l+1)\,\delta\phi\,S^y}|\vec{\Omega}\rangle \\
&= -\frac{1}{4}\sin^2 2\theta\langle\vec{\Omega}|\,(1-|A\rangle\langle A|)\,e^{i\,\delta\phi\,S^y}|\vec{\Omega}\rangle \\
&\simeq -\langle G^l_{AV}\rangle\langle G^{l+1}_{VA}\rangle - \frac{1}{4}\sin^2 2\theta\left(1-\frac{1}{2}\delta\phi^2\underbrace{\frac{\langle\vec{\Omega}|S^{y\,2}|\vec{\Omega}\rangle}{\sin^2\chi}}\right), \\
\langle G^l_{AV}\rangle\langle G^{l+1}_{VA}\rangle &= -\frac{1}{4}\sin^2 2\theta\cos^2\chi\cos^2\left(\frac{1}{2}\alpha^2\,\delta\phi^2\right) \\
&\simeq -\frac{1}{4}\sin^2 2\theta\cos^2\chi\left(1-\frac{1}{4}\alpha^2\delta\phi^2\right).
\end{aligned}
\tag{5.4.4}
$$

Taking these contributions together, the energy-increase is found to be

$$
\begin{aligned}
\Delta E &= \frac{1}{4}N\,\delta\phi^2\left(2\sin^2 2\theta\left[(t_1+t_2)\sin^2\chi - t_2\alpha^2\cos^2\chi\right]\right. \\
&\quad \left. + \sin^2 2\chi\cos^4\theta(1-\alpha)^2 + 2J\alpha^2\cos^2\theta\cos^2\chi\right) \\
&\equiv N\left(\frac{1}{2}\delta\phi\right)^2\rho_s.
\end{aligned}
\tag{5.4.5}
$$

The distribution of the total twist over the two types of bonds is determined by minimizing this energy with respect to α, which yields

$$
\alpha = \frac{n(1-\cos 2\chi)}{n(1-\cos 2\chi) + J - 4t_2(1-n)}.
\tag{5.4.6}
$$

For J_F much larger than J and t_2 (or just J for $n=1$), the twist is entirely localized on the antiferromagnetic bonds. At the transition to the spin disordered phases, it is localized on the ferromagnetic bonds.

Inserting this expression for α into eq. (5.4.5) yields the spin-stiffness. Like the susceptibility, it vanishes at the transition to a spin-disordered phase and reduces to the $S=2$-form for $J\gg J_F$ at half-filling (upto a numerical constant which depends on the precise definition of the stiffness).

The bare coupling constant of the QNLS is given by $g_0 = \frac{1}{\sqrt{\rho_s\chi_\perp}}$. It indeed diverges at the transitions to the singlet superconductor and the spin liquid phase, where both the

susceptibility and the stiffness vanish. In order to obtain a more precise estimate of g_0, its value is shifted by a constant factor such that it agrees with the result for the $S = 2$ antiferromagnet at $n = 1$, $J_F \gg J$. The bare coupling for the $S = 2$ antiferromagnet is obtained from spin-wave results by the procedure discussed in section 1.3.4. It reads

$$g_0^{S=2} \simeq 3.85 . \tag{5.4.7}$$

For the half-filling antiferromagnet, we obtain

$$g_0 = g_0^{S=2} \frac{2}{2 - J} , \tag{5.4.8}$$

while we find for the NSC phase,

$$g_0 = g_0^{S=2} \frac{2\sqrt{(2n + J)(J - 8t_2(1 - n))}}{n(2 - 8t_2) - J + 8t_2} \times \tag{5.4.9}$$

$$\times \frac{1}{\sqrt{J(2n + J) + (1 - n)[4J(t_1 - 2t_2) + 8t_1 n - 64t_1 t_2 n + 32t_2^2(1 - 3n)]}} .$$

The order-disorder transition at $g_0 = 4\pi$ is indicated by a dotted line in the mean field phase diagrams fig.s 5-3-5-5. At finite temperatures, a region with quantum-critical behavior opens up around these lines. This agrees with the observations of Aeppli *et al.* of quantum-criticality in the spin sector of underdoped $La_{2-x}Sr_xCuO_4$. It was argued in [67] that the explanation of this behavior in terms of the nearby charge- and spin-ordered stripe phase requires the existence of a coexistence phase. From this analysis, we find that such a coexistence phase can in principle exist, and that it indeed gives rise to a superconducting state with quantum-critical behavior in the spin-sector.

5.5 SO(5) symmetric point

The NSC phase has an interesting property. Let us consider the SO(5) superspin-vector [29] for this model.

$$\vec{N}_P = \left(\frac{1}{2}(G_{AV} + G_{VA}), \frac{1}{2}\vec{S}, \frac{1}{2i}(G_{AV} - G_{VA}) \right) . \tag{5.5.1}$$

The label 'P' indicates that $\vec{N}_P$ is defined in the projected Hilbertspace, where double site-occupancy is forbidden. The mean-field expectation value of $\vec{N}_P$ satisfies

$$\left. \frac{\partial \langle \vec{N}_P \rangle^2}{\partial n} \right|_{t_2 = -\frac{1}{4}} = 0. \tag{5.5.2}$$

Hence, at the mean-field level and for this particular choice of t_2, the NSC phase can be interpreted as a gradual rotation of the SO(5) supspin from the antiferromagnet to the singlet superconductor. As one approaches the tricritical point, the NSC states with different n become degenerate (fig.5-3) and the mean field state becomes invariant under rotations of $\vec{N}_P$. For $t_2 = -\frac{1}{4}$ the tricritical-critical point is located at $t_1 = t^* = \frac{1}{4}$, $\mu = \mu^* = \frac{J}{4}$.

It should perhaps come as no surprise that we find a 'mean field SO(5) symmetry' for this model. The special lattice used here has two orbitals per unit cell. This seems to be one of the requirements for constructing an SO(5) symmetric model with short-range interactions [35]. In the following, an exact SO(5) symmetric point is derived for the present model. The procedure used is similar to that for the SO(5) symmetric ladder [71].

At the mean-field SO(5)-point, the Hamiltonian is given by

$$\mathcal{H} = \mathcal{H}_0 + \mathcal{H}_1, \tag{5.5.3}$$

where

$$\mathcal{H}_0 = -\sum_{<l,m>} \vec{N}_P^l \cdot \vec{N}_P^m - J \sum_l n_A^l, \tag{5.5.4}$$

$$\mathcal{H}_1 = \sum_{<l,m>} \frac{1}{4} \left[\vec{\tilde{S}}_l \cdot \vec{S}_m + \vec{S}_l \cdot \vec{\tilde{S}}_m + \vec{S}_l \cdot \vec{S}_m \right], \tag{5.5.5}$$

and where a d-wave staggering has been absorbed into the $|V_l\rangle$-state.

The second term, $\mathcal{H}_1$, is manifestly not invariant under rotations of $\vec{N}_P$. Since $\langle \vec{S} \rangle = 0$ in the NSC phase, this symmetry-breaking does not show up at the mean field level. As a first step towards an $SO(5)$-symmetric Hamiltonian, $\mathcal{H}_1$ is subtracted from $\mathcal{H}$. This introduces second- and third-neighbor spin-spin interactions into the model. The somewhat peculiar interactions are shown in fig. 5-7.

The second term in $\mathcal{H}_0$ is an $SO(5)$-invariant (this is discussed below). The first term is invariant under rotations of $\vec{N}_P$, but this does not imply that it is SO(5) symmetric. There is no representation of the SO(5) algebra on the projected Hilbertspace under which $\vec{N}_P$ transforms as a vector. The rotation-symmetry is therefore broken at the quantum level.

To obtain true SO(5) symmetry, the constraint which forbids double site-occupancy has to be relaxed, as it is in the SO(5)-ladder systems. The basis of the single-bond Hilbert-space is extended to include the doubly occupied state $|D\rangle$. It then consists of one SO(5) singlet (A) and one SO(5) quintet (spin-triplet, D and V). The details of this representation of the SO(5) algebra are discussed in section 5.7. We introduce an on-site repulsion $U \sum_{i\delta} n_{D i\delta}$. The Hamiltonian on the unprojected Hilbert space is given by

$$\mathcal{H} = -\sum_{<lm>} \left[4(t_1 + t_2) \left(\text{Re}\vec{\pi}_l \cdot \text{Re}\vec{\pi}_m + \text{Im}\vec{\pi}_l \cdot \text{Im}\vec{\pi}_m \right) \right.$$
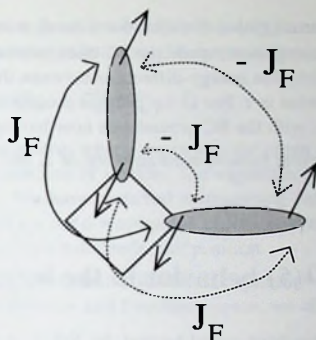
Figure 5-7. Inter-dimer spin-spin interactions in the $SO(5)$ symmetric model.

$$+(t_1 - t_2)\vec{\Delta}_l \cdot \vec{\Delta}_m + \frac{1}{4}\left(\vec{S}_l + \vec{\bar{S}}_l\right) \cdot \left(\vec{S}_m + \vec{\bar{S}}_m\right)\Bigg] \tag{5.5.6}$$
$$+ \sum_l \left[\frac{J}{4}(1 - 4n_A^l) + \left(U - \frac{J}{4} - \mu\right)n_D^l + \left(\mu - \frac{J}{4}\right)n_V^l\right],$$

where $\vec{\Delta} = (\mathrm{Re}\Delta, \mathrm{Im}\Delta)$ (see section 5.7). The value of U has to be fine-tuned in order to obtain SO(5) symmetry on a single bond. The resulting constraint is $\mu = \frac{J}{4}$ (as before), $U = \frac{J}{2}$. Note that this is more restrictive than the local constraint for the ladder model [71], which leaves two free parameters. Since we only consider states of paired electrons, this model has fewer local SO(5) invariants than the ladder.

To establish SO(5) symmetry of the inter-dimer interactions, one now has to take $t_1 = -t_2 = \frac{1}{8}$. After subtraction of $\mathcal{H}_1$, this yields the Hamiltonian

$$\mathcal{H}_{SO(5)} = -\frac{1}{4} \sum_{<l,m>} \vec{N}_l \cdot \vec{N}_m - J \sum_l n_A^l, \tag{5.5.7}$$

where $\vec{N}$ is given by eq. (5.7.1). The local SO(5) invariant n_A is related to the length of the superspin through $\vec{N}^2 = 1 + 4n_A$.

The mean field SO(5) symmetry at $U \to \infty$ evolves from the true SO(5) symmetric point at fine-tuned U in the following way. Let us assume we have $t_1 = -t_2 = t$ and $U = \frac{J}{2} + \bar{U}$.

$$\mathcal{H} = -\sum_{<l,m>} \left(2t\vec{\Delta}_l \cdot \vec{\Delta}_m + \frac{1}{4}\vec{\bar{S}}_l \cdot \vec{\bar{S}}_m\right)$$
$$+ \sum_l \left(\bar{U}n_D^l - Jn_A^l\right). \tag{5.5.8}$$

The superspin has no preferred global direction for $\bar{U} = 0$, $t = \frac{1}{8}$. Since the AF ground-state does not have a $|D\rangle$ component, while the SC does, a small positive $\bar{U}$ will flop the superspin to the AF direction. The energy-difference between the AF and the SC state can be compensated by an increase in t. For $\bar{U} \to \infty$, this procedure shifts the superspin-flop point from $t = \frac{1}{8}$ to $t = \frac{1}{4}$, with the SC groundstate now having $\langle n_D \rangle = 0$. The shift in t is accounted for by the different relative normalization of $\vec{\Delta}$ and $\vec{S}$ in the definitions of $\vec{N}_P$ and $\vec{N}$.

5.6   Remnant $SO(5)$ behavior in the large U limit

One of the criticisms that has been raised against the $SO(5)$ approach, is that it does not take properly into account the effects of projecting onto the lower Hubbard band [73]. While it aims to be a description of the low-energy physics of the t-J model, the expressions for the π-operators in the $SO(5)$ algebra and the superconductivity order-parameter in the superspin are in terms of electrons, not of the hard-core fermions which appear in the t-J model. After projecting onto the lower Hubbard band, the π- spin- and charge-operators no longer form an $SO(5)$-algebra, which was the problem encountered in the previous section. To obtain $SO(5)$ symmetry, U has to be fine-tuned to a value $\sim J$. This is a strange procedure, because the antiferromagnetic interaction in the t-J model arose in the first place as a result of the projection onto the lower Hubbard band [3]. Moreover, the value of $J \sim \frac{t^2}{U}$ is assumed to be much smaller than U, so the fine-tuning condition seems to take you outside the range of validity of the t-J model.

It is therefore interesting to see what remains of the $SO(5)$ symmetry if we apply the projection in earnest. This is not a weak breaking of the symmetry. such as has been studied using a QNLS description [75] , since U is tuned very far away from its value at the symmetric point.

It was already seen that the symmetry survives at the mean field level. The collective modes around the mean field states are studied to examine what is the fate of the π-modes. We focus on the singlet superconductor and the spin liquid phase and some remarks are made about the antiferromagnet and the Néel superconductor. The modes are analysed using the random phase approximation [74]. This approach is similar to the expansion of the action around the mean field state, which was used in section 4.5. For the normal antiferromagnet, the approximation is equivalent to the lowest order of the $\frac{1}{S}$-expansion.

We are interested in the equations of motion of the operators $G_{\alpha\beta}$, which are given by

$$i\partial_t G^l_{\alpha\beta} = [G^l_{\alpha\beta}, \mathcal{H}] . \tag{5.6.1}$$

[3]Although in this particular model we can think of J as arising from the projection onto the paired-electron states, this is however not the case for the ladder model [71], where the same problem occurs

The right-hand side contains products of operators on nearest-neighbor bonds. A mean field decoupling is used to bring it into a single-operator form.

$$G_{\alpha\beta}^l G_{\alpha'\beta'}^m \rightarrow \langle G_{\alpha\beta}\rangle G_{\alpha'\beta'}^m + G_{\alpha\beta}^l \langle G_{\alpha'\beta'}^m\rangle. \tag{5.6.2}$$

The additional zero-operator term which appears in the mean field decoupling eq. (4.3.1) is not important for the equations of motion. The expectation value is taken with respect to the fully ordered state. We have absorbed a staggering-factor for the Néel order into the singlet-operator $A_l^\dagger$ and for the d-wave phase order into the hole pair-operator $V_l^\dagger$. The expectation values are therefore independent of position.

Using this decoupling, a set of first-order differential equations is obtained for the operators $G_{\alpha\beta}^l$. Transforming to momentum- and frequency-space, we obtain

$$\omega\, G_{\alpha\beta}(\vec{k}, \omega) = \sum_{\alpha'\beta'} M_{\alpha\beta}^{\alpha'\beta'}(\vec{k}) G_{\alpha'\beta'}(\vec{k}, \omega), \tag{5.6.3}$$

which has the form of an eigenvalue equation. The dispersion-relations of the collective modes follow from the eigenvalues of the dynamical matrix M. Its eigenvectors give the operators which generate the modes.

Since we want to focus here on the symmetry-breaking effect of the large U limit, the Hamiltonian $\mathcal{H}_0$ with the symmetrized spin-spin interactions is used.

Only operators which refer to the mean field groundstate appear in the equations of motion, so at least one of the indices of $G_{\alpha\beta}$ has to be either A or V (just A for the spin liquid phase). These operators separate into four sets. Three sets describe the longitudinal spin-modes of the bilayer model (singlet-triplet fluctuations) and the π-modes of $SO(5)$-theory (hole-pair triplet fluctuations). They are given by $\{G_{0V}, G_{0A}, G_{V0}, G_{A0}\}$, $\{G_{1V}, G_{1A}, G_{V-1}, G_{A-1}\}$ and the hermitian conjugate of the last set. The dynamical matrix of the first set is given by (for the singlet SC phase)

$$M_1 = \begin{pmatrix} A & -B \\ B & -A \end{pmatrix}, \tag{5.6.4}$$

with A and B the 2×2 matrices

$$A = \begin{pmatrix} -J + \Delta t\, \bar{\mu} + \frac{1}{2}\Sigma t\, \gamma_k(4 - \bar{\mu}) & -\frac{1}{2}(\Delta t - \gamma_k \Sigma t)\sqrt{16 - \bar{\mu}^2} \\ -\frac{1}{8}(4\Delta t - \gamma_k)\sqrt{16 - \bar{\mu}^2} & -J + \frac{1}{8}\gamma_k(4 + \bar{\mu}) \end{pmatrix},$$

$$B = \begin{pmatrix} 0 & 0 \\ -\frac{1}{8}\gamma_k\sqrt{16 - \bar{\mu}^2} & -\frac{1}{8}\gamma_k(4 + \bar{\mu}) \end{pmatrix}, \tag{5.6.5}$$

where $\Sigma t = t_1 + t_2$, $\Delta t = t_1 - t_2$, $\bar{\mu} = \left(\mu + \frac{3}{4}J\right)/\Delta t$ and $\gamma_k = \frac{1}{2}(\cos k_{x+y} + \cos k_{x-y})$. The second set has the same matrix with $B \rightarrow -B$, while the third set has $A \rightarrow -A$.

The fourth set describes the phase and number fluctuations in the singlet superconductor phase. It contains the operators $\{n_A - n_V, G_{AV}, G_{VA}\}$. Its dynamical matrix reads

$$M_0 = \begin{pmatrix} 0 & -\frac{1}{2}\Delta t\sqrt{16 - \bar{\mu}^2} & \frac{1}{2}\Delta t\sqrt{16 - \bar{\mu}^2} \\ -\Delta t(1 - \gamma_k)\sqrt{16 - \bar{\mu}^2} & \Delta t\,\bar{\mu}\,(1 - \gamma_k) & 0 \\ \Delta t(1 - \gamma_k)\sqrt{16 - \bar{\mu}^2} & 0 & -\Delta t\,\bar{\mu}\,(1 - \gamma_k) \end{pmatrix}. \quad (5.6.6)$$

For the spin liquid phase at half-filling, these matrices take the simpler form

$$M_1 = \begin{pmatrix} 4\Delta t - J & 0 & 0 & 0 \\ 0 & \gamma_k - J & 0 & \gamma_k \\ 0 & 0 & J - 4\Delta t & 0 \\ 0 & -\gamma_k & 0 & J - \gamma_k \end{pmatrix}, \quad (5.6.7)$$

and

$$M_0 = \begin{pmatrix} 0 & 0 & 0 \\ 0 & \Delta t(\bar{\mu} - 4\gamma_k) & 0 \\ 0 & 0 & -\Delta t(\bar{\mu} - 4\gamma_k) \end{pmatrix}. \quad (5.6.8)$$

The mode-spectrum in the singlet SC and spin liquid phase and at the different transitions is sketched in fig. 5-8

In the spin liquid phase, there are two dispersive modes. One is related to triplet excitations over the singlet groundstate. Its dispersion is given by

$$\omega_k = \pm\sqrt{J^2 - 2J\gamma_k}. \quad (5.6.9)$$

This mode softens at the transition to the spin-ordered $n = 1$ state, as it did for the bilayer model. In addition, there is a gapped pairing mode with eigenvector G_{AV} (G_{VA}), which is given by

$$\omega_k = \pm\Delta t(\bar{\mu} - 4\gamma_k) \quad (5.6.10)$$

The pairing-gap closes at the transition to the singlet SC, at $\bar{\mu} = 4$.

At $n < 1$, the pairing mode of the insulating phase becomes the phase-mode of the superconductor. It is given by

$$\omega_k = \pm\sqrt{(1 - \gamma_k)[\Delta t^2(16 - \bar{\mu}^2) - \bar{\mu}^2(1 - \gamma_k)]}, \quad (5.6.11)$$

which has a linear dispersion for $k \rightarrow 0$. The corresponding eigenvector in this limit is $n_A - n_V$, which indeed generates phase rotation of the singlet SC groundstate.
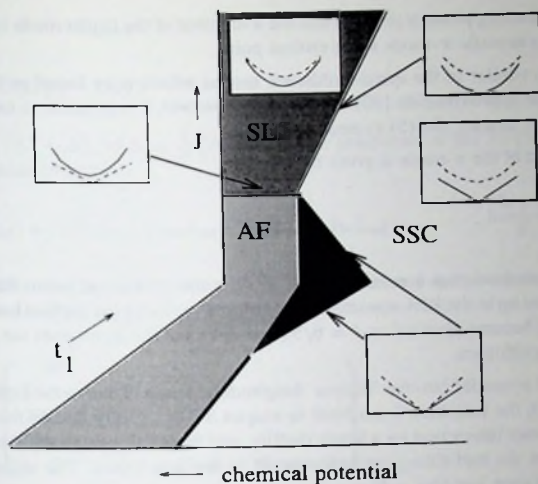
Figure 5-8. Sketch of the mode-spectrum in the spin liquid and singlet superconductor phase. The dashed line refers to the triplet modes.

The triplet modes are gapped in the singlet SC phase. They soften at the transition to the spin-ordered Néel superconductor. The system then has four acoustic modes: one phase-mode and three triplet-modes.

We consider the case where μ is at the transition to the Néel SC phase, $t_2 = -\frac{1}{4}$ and t_1 is tuned towards the mean-field $SO(5)$ point at $t_1 = \frac{1}{4}$. The $k \to 0$ eigenvectors corresponding to the acoustic $m = 0$ triplet mode is then given by

$$\sqrt{\frac{2-J}{2+J}} \frac{2}{4t_1 - 1} (G_{0V} - G_{V0}) + G_{0A} - G_{A0}. \tag{5.6.12}$$

and the same form for the other triplet modes.

For t_1 far from its critical value, the triplet-mode is a pure singlet-triplet fluctuation -the same mode which softens at the transition from the spin liquid to the antiferromagnet. As t_1 is tuned towards the mean field $SO(5)$ point, hole-pair to triplet excitations are mixed in until, at $t_1 = \frac{1}{4}$, it has become a pure π-mode. Even though the $SO(5)$ symmetry is explicitly broken, π-modes are still found to linear approximation around the ordered state.

The same behavior is found if the symmetric point is approached from the singlet SC by varying the chemical potential. As μ is tuned towards its critical value, the triplet-gap in

the superconducting phase is reduced and the π-content of the triplet mode increased, until it becomes an acoustic π-mode at the critical point.

This result is similar to the quasi-Goldstone modes which were found in the t-J model using a similar approximation [30]. In this case, however, it is possible to explicitly relate the modes to a 'nearby' $SO(5)$ symmetric point.

The dispersion of the π-mode is given by

$$\omega_k = \frac{2+J}{4}k\,,\tag{5.6.13}$$

while the phase-mode has a velocity $\sqrt{1 - J^2/4}$ at the symmetric point. The symmetry-breaking shows up in the RPA-spectrum by a different velocity for the two kinds of modes. The velocities become identical at $J = 6/5$ ($n = 4/5$), but this point does not seem to have any special significance.

The mixing of π-modes into the 'bilayer' longitudinal mode is due to the hopping process t_2. For $t_2 = 0$, the transition from Néel to singlet SC is entirely due to the suppression of the inter-dimer interaction by a lower density, and therefore essentially the same as the transition from the half-filling antiferromagnet to the spin liquid. The softening triplet-mode is in that case just $G_{0A} - G_{A0}$.

The continuous evolution of the triplet magnon of the spin-liquid state into the π-mode of the superconductor at the symmetric point, which is depicted in fig. 5-8, was also found for the ladder model with unbroken $SO(5)$ symmetry. We conclude that tuning U away from its $SO(5)$ symmetric point only weakly affects the modespectrum in the spin-disordered phases , at least at the RPA level.

The situation is different for the spin-ordered phases. In the AF phase, the π-mode of the $SO(5)$-symmetric model becomes a bilayer-type longitudinal spin-mode after projection, which is gapped at the tricritical-critical point. The RPA modespectrum in the Néel SC phase interpolates between the gapped mode in the AF phase and the acoustic mode in the singlet SC.

5.7   The $SO(5)$ algebra.

In this and the next section, the focus is on the $SO(5)$ symmetric point. Here, the representation of the $SO(5)$-algebra for this model is discussed. In the next section, an $SO(5)$ QNLS-action is derived which described the long-wavelength physics at the symmetric point.

In the unprojected Hilbertspace, a representation of the $SO(5)$ algebra can be defined which transforms the superspin $\vec{N}$ as a vector. The superspin is given by

$$\vec{N} = \left(\mathrm{Re}\Delta, \vec{S}, \mathrm{Im}\Delta\right)\,,\tag{5.7.1}$$

where

$$\Delta^\dagger = \sqrt{2}\,(G_{DA} - G_{AV}) \tag{5.7.2}$$

and $\mathrm{Re}\,\Delta = \frac{1}{2}\left(\Delta^\dagger + \Delta\right)$, $\mathrm{Im}\,\Delta = \frac{1}{2i}\left(\Delta^\dagger - \Delta\right)$. The generators of the $SO(5)$-algebra satisfy the commutation relation

$$[L_{ab}, L_{cd}] = i\,(\delta_{ac}L_{bd} + \delta_{bd}L_{ac} - \delta_{ad}L_{bc} - \delta_{bc}L_{ad})\,, \tag{5.7.3}$$

where the indices take the values 1 through 5. The L_{ab} are anti-symmetric under an interchange of a and b. They are given by [29]

$$L_{ab} = \begin{pmatrix} 0 & & & & \\ 2\mathrm{Re}\pi_x & 0 & & & \\ 2\mathrm{Re}\pi_y & -S^z & 0 & & \\ 2\mathrm{Re}\pi_z & S^y & -S^x & 0 & \\ Q & 2\mathrm{Im}\pi_x & 2\mathrm{Im}\pi_y & 2\mathrm{Im}\pi_z & 0 \end{pmatrix} \tag{5.7.4}$$

where the π-operators read $\pi_\alpha^\dagger = -\frac{1}{2}c_1^\dagger \sigma_\alpha \sigma_y c_2^\dagger$, with $\vec{\sigma}$ the Pauli matrices [71]. Projecting onto the paired-electron states, we obtain

$$\begin{aligned}
\pi_x^\dagger &= \frac{1}{2i}\,(G_{D1} - G_{D-1} + G_{1V} - G_{-1V})\,, \\
\pi_y^\dagger &= \frac{1}{2}\,(G_{D1} + G_{D-1} - G_{1V} - G_{-1V})\,, \\
\pi_z^\dagger &= \frac{i}{\sqrt{2}}\,(G_{D0} + G_{0V})\,.
\end{aligned} \tag{5.7.5}$$

The charge-operator is given by

$$Q = n_D - n_V\,. \tag{5.7.6}$$

It can be checked that $\vec{N}$ indeed transforms as a vector under this $SO(5)$-algebra:

$$[L_{ab}, N_c] = i\,(\delta_{ac}N_b - \delta_{bc}N_a)\,, \tag{5.7.7}$$

and furthermore that

$$[N_a, N_b] = iL_{ab}\,. \tag{5.7.8}$$

5.8   Coherent state path integral

We derive the coherent-state path-integral for the symmetric model . It follows from equations (5.7.3), (5.7.7) and (5.7.8) that an $SO(6)$-algebra l_{ab} can be constructed by taking $l_{a+1\,1} = N_a$ and $l_{a+1\,b+1} = L_{ab}$. Since the coherent state has to parametrize the rotations of the superspin-vector, generated by L_{ab}, as well as the fluctuations of $\vec{N}^2$, generated by N_a, it makes sense to start from an $SO(6)$ description, which incorporates both. The coherent state appropriate to the description of this system was derived in chapter 3, eq.s (3.4.5) and (3.4.6).

The coherent state path integral is constructed in the usual way [13] [3]. The kinetic term in the action derives from the overlap eq. (3.4.12), the potential energy comes from the expectation value of the Hamiltonian with respect to the coherent state. We obtain

$$\mathcal{Z} \propto \int \left[\prod_l d\chi_l d\hat{\alpha}_l d\hat{\beta}_l \delta(\hat{\alpha}_l \cdot \hat{\beta}_l) \Theta(\alpha_l^1) \right] e^{-\mathcal{S}}, \tag{5.8.1}$$

with the imaginary time action

$$\mathcal{S} = \int_0^\beta d\tau \left[i \sum_l \sin 2\chi_l \left(\partial_\tau \phi + \vec{n}_l \cdot \partial_\tau \hat{\bar{n}}_l \right) \right.$$
$$- \frac{1}{4} \sum_{<ij>} \sin 2\chi_i \sin 2\chi_j \sqrt{1 - \vec{n}_i^2} \sqrt{1 - \vec{n}_j^2} \, \hat{\bar{n}}_i \cdot \hat{\bar{n}}_j$$
$$\left. - J \sum_i (1 - \vec{n}_i^2)(\cos^2 \chi \cos^2 \phi + \sin^2 \chi \sin^2 \phi) \right], \tag{5.8.2}$$

where, as before, $\vec{n} = \sin \psi \hat{n}$ (ψ is now not the phase but one of the angles entering the coherent state eq. (3.4.6)). In terms of the $SO(5)$ operators L_{ab}, the second part of the kinetic term reads

$$\sin 2\chi \vec{n} \cdot \partial_\tau \hat{\bar{n}} = \sum_{a<b} \langle L_{ab} \rangle \partial_\tau \hat{\bar{n}}_a \hat{\bar{n}}_b$$
$$= \langle Q \rangle (\hat{\bar{n}}_5 \partial_\tau \hat{\bar{n}}_1 - \hat{\bar{n}}_1 \partial_\tau \hat{\bar{n}}_5) + \langle \vec{S} \rangle \cdot \partial_\tau \hat{\bar{n}}_{234} \times \hat{\bar{n}}_{234}$$
$$+ (2\text{Re}\vec{\pi}) \cdot (\hat{\bar{n}}_1 \partial_\tau \hat{\bar{n}}_{234} - \hat{\bar{n}}_{234} \partial_\tau \hat{\bar{n}}_1)$$
$$+ (2\text{Im}\vec{\pi}) \cdot (\hat{\bar{n}}_5 \partial_\tau \hat{\bar{n}}_{234} - \hat{\bar{n}}_{234} \partial_\tau \hat{\bar{n}}_5), \tag{5.8.3}$$

where $\hat{\bar{n}}_{234} = (\hat{\bar{n}}_2, \hat{\bar{n}}_3, \hat{\bar{n}}_4)$.

The first term describes the phase dynamics. It has the same form as the kinetic term for an XY spin model, where $\langle Q \rangle$ plays the role of the z-component of the spin. The second term was also obtained for the bilayer model. It describes the spin-dynamics. The last two terms describe the π-fluctuations.

The need to go to a finite, fine-tuned U in order to obtain $SO(5)$ symmetry can be understood from the phase-dynamics term. Due to the fine-tuning of U, the $SO(5)$-symmetric system remains at half-filling, where $\langle Q \rangle = 0$, as the superspin is rotated from the AF to the SC direction. $\langle Q \rangle$ is therefore a purely fluctuating quantity. It can be integrated out to yield a time-gradient squared term in the effective action, which consequently gives $z = 1$ for the phase-sector, the same as for the spin-sector.

Away from the fine-tuned value of U, π-rotations of the superspin will move the system away from half-filling, since the V and the D component of the SC state no longer have the same amplitude. As a result, $\langle Q \rangle$ acquires a non-fluctuating part Q_0. The long-wavelength action will therefore contain the single-derivative phase-dynamics term of eq. (5.8.3) with $\langle Q \rangle = Q_0$, in addition to the time-derivative squared term mentioned before. This single-derivative term gives rise to a critical exponent $z = 2$ for the phase-sector, leading to very different behavior for the spin and phase degrees of freedom at low temperatures.

At the symmetric point, $\vec{n}$ is a fluctuating quantity. Expanding the action to second order in $\vec{n}$ and integrating it out, we obtain an $SO(5)$ generalization of the bilayer QNLS eq. (4.6.3)

$$S_{\text{Eff}} = \frac{1}{2} \int_{J_0}^{\beta\hbar} d\tau \int d^d x \left[\chi_\perp \left(\partial_\tau \hat{\vec{n}}(\vec{x}, \tau) \right)^2 + \rho_s \left(\vec{\nabla} \hat{\vec{n}}(\vec{x}, \tau) \right)^2 \right]. \tag{5.8.4}$$

Its stiffness and susceptibility have the saddle-point values

$$\chi_\perp = a^{-d} \frac{2 - J}{(2 + J)(1 + \frac{3}{2}J)},$$

$$\rho_s = a^{2-d} \frac{1}{4} \left(1 - \frac{J^2}{4} \right). \tag{5.8.5}$$

This action describes the transition from the small J phase, where the $SO(5)$ symmetry is spontaneously broken and the system has long-range spin- and/or phase-order, to an $SO(5)$ symmetric phase at $J > J_c$. The symmetric phase continuously evolves into the mean-field $n = 1$ spin liquid state at large J. That the same transition occurs in this model as in the bilayer model is related to the fact that $|A\rangle$ is an $SO(5)$ singlet as well as a spin-singlet.

5.9 Summary and outlook

We have introduced a model which can describe in a simple way the interplay between spin-ordering and superconductivity. It demonstrates the point that a smooth transition from an insulating antiferromagnet to a spin-disordered superconductor is only possible through an intermediary phase, which can be a spin-disordered insulator or a superconducting antiferromagnet. The latter appears here as the more natural scenario, since the system can be tuned through it by varying the density of charge-carriers (the former requires first varying a spin-exchange constant and then varying the charge density). At finite temperatures, a

superconducting system which is close to the coexistence region is found to show quantum critical behavior in the spin sector. This behavior has been observed in various experiments for the high T_c superconductors [66] [65].

The model is formulated on a $\frac{1}{5}$-depleted lattice. Since the goal of this work has been to demonstrate the possibility of a coexistence phase and to investigate its long-wavelength properties, we had some liberty regarding the microscopic input. The occurrence of the coexistence phase is not expected to be an artefact of our specific choice for the lattice. It can for instance easily be seen that a system with paired *holes* near half-filling (low density limit) on a square lattice should have very similar behavior to what is found here.

The most likely place in the high-T_c's phase-diagram for coexisting antiferromagnetism and superconductivity is not near half-filling, but in the underdoped superconducting region. The antiferromagnetism is in this case of the stripe-variety. The charge-ordering which is also present in a stripe-state was not addressed in the present analysis. The possibility of coexisting charge-order and superconductivity has however already been demonstrated in various models [51].

The model is found to have an $SO(5)$ symmetric line in its phase-diagram. This is a property which *is* specific to its microscopy. The $SO(5)$-symmetric models in dimensions larger than 1 formulated up to now all involve long-range interactions. Because of the special choice for the lattice and the pairing-interaction, $SO(5)$-symmetry can be obtained here with only local interactions. This model can therefore be useful as a 'fixed point Hamiltonian' to study the physics of higher dimensional systems with a (near) $SO(5)$-symmetry. Here, we have focussed on the strong-pairing limit, which yields only the bosonic $SO(5)$-sector. It is however possible to go to the regime of weaker pairing while keeping the $SO(5)$-symmetry. One can then study for instance the quasi-particle properties.

The extension of the model to general pairing-strength is a future project. There will also be a more thorough analysis of the remaining $SO(5)$-properties after projecting onto the lower-Hubbard band, especially with regard to the finite temperature behavior.

Bibliography

[1] J. G. Bednorz and K. A. Müller, Z. Phy. B, 64 (1986), 189.

[2] A. J. Millis and H. Monien, Phys. Rev. Lett. **70**, 2810 (1993); *ibid.* Phys. Rev. B **50**, 16606 (1994).

[3] A. Auerbach, Interacting electrons and quantum magnetism, Springer-Verlag New York (1994).

[4] H. Ding *et al.*, cond-mat/9712100 (1997).[4]

[5] N. D. Mermin and H. Wagner, Phys. Rev. Lett. **17**, 1133 (1966).

[6] T. Holstein and H. Primakoff, Phys. Rev. **58**, 1908 (1940).

[7] Ch. Niedermayer *et al.*, Phys. Rev. Lett. **80**, 3843 (1998).

[8] P. W. Anderson, Science **235**, 1196 (1987).

[9] B. Keimer *et al.*, Phys. Rev. B **46**, 14034 (1992).

[10] J. Igarahsi, Phys. Rev. B **46**, 10763 (1992).

[11] J. Kim and M. Troyer, Phys. Rev. Lett. **80**, 2705 (1998).

[12] S. Chakravarty, B. I. Halperin and D. R. Nelson, Phys. Rev. Lett. **60**, 1057 (1988); *ibid.* Phys. Rev. B **39**, 2344 (1989).

[13] E. Fradkin, Field theories of condensed matter systems, Addison Wesley (1991)

[14] J. A. Hertz, Phys. Rev. B **14**, 1165 (1976).

[15] F.D.M. Haldane, Phys. Lett. **93 A**, 464 (1983), Phys. Rev. Lett. **50**, 1153 (1983).

[16] A. V. Chubukov and S. Sachdev, Phys. Rev. Lett. **71**, 169 (1993).

[17] D. Sénéchal, Phys. Rev. B **52**,15319 (1995).

[18] A. Perelomov, Generalized coherent states and their applications, Springer-Verlag Berlin Heidelberg (1986).

[19] M. Troyer and M. Imada, Computer Simulations in Condensed Matter Physics X, ed. D. P. Landau *et al.* (Springer-Verlag Heidelberg, 1997); cond-mat/9703049.

---

[4] 'cond-mat' refers to the Los Alamos E-print archive: http://xxx.lanl.gov/archive/cond-mat.

[20] H.Q. Lin and J.L.Shen cond-mat/9805269, PRB **42**,4561 (1990)

[21] M. den Nijs and K. Rommelse, Phys. Rev. B **40**, 4709 (1989)

[22] J. M. Tranquada *et al.*, Nature **375**, 561 (1995);J. M. Tranquada cond-mat/9802034 (1998).

[23] J. Zaanen and O. Gunnarsson, Phys. Rev. B **40**, 7391 (1989)

[24] H. J. Schultz, Phys. Rev. Lett. **64**, 1445 (1990), *ibid* J. Phys. (Paris) **50**, 2833 (1989); D. Poilblanc and T. M. Rice, Phys. Rev. B **39**, 9749 (1989); K. Machida, Physica C **158**, 192 (1989).

[25] S. R. White and D. J. Scalapino, cond-mat/9705218 (1997).

[26] V. J. Emery and S. A. Kivelson, Nature **374**, 434 (1995).

[27] H. Kimura *et al.*, Phys. Rev. B **59**, 6517 (1999); T. Suzuki *et al.*, Phys. Rev. B **57**, R3229 (1998).

[28] J. M. Tranquada *et al.*, cond-mat/9608048 (1996).

[29] S. C. Zhang, Science **275**, 1089 (1997).

[30] E. Demler and S. C. Zhang, Phys. Rev. Lett. **75** , 4126 (1995).

[31] W. Hanke *et al.*, cond-mat/9807015 (1998).

[32] S. Alama *et al.*., cond-mat 9812283 (1998).

[33] Demler *et al.*, Phys. Rev. Lett. **80**, 2917 (1998).

[34] P. Bouwknegt and K. Schoutens, cond-mat/9805232 (1998).

[35] S. C. Zhang, Proceedings of the Grand Finale Taniguchi Symposium on "The Physics and Chemistry of Transition Metal Oxides"; cond-mat/9808309 (1998).

[36] H. Lin, L. Balents and M. Fisher, Phys. Rev. B **58**, 1794 (1998).

[37] O. Zachar, S. A. Kivelson and V. J. Emery, Phys. Rev. B **57**, 1422 (1998).

[38] V. J. Emery, S. A. Kivelson and H. Q. Lin, Phys. Rev. Lett. **64**, 475 (1990).

[39] V. Sachan *et al.*, Phys. Rev. B **54**, 12318 (1996).

[40] A. H. Castro Neto and D. Hone, Phys. Rev. Lett. **76**, 2165 (1996); *ibid* cond-mat/9701042.

[41] J. Tworzydlo *et al.*, Phys. Rev. B **59**, 115 (1999).

[42] Y. J. Kim *et al.*, cond-mat/9902248.

[43] A. Parola, S. Sorella, and Q. F. Zhong, Phys. Rev. Lett. **71**, 4393 (1993).

[44] I. Affleck and B. I. Halperin, J. Phys. **A29**, 2627 (1996).

[45] Ziqiang Wang, Phys. Rev. Lett. **78**, 126 (1997)

[46] J. M. Tranquada, P. Wochner and D. J. Buttrey, cond-mat/9612007.

[47] V. Kataev *et al.*, Phys. Rev. B **55**, R3394 (1997).

[48] A. Aharony *et al.*, Phys. Rev. Lett. **60**, 1330 (1988).

[49] U. Löw *et al.*, Phys. Rev. Lett. **72**, 1918 (1994).

[50] S.-H. Lee and S.-W. Cheong, cond-mat/9706110.

[51] A. van Otterlo *et al.*, cond-mat/9508065 (1995).

[52] D. R. Nelson and R. A. Pelcoqqvits, Phys. Rev. B **16**, 2191 (1977).

[53] E. Brézin, J. Zinn-Justin and J. C. Le Guillou, Phys. Rev. D **14**, 2615 (1976).

[54] J. Bardeen, L. N. Cooper and J. R. Schrieffer, Phys. Rev. **108**, 1175 (1957).

[55] J. Zaanen, 'The classical condensates', lecture notes to condensed matter theory course, Leiden University.

[56] A. W. Sandvik and D. J. Scalapino, Phys. Rev. Lett. **72**, 2777 (1994).

[57] T. Matsuda and K. Hida, J. Phys. Soc. Jpn. **59**, 2223 (1990).

[58] K. Hida, J. Phys. Soc. Jpn. **59**, 2230 (1990).

[59] K. Hida, J. Phys. Soc. Jpn. **61**, 1013 (1992).

[60] Z. Weihong, cond-mat/9701214 (1997).

[61] A. V. Chubukov and D. K. Morr, Phys. Rev. B **52**, 3521 (1995).

[62] C. Gros, W. Wenzel and J. Richter, Europhys. Lett. **32**, 747 (1995). It is noted that the spectrum of physical excitations is in this case gapped. The mode-softening transition discussed by Gros et al occurs actually in the thermodynamically irrelevant thin spectrum. E. Lieb and D. Mattis, J. Math. Phys. **3**. 749 (1962); T. A. Kaplan, W. von der Linden and P. Horsch, Phys. Rev. B **42**, 4663 (1990).

[63] For instance, the so-called singlet-triplet models:P. Fulde and I. Peschel, Adv. Phys. 21, 1 (1972).

[64] A. V. Chubukov, S. Sachdev and J. Ye, Phys. Rev. B. **49**, 11919 (1994).

[65] V. Barzykin and D. Pines, Phys. Rev. B **52**, 13585 (1995) ;Y. Zha, V. Barzykin and D. Pines, cond-mat/9601016.

[66] G.Aeppli *et al.* Science **278**, 1432 (1997).

[67] J. Zaanen, cond-mat/9811078 (1998).

[68] R. Micnas, J. Ranninger and S. Robaszkiewicz, Rev. Mod. Phys. **62**, 113 (1990).

[69] P. Nozieres, S. Schmitt-Rink, J. Low-Temp. Phys. **59**, 159 (1985).

[70] A. van Otterlo, Quantum phase transitions and vortex dynamics in two-dimensional Bose systems, Dissertation, Universität Karlsruhe (1994).

[71] D. Scalapino, S. C. Zhang and W. Hanke, Phys. Rev. B **58** 443 (1998).

[72] R. Eder *et al.*, cond-mat/9805120 (1998).

[73] G. Baskaran and P. W. Anderson, cond-mat/9706076 (1997) ; R. B. Laughlin, cond-mat/9709195; (1997) P. W. Anderson and G. Baskaran, cond-mat/9711197 (1997).

[74] S.B. Haley and P. Erdös, Phys. Rev. B **5**, 1106 (1972).

[75] C. P. Burgess and C. A. Lütken, Phys. Rev. B **57**, 8642 (1998).

Summary

The subject of this thesis is magnetic ordering as it appears in the cuprate superconductors. These materials have a quasi 2-dimensional structure: they are layered, and the interactions between the degrees of freedom in the different layers are very weak. When undoped, they are spin-$\frac{1}{2}$ antiferromagnetic insulators. By doping holes into the layers, it is however possible to induce some conductance, and, above a critical doping, superconductivity. The antiferromagnetic order is rapidly suppressed with doping, but it reappears in a different form at higher hole-concentrations. The problems studied in chapters 2 and 5 are related to this different form of antiferromagnetism: the stripe-ordered state.

The undoped cuprate superconductors are, as said, quasi 2-dimensional antiferromagnets. In sections 1.2 through 1.4, a review is given of the semi-classical theory of the two-dimensional quantum Heisenberg antiferromagnet. At zero-temperature, this system has long-range antiferromagnetic order. It is then possible to analyse its properties by expanding in small perturbations around the perfectly ordered state. The expansion parameter is one over the spin size S. This expansion gives reasonable results even for $S = \frac{1}{2}$ antiferromagnets, since the prefactors of the higher order terms fall off rapidly.

At finite temperatures, the long-range order in two-dimensional antiferromagnets is destroyed by thermal fluctuations. An expansion around the globally ordered state is then no longer possible. One can, however, still use a mapping of the low-energy sector of the system onto an effective field-theory: the non-linear sigma model. This mapping relies on the assumption that, for low enough temperatures, there still is well-developed antiferromagnetic order at short distances. One can then define a local order-parameter vector, whose length is associated with the strength of the antiferromagnetic order, and whose direction is related to the average local orientation of the spins. The low-energy fluctuations of the system are slow variations in the orientation of the order-parameter. It is these transversal fluctuations which are described by the non-linear sigma model. This model can be analyzed by a renormalization-group procedure, which is reviewed in the appendix to chapter 2.

The non-linear sigma model contains two parameters: temperature, and a parameter g which determines the strength of the quantum fluctuations. This parameter is inversely proportional to the spin-size S. For large S, quantum-fluctuations are therefore weak and the tendency to order at zero-temperature is strong. The quantum-fluctuations grow stronger as S is decreased, until the spin-order disappears at a critical value of $S \simeq \frac{1}{3}$. This spin-size is unphysically small, and two-dimensional antiferromagnets are therefore always ordered at zero-temperature.

The models which are discussed in chapter 2, 4 and 5 all have the property that they do undergo a zero-temperature order-disorder transition. At non-zero temperature, and for g close to this phase-transition, the renormalization-group analysis predicts the existence of

a region where the system becomes insensitive to all energy-scales except temperature: the quantum-critical regime. There are a number of experiments which indicate that this type of behavior occurs in the spin-sector of the cuprate superconductors. This implies that these materials are 'close' to an antiferromagnetically ordered state. In view of the dopings at which the quantum-critical behavior is found, it seems reasonable to identify this nearby antiferromagnetic state with the aforementioned stripe-phase.

Stripe-ordering can emerge when a two-dimensional antiferromagnet is doped with a sufficient quantity of holes. In the stripe-ordered phase, the holes form lines, while the spins in the hole-free regions between the lines order antiferromagnetically. The lines are localized on anti-phase domain-walls in the spin-system. At the dopings where quantum-critical behavior is observed, neutron-scattering experiments show dynamical stripe-correlations. Recently, static stripe-order coexisting with superconductivity has been found around a specific doping, where the stripes are particularly stable due to a commensuration effect.

In chapter 2, the disordering influence of static stripe-order on an antiferromagnetic spin system is investigated. The antiferromagnetic interaction between two spins separated by a hole is weaker than between two neighboring spins. In the limit where the first interaction vanishes, the spin-system in the static stripe phase becomes effectively one-dimensional. Since quantum-fluctuations destroy antiferromagnetic order in one dimension even at zero-temperature, it is clear that the presence of stripes drives the spin-system closer to its order-disorder transition. This effect is investigated using a renormalization-group analysis of a generalized non-linear sigma model. It is found that the weakening of the spin-spin interaction across the stripes indeed reduces the zero-temperature spin-ordering, but that the effect on the finite-temperature properties of the system is even more dramatic. The onset-temperature of antiferromagnetic order is for instance much more strongly reduced by the presence of static stripes than the zero-temperature antiferromagnetic order-parameter [5]. This effect is of significance if one tries to understand the mechanism underlying stripe-ordering, as is discussed in section 2.1.

Chapter 3 is more technical in nature. In order to construct a semi-classical description of a system, so-called coherent states are often used. These states are locally 'optimally classical' and form a basis on the Hilbert space of the system that one wants to study. If the theory is constructed using this basis, it becomes easy to identify the dangerous long-wavelength fluctuations around the classical state. There are however systems for which the local state is not maximally classical. Two examples of such systems are treated in chapters 4 and 5. In order to arrive at a semi-classical description of these kinds of systems, a new type of coherent state is constructed, in which local quantum-fluctuations are incorporated. This state is applied to the problems discussed in the next two chapters.

Another spin-system which undergoes a zero-temperature order-disorder transition is studied in chapter 4: the Heisenberg bilayer antiferromagnet. As was the case in the static stripe-phase, this system is driven towards the disordering transition by effectively reducing the dimensionality. In the bilayer Heisenberg model, each spin in layer 1 is antifer-

---

[5]In *quasi* two-dimensional spin-systems, like the cuprates, the spin-ordering temperature is small but non-zero.

romagnetically coupled to a spin in layer 2. If this coupling is much stronger than the coupling between spins in the same layer, the system is effectively zero-dimensional. Each spin then pairs into a singlet-state with its neighbor on the opposite layer. This is one example of a local state which which is strongly quantum-correlated. Using the coherent state constructed in the previous chapter, the long-wavelength sector of this system is mapped onto a non-linear sigma model, where the parameter g is now a function of the ratio of the inter-layer and the intra-layer spin-spin interaction. This parameter diverges at the value of the ratio where, according to mean-field theory, the system undergoes a transition to a state consisting of local singlet pairs. Since g has a finite critical value, transversal fluctuations will destroy the antiferromagnetic order before this mean-field transition can occur.

As was noted earlier, there are indications that antiferromagnetic stripe-order can coexist with superconductivity. The goals of chapter 5 is to investigate in a simple setting the interplay between antiferromagnetism and superconductivity. The model which is investigated describes a strong-coupling limit where attractive interactions have caused all electrons to form nearest-neighbor pairs. These pairs carry spin degrees of freedom and can hop on an unusual type of two-dimensional lattice (this particular lattice is used to allow for a strong-coupling limit in which electron-pairing occurs, instead of phase-separation). This system has a rich phase-diagram, in which various types of spin-order and superconductivity appear. Specifically, it exhibits a phase where the system is superconducting while at the same time having antiferromagnetic order. It is discussed how this work relates to the $SO(5)$ theory of high-temperature superconductivity. In this theory, it is attempted to arrive at a unified description of antiferromagnetism and superconductivity in the cuprates, by assuming that these two types of order are approximately related through a higher symmetry than is manifestly present in these materials. We find that this higher symmetry can be obtained in this model for specific, not very realistic, values of the system parameters. Some of the properties which are related to this symmetry survive at the mean-field level and to linear approximation around it, even if the symmetry is explicitly broken by imposing the physical constraint that the Coulomb repulsion between two electrons on the same site has to be very strong.

Samenvatting

Dit proefschrift heeft als onderwerp de magnetische ordening zoals die optreedt in hoge temperatuur supergeleiders. Deze materialen zijn quasi twee-dimensionaal: ze hebben een gelaagde structuur, met zwakke interacties tussen de vrijheidsgraden in de verschillende lagen. In hun pure toestand zijn ze isolerende spin-$\frac{1}{2}$ antiferromagneten, maar door doping van gaten in de lagen kan een gebrekkig soort geleiding, en uiteindelijk, boven een bepaalde doping, supergeleiding worden geinduceerd. De antiferromagnetische ordening verdwijnt snel wanneer het materiaal gedoopt wordt, maar duikt bij hogere gatenconcentraties in een andere vorm weer op. Deze andere vorm van antiferromagnetisme, de stripe-toestand, vormt de aanleiding voor het werk in de hoofdstukken 2 en 5.

De ongedoopte supergeleiders zijn, zoals gezegd, quasi twee-dimensionale antiferromagneten. In secties 1.2 tot en met 1.4 wordt een overzicht gegeven van de semi-klassieke theorie van de quantum Heisenberg antiferromagneet in twee dimensies. Bij nul-temperatuur heeft dit systeem lange-drachts antiferromagnetische orde. Het is dan mogelijk de eigenschappen te berekenen door te expanderen in kleine afwijkingen rond de perfect geordende toestand. De expansie parameter is één gedeeld door de spin-lengte S. Zelfs voor $S = \frac{1}{2}$ antiferromagneten geeft deze expansie nog redelijke resultaten, daar de voorfactoren van de hogere orde termen snel afvallen.

Bij eindige temperaturen wordt de lange-drachts orde in twee-dimensionale antiferromagneten vernietigd door spin-fluctuaties. Het is dan niet meer mogelijk om een expansie rond een globale geordende toestand te gebruiken om het systeem te analyseren. Het is echter nog wel mogelijk om de lage-energie sektor van het systeem af te beelden op een effectieve veldentheorie: het niet-lineaire sigma model. Deze afbeelding gaat uit van de aanname dat er, als de temperatuur laag genoeg is, op korte afstanden wel goed ontwikkelde antiferromagnetische orde is. Het is dan mogelijk om een lokale orde-parameter vektor te definiëren, waarvan de lengte de mate van ordening aangeeft, en de richting de gemiddelde oriëntatie van de spins. De lage-energie fluctuaties van het systeem zijn geleidelijke veranderingen van de richting van de orde-parameter. Het zijn deze transversale fluctuaties die worden beschreven door het niet-lineaire sigma model. In de appendix van hoofdstuk 2 wordt de renormalisatie-groep procedure besproken waarmee dit model geanalyseerd kan worden.

Het niet-lineaire sigma model bevat twee parameters: de temperatuur en een parameter genaamd g, die de sterkte van de quantum-fluctuaties bepaald. Deze laatste parameter is omgekeerd evenredig aan de spin-lengte S. Voor grote S zijn de quantum-fluctuaties dus zwak en is de neiging tot orde bij nul-temperatuur sterk. De quantum-fluctuaties nemen toe met afnemende S, totdat, bij een kritische waarde van ongeveer $\frac{1}{3}$, de spin-orde verdwijnt. Deze spin-lengte is onfysisch klein, en een twee-dimensionale antiferromagneet is dan ook altijd geordend bij nul-temperatuur.

De modellen die in de hoofdstukken 2, 4 en 5 worden beschouwd hebben als eigenschap dat ze wèl de nul-temperatuur fase-overgang naar een wanordelijke spin-toestand kunnen ondergaan. Bij eindige temperaturen en voor g in de buurt van deze fase-overgang voorspelt de renormalisatiegroep-analyse een gebied waar het spin-systeem ongevoelig wordt voor elke energieschaal behalve de temperatuur: het quantum-kritische regime. Er zijn verschillende experimenten die erop wijzen dat de spin-sektor van de hoge-temperatuur supergeleiders dit soort gedrag vertoont. Dit betekent dat deze materialen dicht bij een antiferromagnetisch geordende toestand zijn . Gezien de dopings waarbij het quantum-kritische gedrag wordt waargenomen, ligt het voor de hand om de 'nabije' spin-geordende toestand te identificeren met de eerder genoemde stripe-fase.

Stripe-ordening kan ontstaan wanneer een twee-dimensionale antiferromagneet met voldoende gaten wordt gedoopt. In de stripe-geordende fase vormen de gaten lijnen, terwijl de spins in de gebieden tussen de lijnen antiferromagnetisch ordenen. De lijnen bevinden zich op domein-wanden in de spin-orde: de antiferromagnetische orde-parameter verandert 180 graden van richting wanneer men een lijn passeert. In het dopingsgebied waar het quantum-kritische gedrag optreedt worden met neutronen-verstrooiing dynamische stripe-correlaties waargenomen. Rond een specifieke doping, waar stripe-orde extra stabiel is door een commensuratie-effect, zijn recentelijk statische stripes waargenomen, coexisterend met supergeleiding.

In hoofdstuk 2 wordt de verstorende invloed van een statische stripe-configuratie op de spin-sektor bestudeerd. De antiferromagnetisch spin-spin wisselwerking tussen twee spins aan weerszijden van een gat is zwakker dan tussen twee naburige spins. In de limiet waar deze eerste wisselwerking nul is, is het spin-systeem in de statisch stripe-fase effectief één-dimensionaal. Aangezien in één dimensie quantum-fluctuaties de spin-orde zelfs bij nul-temperatuur vernietigen, is het duidelijk dat de aanwezigheid van de stripes het spin-systeem dichter naar zijn orde-wanorde overgang drijft. Dit effect wordt bestudeerd met een renormalisatie-groep analyse van een gegeneraliseerd niet-lineair sigma model. Het blijkt dat de zwakkere spin-spin koppeling over de stripes inderdaad de antiferromagnetische orde bij nul-temperatuur verzwakt, maar dat het nog dramatischer effecten heeft op de eigenschappen van het systeem bij eindige temperaturen. Zo wordt de temperatuur waar het spin-systeem ordent [6] veel sterker gereduceerd door de aanwezigheid van de stripes dan de nul-temperatuur antiferromagnetische orde-parameter. Dit effect is van belang om zicht te krijgen op het mechanisme achter de formering van de stripes, zoals besproken in sectie 2.1.

Hoofdstuk 3 is meer technisch van aard. Om tot een semi-klassieke beschrijving van een systeem te komen, worden vaak zogenaamde coherente toestanden gebruikt. Deze toestanden zijn lokaal 'maximaal klassiek' en vormen een basis op de Hilbertruimte van het te bestuderen systeem. Wanneer de theorie in zo'n basis geformuleerd wordt, is het eenvoudig om de gevaarlijke lange-golflengte fluctuaties rond de klassieke toestand te identificeren. Er zijn echter systemen waarin de lokale toestand niet maximaal klassiek is. Voorbeelden

---

[6]Deze temperatuur is niet precies nul in aanwezigheid van kleine spin-anisotropien en een koppeling tussen verschillende twee-dimensionale lagen, zoals het geval is voor de hoge-temperatuur supergeleiders.

hiervan worden behandeld in de hoofdstukken 4 en 5. Om tot een semi-klassieke beschrijving van dit soort systemen te komen, wordt in hoofdstuk 3 een coherente toestand geconstrueerd waarin quantum-correlaties op korte afstanden zijn verwerkt. Deze toestand wordt toegepast op de problemen in de volgende hoofdstukken.

Een ander spin-systeem waarin een nul-temperatuur orde-wanorde overgang kan plaatsvinden wordt bestudeerd in hoofdstuk 4: de dubbellaags Heisenberg antiferromagneet. Evenals in de statische stripe-fase, wordt het systeem hier naar de overgang gedreven door effectief de dimensie te verlagen. In het dubbellaags Heisenberg model is elke spin in laag 1 antiferromagnetisch gekoppeld aan een spin in laag 2. Als deze koppeling veel sterker wordt dan de koppeling tussen spins in dezelfde laag, wordt het systeem feitelijk nul-dimensionaal. Elke spin vormt in dat geval een singlet toestand met de buur in de andere laag. Dit is een voorbeeld van een lokale toestand die sterk quantum-mechanisch is. Gebruik makend van de coherente toestand uit het vorige hoofdstuk, wordt een langegolflengte theorie voor dit model afgeleid: een niet-lineair sigma model, waarin de parameter g nu een functie is van de verhouding tussen de spin-spin koppeling in de laag en die tussen de lagen. Deze parameter divergeert bij de waarde van de inter-laag spin-spin interactie waar, volgens de gemiddeld-veld theorie, het systeem overgaat naar een toestand van lokale singlets. Aangezien g een eindige kritische waarde heeft, betekent dit dat transversale spin-fluctuaties de antiferromagnetische orde in het systeem vernietigen voordat de gemiddeld-veld overgang plaats kan vinden.

Zoals eerder opgemerkt zijn er aanwijzingen dat het stripe-antiferromagnetisme in de hoge temperatuur supergeleiders coexisteert met supergeleiding. Het doel van hoofdstuk 5 is om de wisselwerking tussen spin-ordening en supergeleiding te bestuderen in een eenvoudig microscopisch model. Dit model beschrijft een sterke-koppelings limiet, waarin de elektronen door een sterke attractieve wisselwerking naaste-buur paren gevormd hebben. Deze paren hebben spin-vrijheidsgraden en kunnen bewegen over een wat ongewoon soort 2-dimensionaal rooster (dit rooster wordt gebruikt zodat in de sterke koppelingslimiet naaste-buur paring optreedt, in plaats van fasescheiding). Dit systeem heeft een rijk fasediagram, waarin verschillende vormen van spin-orde en supergeleiding voorkomen. Het vertoont met name een fase waarin het systeem tegelijkertijd supergeleidend is en antiferromagnetische orde heeft. Er wordt bediscusieerd hoe de resultaten van dit model zich verhouden met de $SO(5)$-theorie van hoge temperatuur supergeleiding. In deze theorie wordt getracht tot een geunificeerde beschrijving van supergeleiding en antiferromagnetisme in de hoge temperatuur supergeleiders te komen. door te veronderstellen dat de twee soorten orde bij benadering gerelateerd zijn door een hogere symmetrie dan manifest in deze materialen aanwezig is. We vinden dat deze symmetrie in dit model gerealiseerd kan worden voor specifieke, niet erg realistische, waarden van de model-parameters. Sommige eigenschappen die horen bij de hogere symmetrie overleven op gemiddeld veld-niveau en tot lineaire orde daaromheen, ook wanneer de symmetrie expliciet gebroken wordt door de fysische eis te stellen dat de Coulomb-repulsie tussen twee elektronen op dezelfde roosterplaats zeer sterk is.

List of publications

- Ginzburg-Landau theory of the cluster glass phase.
  Th. M. Nieuwenhuizen and C.N.A. van Duin,
  J. Phys. A **30**, L55 (1997)

- Origin of the quantum critical transition in the bilayer Heisenberg model.
  C.N.A. van Duin and J. Zaanen,
  Phys. Rev. Lett. **78**, 3019 (1997)

- Charge- versus spin-driven stripe order: the role of transversal spin
  fluctuations.
  C.N.A. van Duin and J. Zaanen,
  Phys. Rev. Lett. **80**, 1513 (1998)

- Quantum magnetism in the stripe phase: bond- versus site order.
  J. Tworzydlo, O. Y. Osman, C.N.A. van Duin and J. Zaanen,
  Phys. Rev. B **59**, 115 (1999)

- Spin-only approach to quantum magnetism in the ordered stripe state.
  J. Tworzydlo, C.N.A. van Duin and J. Zaanen,
  to appear in Proc. of 2nd Intern. Conf. on Stripes and High T_c Superconductivity,
  Rome 1998, J. of Superconductivity.

- Theory of site-disordered magnets.
  Th. M. Nieuwenhuizen and C.N.A. van Duin,
  Eur. Phys. J. B. **7**, 191 (1999)

Curriculum vitae

Ik ben geboren op 7 november 1970 te Nijmegen. Mijn middelbare schooltijd bracht ik door aan de Rijksscholengemeenschap in Schagen, waar ik het VWO-examen voltooide in 1989. In datzelfde jaar begon ik met mijn studie natuurkunde aan de Universiteit van Amsterdam. Als afstudeerrichting koos ik voor de theoretische natuurkunde. Ik besloot mijn studie met een stage bij dr. Th. M. Nieuwenhuizen, met wie ik werkte aan een Ginzburg-Landau theorie voor positioneel wanordelijke spinglazen, en behaalde mijn doctoraal examen in maart 1995. Gedurende mijn studie-periode heb ik als student-assistent een werkcollege speciale relativiteit en klassieke mechanica gegeven, en als steundocent wis- en natuurkunde les gegeven aan kleine groepen leerlingen op een middelbare school.

In april 1995 trad ik in dienst van de stichting FOM (Fundamenteel Onderzoek der Materie) als onderzoeker in opleiding. Ik verrichtte promotie-onderzoek op het gebied van de theorie van de gecondenseerde materie, onder begeleiding van dr. J. Zaanen, met als promotor prof. dr. ir. W. van Saarloos. De resultaten van dit onderzoek zijn beschreven in dit proefschrift.

Gedurende mijn promotie-periode heb ik verschillende congressen en scholen bezocht, en daar mijn werk gepresenteerd. In januari 1998 heb ik twee weken doorgebracht in de Los Alamos laboratoria, in de Verenigde Staten. Als onderwijstaak heb ik bijdragen geleverd aan de syllabus voor het college theorie van de gecondenseerde materie van dr. J. Zaanen.
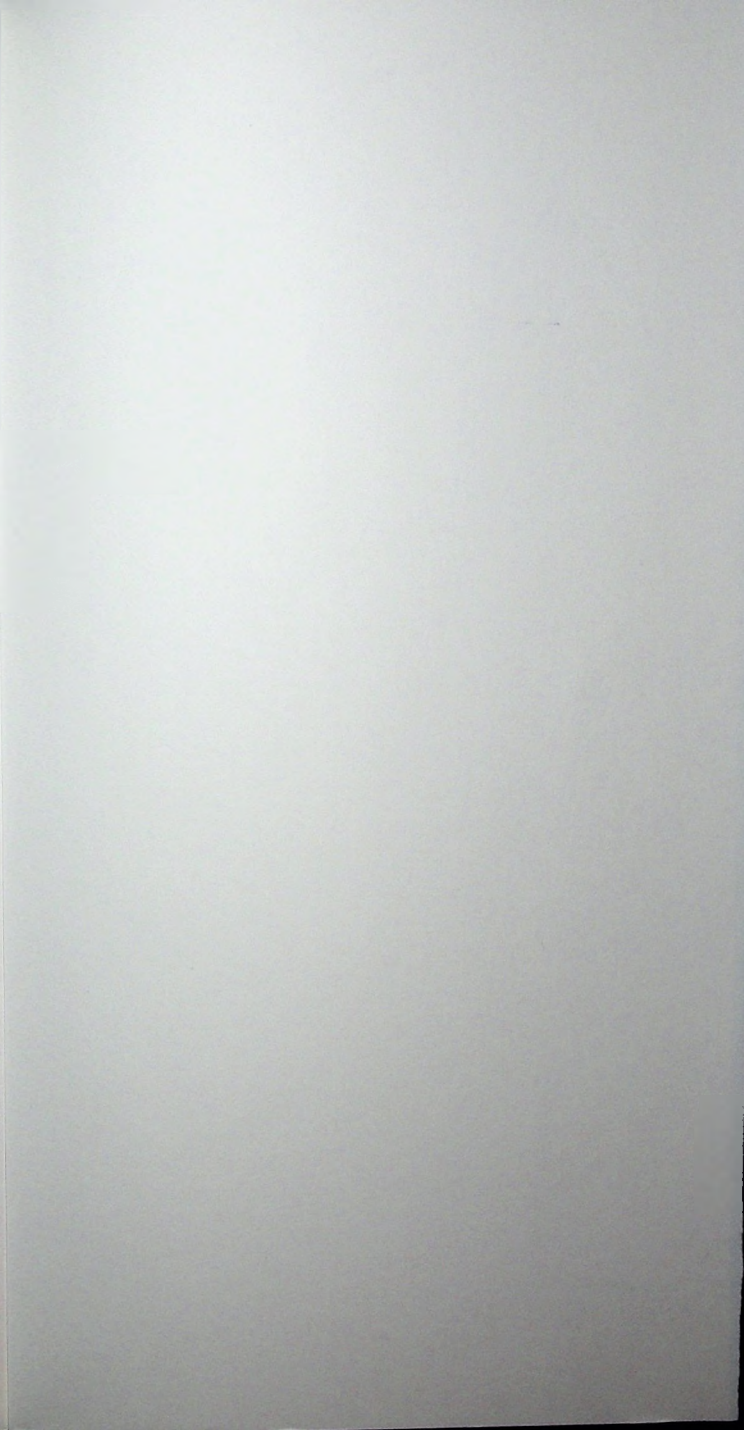
Stellingen
behorende bij het proefschrift
On Quantum Magnetism in Cuprate Superconductors

1. Bij de analyse van een systeem van zwak gekoppelde spin-$\frac{1}{2}$ ketens, bepaalt Wang[1] de koppelingsconstante g van het effectieve 2d niet-lineair sigma model uit de gerenormaliseerde spin stijfheid (ρ_s) en susceptibiliteit ($\chi_\perp$) van de individuele spin ketens. De relatie $g = 1/\sqrt{\rho_s \chi_\perp}$ die hij daarvoor gebruikt, is echter alleen geldig voor de parameters gedefinieerd op roosterniveau en hier dus niet toepasbaar.
Hoofdstuk 2, dit proefschrift

[1] Z. Wang, Phys. Rev. Lett. **78**, 126 (1996).

2. Een zelf-consistent doorgevoerde RPA analyse van het dubbellaags Heisenberg model leidt tot pathologische resultaten in het gebied waar de lagen sterk gekoppeld zijn. Voor zwakke koppeling van de lagen geeft het beduidend slechtere resultaten dan de niet zelf-consistente RPA.
Hoofdstuk 3, dit proefschrift.

3. Het 'dynamische principe' dat Eder *et al.*[2] introduceren ter verheldering van de aard van $SO(5)$ symmetrie, beschrijft de gemiddeld veld $SO(5)$-symmetrie zoals die in hoofdstuk 5 gevonden wordt, niet de onverstoorde $SO(5)$-symmetrie in de ongeprojecteerde Hilbert ruimte.
Hoofdstuk 5, dit proefschrift.

[2] R. Eder *et al.*, http:xxx.lanl.gov/abs/cond-mat/9805120

4. Twee antiferromagnetisch gekoppelde, antiferromagnetische spin-1 ketens, ondergaan bij een zwakke, maar eindige koppeling een faseovergang van de incompressibele Haldane fase naar een incompressibele lokale singletfase. De spin-gap sluit bij de overgang.
Sectie 1.4, dit proefschrift.

5. In een niet-lineair sigma model met een kleine rotatie-symmetrie breking van de vorm

$$S = \frac{1}{T} \int d^2x \left[(\vec{\nabla}\hat{n})^2 + \alpha(\vec{\nabla}n_1)^2 \right],$$

waar n_1 een component van de eenheidsvektor $\hat{n}$ is en $\alpha \ll 1$, is de parameter α irrelevant[3]. De aanwezigheid van deze symmetrie-breking zorgt er echter voor dat in het renormalisatie-proces andere symmetrie-brekende

termen aanschakelen, die wél relevant zijn (op tree level). Dit suggereert dat het model ondanks de irrelevantie van α niet naar het symmetrische punt stroomt.[4]

[3] R. A. Pelcovits and D. R. Nelson, Phys. Lett. **57A**, 23 (1976)
[4] S. C. Zhang, Science **275**, 1089 (1997)

6. In Friedan's[5] generalisatie van het niet-lineaire sigma model, wordt het hierboven beschreven effect voorkomen door de symmetrie-breking niet alleen in de actie, maar ook in de constraint op het vektorveld te introduceren. De $SO(5)$ symmetrie-breking voorgesteld door Zhang[4] ter beschrijving van de fysica van hoge temperatuur supergeleiders, is echter niet van deze vorm. Friedan's werk kan daardoor niet gebruikt worden om te beargumenteren dat deze breking bij lange golflengtes verdwijnt.

[5] D. H. Friedan, Ann. Phys. **163**, 318 (1985)

7. Bij het berekenen van de hogere orde diagrammen in een impuls-schil renormalisatiegroep-analyse, geeft het gewetensvol integreren van alle deltafuncties niet het juiste resultaat. Het tactisch negeren van bepaalde integratiegrenzen doet dat wel. Dit wordt vaak verzwegen in didactisch bedoelde beschrijvingen van deze methode[6] (en ook lezers van dit proefschrift moeten de Nederlandse taal machtig zijn om deze informatie te krijgen).

[6] R. Shankar. Rev. Mod. Phys. **66**, 129 (1994)

8. Het kennelijke succes waarmee bepaalde conflict-theorie modellen toegepast kunnen worden op de werken van Shakespeare[7], doet vrezen dat ze maar weinig geschikt zijn voor de beschrijving van het echte leven, waarin jaloerse bosgeesten, bloeddorstige Schotten en suicidale verliefden doorgaans slechts een kleine rol spelen.

[7] N. Howard in de Volkskrant, wetenschapsbijlage, 17-4 1999.

9. Om iets te doen aan het softe imago van alternatieve straffen, zou gedwongen vestiging in Urk in het pakket opgenomen kunnen worden.

<div align="right">
Coen van Duin
27 april 1999
</div>